UNIVERSITY OF OKLAHOMA GRADUATE COLLEGE

Plasma-catalysis-enhanced dry reforming of methane facilitated by electrically conductive carbide catalysts

A THESIS

SUBMITTED TO THE GRADUATE FACULTY

in partial fulfillment of the requirements for the

Degree of

MASTER OF SCIENCE

By MUHAMMAD ABDULLAH

Norman, Oklahoma

2024

Plasma-catalysis-enhanced dry reforming of methane facilitated by electrically conductive carbide catalysts

A THESIS APPROVED FOR THE
MEWBOURNE SCHOOL OF PETROLEUM AND GEOLOGICAL ENGINEERING

BY THE COMMITTEE CONSISTING OF

Dr. Baharak Sajjadi, Chair

Dr. Rouzbeh Ghanbar Moghanlo

Dr. Hamidreza Karami

Dr. Catalin Teodoriu

ACKNOWLEDGEMENTS

Gaining knowledge is rewarding but using it to make a difference is a true gift. This thesis marks the end of a journey filled with challenges and personal growth, and I am grateful to everyone who helped me along the way.

First, I thank Allah SWT, my parents, and my siblings. To my loved ones, Babar Hussain and Khizar Abid, thank you for being my strength and biggest supporters. Your love and encouragement have driven my determination every step of the way. I feel lucky to have a supportive extended family. Their faith in me and encouragement have been a constant inspiration.

Academically, I thank my advisor, Dr. Baharak Sajjadi, for the opportunity to work on this project. Under Dr. Sajjadi's guidance, I gained valuable insights and found a role model. I also thank my committee members, Dr. Catalin Teodoriu, Dr. Hamidreza Karami, and Dr. Rouzbeh Ghanbar Moghanlo.

Finally, I thank Mr. Gary Stowe, Ms. Katie Shapiro, and Mr. Derrick Whitney for their support over the past two years.

To all of you, my deepest thanks. This thesis would not have been possible without your constant support.

Table of Contents

LIST OF TABLES

LIST of Figures

ABSTRACT

DRM process, despite its potential for sustainable H_2 production, faces significant challenges due to high energy requirements and catalyst instability at temperatures exceeding 700^0C. To address these issues, NTP (DBD-plasma) was used to process DRM reaction, and TMCs (specifically Mo_2C and WC) were investigated as innovative catalysts for the reaction. Mo_2C and WC catalysts were synthesized by mechanical activation process followed by molten-salt synthesis method, using different sizes of Mo or W powders (nano-powder vs. micro-powder), carbon sources (super-activated carbon vs. carbon black), and metal/carbon ratios. The results showed that Mo_2C catalysts synthesized with micro-powder Mo and carbon black at a 1:1 metal/carbon ratio demonstrated exceptional catalytic activity, increasing H_2 yield by 170% and CO_2 conversion by 277% compared to un-catalyzed reaction. Similarly, WC catalysts synthesized with nano-powder W and carbon black at a 1:1 ratio boosted H_2 yield by 40% and CO_2 conversion by 31%. The high electrical conductivity of TMCs, particularly Mo_2C, facilitated high energy plasma discharge species' transfer to the DRM reactants, thereby improved the interaction between plasma-generated reactive species and DRM reactants, and increased the overall feed-conversion and reaction-yield. Temperature in the discharge region also remained significantly low for the whole time-on-stream. This study effectively addressed the limitations of conventional thermal catalysis, promoting energy efficiency, enhancing catalytic performance, and improving operational stability, thus offering a promising pathway towards more sustainable and efficient methane reforming processes.

CHAPTER 1: INTRODUCTION

1.1 Background

Natural gas (NG) is a mixture of light hydrocarbons, mainly from C_1 to C_4, but some higher HCs and impurities may also be present [3]. The crucial and requisite constituent of NG is methane (CH_4), about 87-97mole %, CH_4 is a flammable, colorless, odorless, and heat-trapping gas [3, 4]. CH_4 has direct and indirect disparate impacts on climate, but only indirect adverse effects on bionetwork and human health [5, 6]. After discharge, it remains in the atmosphere for a decade or more precisely for 11.8 ± 1.8 years. Still, it's short-term effect on the eco-system, in terms of radiative forcing and global warming potential (GWP) is far beyond carbon dioxide (CO_2), though, CO_2 stays in the atmosphere for hundreds of years [7-9]. The presence of CH_4 presence in the atmosphere gives rise to the formation of other greenhouse gases as well, such as it causes an increase in the volume of stratospheric water (H_2O) vapors, and its oxidation results in the formation of CO_2 and ozone (O_3) [7, 8, 10, 11]. As a precursor for O_3, CH_4 indirectly negatively influences the environment and human life. [12-15]. The above-explained negative effects of CH_4 make it the second most dangerous greenhouse gas after CO_2. There are various natural and human-induced sources of CO_2 and CH_4 emission in the atmosphere [16-19]. Besides the cons related to environs and life, CH_4 plays an important role in the artificial preparation of different chemicals. As the main component of NG, it is also used as a fuel in different sectors to meet energy needs [20, 21]. NG and other fossil fuels are responsible for fulfilling around 80% of the global energy demand and are also the main cause of CO_2 emission in the atmosphere [16]. Fossil fuels' consumption will cause the CO_2 emission to increase to 37 billion metric tons per year, by 2025 [16]. The present role of fossil fuels in Earth's energy sectors makes them the main important source of energy, but the remaining quantity, apace depletion, non-renewable nature, harmful impacts (on the global climate and humanity), and fluctuation in the price/supply (depending upon the regional and international politics) of fossil fuels demand a shift towards renewable and green energy, and this shift is only possible with a boost in investment in the renewable energy sector than in fossil fuels, in the current energy market [16, 22-24]. There is an estimation that the current investment amount ($1.3T) in pollution-free energy will increase to a figure above $2T by the year 2030 [16].

Hydrogen gas (H_2) as a fuel can solve the energy and climate-related problems of today's humanity because of its energy density (by mass) value (141.8 MJ/kg), higher than any other source of energy,

and only H_2O (liquid/steam) is produced as a result of its combustion [25-31]. Very high energy content per unit mass and eco-friendly nature highlights the importance of H_2 as the fuel for the future [28, 32]. Technically, H_2 is not a fuel but an energy carrier, and despite being the most common chemical element in the universe, it does not exist freely but is present most commonly in fossil fuels and other chemical compounds, and various technologies are available for its production, by using fossil fuels and other chemical compounds as feed [25, 27, 29-40]. To use and make H_2 an economical source of energy, there must be efficient and cost-effective technologies for its production and storage. Presently, H_2 applications as a fuel are very limited due to its very high production cost [35], but it is utilized in refining (for hydrocracking and hydro-treating), in the chemical industry (for the synthesis of ammonia (NH_3) and methanol (CH_3OH)), in the electric power industry (for producing electricity), and in some other sectors of great importance [30, 37, 41-43]. Production of pure H_2 affordably and reliably can replace the usage of fossil fuels. But benefits, opportunities, expenses, and risks related to every H_2 production method must be considered for a desirable and successful shift towards H_2 economy [36].

Carbon (C) and hydrogen (H) are the two principal constituents of CH_4. Easy access, inexpensive availability, and high H to C ratio ($H/C = 4:1$), which is higher than any other chemical compound, make CH_4 an ideal and very attractive source of H_2. In the contrary, enormous energy requirements and the unavailability of an economical catalyst with desireable activity/stability/product-selectivity, are the issues, that limit the use of CH_4 for getting H_2. Noble-metal based, Ni-based and other non-noble metal based catalysts have been investigated widely for H_2 production by CH_4 reforming reactions [44-51]. Noble-metal based catalysts have been proven very good due to their remarkable thermal/oxidation stability and coking resistance, but their use to catalyze CH_4 reforming reactions is economically not justified [44, 45, 47, 49-51]. Ni-based catalysts are the most investigated catalysts [44, 46-51]. Although, Ni-based catalysts are highly cost-effective and are active for the CH_4 decomposition, but deposition of the solid C ($C_{(s)}$, filamentous and graphitic), produced due to the decomposition of CH_4, on the surface leads to their deactivation [44, 46-51]. Other problems associated with the Ni-based catalysts are oxidation and sintering (due to very high reaction temperature) of Ni particles [44, 46-51]. Using different methods/process-conditions for synthesizing the catalyst, modifying the catalyst by using a promoter/support, and optimizing the reaction conditions have not been proven economically

successful in improving the catalytic activity/stability/product-selectivity of Ni-based catalysts [44, 46-53].

NG reforming-based H_2 production reactions are surface catalytic reactions in nature. Therefore, any element/molecule/compound with a surface catalytic action, similar to that of noble metals can be proved as an appropriate catalyst for these processes. The addition of C in the interstitial sites (voids within the crystal lattice) of a transition-metal (TM)) helps in forming a new compound, called transition-metal carbide (TMC) (Figure 1[54]) [55, 56]. The inclusion of C in the interstitial sites of a TM, alters the electron (e^-) arrangement as well, within the atomic structure [55-57]. Due to the changed e^- distribution, the new chemical compound (TMC) exhibits elctronic properties which are different from that of the parent TM but resemble that of one of the noble metals. The likeness in the electronic properties of a TMC and a noble metal, leads them to exhibit similar surface catalytic action. For example, Levy et al. [57] found that for the reactions like H_2O formation from H_2 and oxygen gas (O_2) at room temperature, and the isomerization of 2,2-dimethylpropane to 2-methylbutane, platinum (Pt) and tumgsten-carbide (WC) present the identical catalytic role. Since then, TMCs have gotten the attention of researchers as alternatives of noble metals for various purposes. Noble metal type surface catalytic behavior and innate higher tendency to react with oxides (H_2O, CO_2, and O_2, etc.) make TMCs the potential candidates to play the catalytic role for CH_4 reforming based H_2 production reactions. The catalytic activity/stability/product-selectivity of TMCs has been found intermediate between the minimum of TMs and a maximum of noble metals, for the hydrogen evolution reactions (HERs) including water-gas shift reaction (WGSR), aqueous phase methanol-reforming, and NG reforming [58-61]. The improved catalytic performance of TMCs compared to their parent metals for HERs is because TMCs' surfaces are three times more sensitive than their parent metals' surfaces to the weakening of H adsorption due to surface coverage effects [60]. TMCs are also used to catalyze biomass conversion reactions, oxygen evolution reactions (OERs), CH_4 coupling reactions, CO_2 upgrading reactions, CO_2 reduction reactions, hydrogenation reactions, hydrodeoxygenation (HDO) reactions, hydrodenitrogenation reactions (HDN), hydrodesulfurization reactions (HDS), and electrochemical reactions, etc. [58, 59, 62-66].

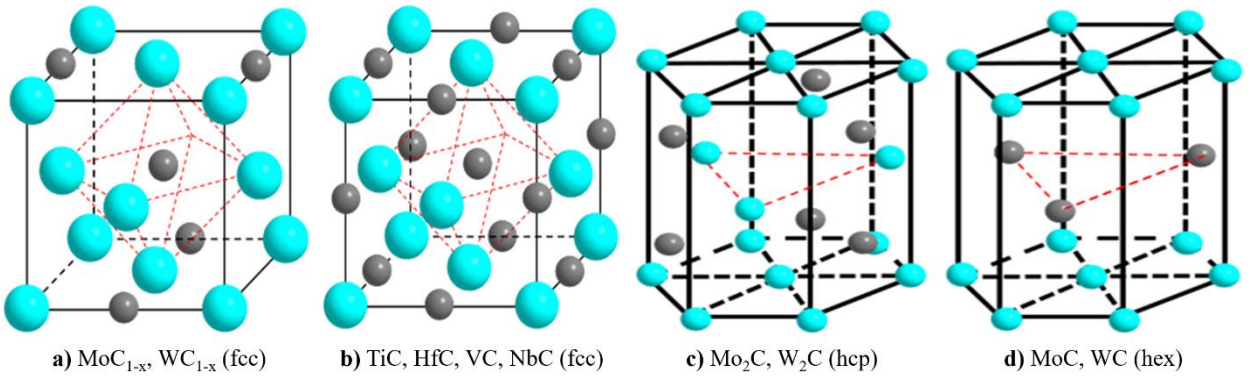

Figure 1. (a) The lattice, associated with carbides, in which M/C ratio can vary, of group-VI metals. (b) The lattice, associated with carbides of group-IV & V metals. (c) The lattice, associated with β-phase of the carbides of group-VI metals. (d) The lattice, associated with α-phase of the carbides of group-VI metals. The blue balls represent the metal atoms, and the dark grey balls represent the C atoms occupying the interstitial sites in the metal structure. Reproduced from [54].

From a thermodynamic standpoint, the dry reforming of methane (DRM) (Equation 11) is an endothermic process, requiring high operating temperatures usually exceeding 700^0C to achieve meaningful conversions of CH_4 and CO_2 [67]. Ni-based catalysts are among the most promising options for DRM due to their impressive performance and cost-effectiveness. However, at these elevated temperatures, they are prone to deactivation through sintering and coke deposition [67, 68]. To address these challenges, various strategies have been investigated. One approach involves adding a second metal to create alloys, such as Ni-Ru or Ni-Re, which can enhance both catalytic activity and stability by improving the dispersion of Ni and reducing coke formation [68, 69]. Another strategy focuses on increasing the basicity of support materials to enhance CO_2 adsorption, thereby maintaining catalytic activity. For example, using supports like $MgAl_2O_4$ with modified acidity can facilitate the DRM reaction pathway [68]. Additionally, constructing core-shell structures is an effective method to limit the sintering of Ni particles. For instance, hollow-NiPt/SiO_2 core-shell catalysts have shown high activity and thermal stability, consistently performing well over extended periods [69]. These strategies have significantly advanced the solutions to the challenges faced by Ni-based catalysts in DRM reactions.

Non-thermal plasma (NTP) or di-electric barrier discharge (DBD) plasma is another useful addition to traditional heat-based catalysis, helping to lower reaction temperatures and speeding up reactions

that would normally be limited by high temperatures, like DRM. In DBD plasma, the temperature of the electrons is in the range of 300 K to 10,000 K, while the temperature of the gas remains relatively low, often near room temperature. Therefore, DBD plasma is commonly referred to as cold plasma**.** In DBD systems, the usual energy of electrons (1-10eV) is enough to break C−H bonds (4.5eV) and C=O bonds (5.5eV), which makes DBD-catalysis a promising method for the DRM reaction [70]. In NTP-assisted catalysis, the sintering of Ni nanoparticles at high operating temperatures is mitigated [68]. Various catalysts have been explored to enhance the conversion of reactants and the selectivity of main products in the DRM reaction. In traditional catalysis, CO_2 conversions are generally higher than CH_4 conversions due to side reactions like the reverse water-gas shift (RWGS) (Equation 13) coupled with DRM. However, in cold-plasma-assisted DRM reactions, especially at low temperatures, CH_4 conversions are higher than CO_2 conversions. This discrepancy is attributed to the direct CH_4 dissociation facilitated by the plasma [71]. Another challenge in the application of DBD plasma is the very short life (nanoseconds to microseconds) of the discharge, which can limit its effectiveness and stability in various processes. DBD plasma generates non-thermal/equilibrium plasma at atmospheric pressure, but the discharge itself is characterized by short-lived reactive species [72, 73]. In the context of catalysis, the short life of discharge can impact on the synergistic effects between the plasma and the catalyst. Electrically conductive materials, such as TMCs, as catalysts, can help in the effective utilization of the short-lived plasma discharge by facilitating the transport of microsecond-discharges to the reactant species, thereby increasing the reactants' conversion and products' yield. TMCs possess a natural high tendency to react with oxides, and in the traditional thermal DRM reaction, TMCs have been proven to be effective catalysts for CO_2 activation/dissociation. Thus, TMCs can also help in creating a balance between CH_4/CO_2 activation/dissociation/conversion.

In this study, we are utilizing two critical TMC catalysts (Mo_2C and WC) that are highly electrically conductive and exhibit a high affinity towards oxides, aiming to address the dual challenges of slow CO_2 activation and the effective utilization of short-lived discharges in Dielectric Barrier Discharge (DBD) plasma-assisted DRM reaction. We can leverage their synergistic effects (natural high tendency to react with oxides and high electrical conductivity) to accelerate CO_2 activation and effectively utilize short-lived discharges in DBD-plasma-assisted DRM reaction. The electrically conductivity of TMCs, as catalysts, can help in the effective utilization of the short-lived plasma discharge by facilitating the transport of microsecond discharges to the reactant species, thereby

increasing the reactants' conversion and products' yield. Additionally, the high affinity of TMCs towards oxides ensures efficient activation and conversion of CO_2, addressing the problem of slow CO_2 activation. This dual-catalyst approach offers a promising solution to enhance the overall efficiency, stability, and energy efficiency of the cold-plasma-assisted DRM reaction. The experimental results demonstrated the remarkable efficacy of catalysts Mo_2C and WC, both synthesized with an M/C ratio of 1:1 (M = Mo or W), in significantly enhancing the H_2 yield. Under identical input power conditions, Mo_2C exhibited an impressive performance, increasing the H_2 yield by 170% and CO_2 conversion by 277% compared to the uncatalyzed reaction. Similarly, WC also showed substantial improvement, boosting the H_2 yield by 40% and CO_2 conversion by 31% relative to the control scenario without any catalyst. Plasma discharge temperature remained significantly low during the whole time-on-stream. The present study elucidates the critical roles of TMCs in plasma-assisted catalysis of the dry reforming of methane (DRM) reaction. Their dual function addresses key challenges in coupled plasma and catalysis, providing practical solutions for optimizing DRM processes and promoting more sustainable methane reforming technology.

1.2 Problem Statement

DRM reaction faces significant challenges due to its endothermic nature and the high operational temperatures, typically exceeding 700°C, which can lead to catalyst deactivation through sintering and coke deposition, especially in Ni-based catalysts commonly used for this process. Conventional strategies to enhance catalyst stability and activity, such as alloying and using basic supports, often fall short of addressing the challenges in DRM. Additionally, while NTP technology (DBD-plasma) can effectively lower the temperature requirements of the DRM reaction, it presents its own set of challenges. The short-lived nature of reactive species in DBD-plasma system limits sustained catalytic performance and has been shown to be more effective for CH_4 activation than for CO_2. Consequently, there is a pressing need for innovative catalytic materials that can enhance both CO_2 activation and discharge utilization, particularly in the context of DBD-plasma-assisted DRM reaction, to improve overall efficiency and sustainability.

1.3 Objectives

This study aims to (1) synthesize and characterize TMC catalysts (Mo_2C and WC), (2) investigate the effectiveness of these synthesized TMC catalysts in improving CO_2 activation rates in DBD/NTP-plasma-assisted DRM process, (3) explore the synergistic effects of TMC catalysts in conjunction with dielectric barrier discharge (DBD) plasma to enhance both CH_4 and CO_2 activation, aiming to overcome the challenges posed by the short-lived reactive species in DBD system, (4) measure/compare H_2 yield and CO_2 conversion rates for TMCs-catalyzed DRM reactions, quantifying improvements over uncatalyzed DBD-plasma-assisted DRM to demonstrate enhanced overall efficiency and sustainability, and (5) control the temperature in the discharge region to avoid the deactivation of the catalyst due to metal sintering.

1.4 Outline of thesis

Chapter 1: Introduction

This chapter introduces the concept of DRM and its potential for H_2 production. We briefly highlight the challenges associated with conventional catalytic DRM reaction, while also outlining the advantages of both the NTP for catalysis and the use of TMCs as catalysts. Additionally, we highlight the key objectives of our work.

Chapter 2: Literature Review

This section delves into a comprehensive review of past studies exploring the utilization of TMCs as catalysts for CH_4-reforming based H_2 production technologies. The analysis focuses specifically on the DRM reaction mechanism over a TMC catalyst, as well as recent advancements and findings related to the applications of TMC catalysts in CH_4-reforming based H_2 production technologies.

Chapter 3: Methodology

This section details the experimental approach employed in this study, encompassing:

1. Catalyst synthesis: Synthesis of TMC catalysts with characterization using appropriate techniques to confirm their structure and properties.
2. Experimental Setup: Description of the DBD plasma setup, including details on gas mixture flow rates, temperature control, and equipment used for the product analysis.
3. Experimental Procedure: Outline of the steps involved in DBD-plasma catalysis experiments, including amount of catalyst used, operating conditions (feed ratio, gas mixture flowrate, voltage, and frequency), and gas product sampling procedures.
4. Analysis of Results: Description of the analytical techniques employed to characterize the gas product obtained, including gas composition analysis and hydrogen yield determination.

Chapter 4: Results and Discussion

This section presents the key findings from the DBD-plasma assisted DRM over TMCs as catalysts experiments. We discuss the composition and concentration of gases produced during the process, focusing on the comparison between the cases with and without catalyst. Additionally, we analyze the influence of applied frequency on the temperature inside the reactor.

CHAPTER 2: LITERATURE REVIEW

Current Methods for H_2 Production by CH_4 Reforming

Above 70% of H2 production technologies are based on reforming of NG [28, 31, 32, 39, 74]. The technologies in which CH_4 is used as the feedstock, include: CH_4 decomposition or catalytic CH_4 decomposition (CMD), CH_4 pyrolysis, steam reforming of CH_4 (SRM), combination of carbon capture and storage (CCS) with SRM, sorption enhanced steam reforming of CH_4 (SE-SRM), sorption enhanced chemical looping SRM, dry reforming of CH_4 (DRM), combined steam and dry reforming of CH_4 (CSDRM) or steam-CO_2 bi-reforming of CH_4 (SCRM), partial oxidation of CH_4 (POM), auto-thermal reforming (ATR) of CH_4, sorption enhanced ATR of CH_4, and tri-reforming of CH_4 (TRM) [36, 39, 75-80]. Feed composition is the most important factor that makes the above-mentioned H_2 production technologies different from each other.

Steam Reforming of Methane (SRM)

In SRM (Equation 1), CH_4 and steam ($H_2O_{(s)}$) react to form synthesis gas or syngas ($H_2 + CO$) with H_2/CO ratio of 3:1 [32, 35, 39, 40, 81, 82]. The H_2/CO ratio is good, but SRM is a highly endothermic reaction in nature, very high pressure (14-20 atmosphere), and a lot of energy (206.2kJ/mol) is required for this reaction to go to completion [38-40, 81]. This is not the only difficulty in SRM. When $H_2O_{(s)}$ is supplied in excess quantity, the reaction's energy demand decreases from 206.2kJ/mol to 165kJ/mol, but CH_4 reacts with $H_2O_{(s)}$ to produce H_2 and CO_2 (the greatest contributor in changing the climate) (Equation 2) [31, 81]. Concurrently, extra $H_2O_{(s)}$ reacts with carbon monoxide (CO) to give extra H_2 along with CO_2, and this reaction is called the WGSR (Equation 3), and is exothermic in nature to some extent [31, 38, 83]. Due to having an exothermic nature, WGSR occurs spontaneously in SRM reaction stream, without even providing extra $H_2O_{(s)}$ in the feed and cannot be avoided. Vigorous nature and side reaction (WGSR) are the two main problems associated with SRM. The unavailability of a perfect catalyst for SRM is still also a challenge because all the metal based catalysts that have been tested to date for SRM suffer from coking and sintering problems [44]. Despite all the issues described above, SRM is the technology that was commercialized long ago and now is responsible for fulfilling more than 90% of the world's total H_2 demand [28, 31, 32, 39, 74]. The commercial role of SRM makes CH_4 the most valuable chemical compound for getting H_2. Although SRM is the most widely accepted method for generating H_2, it also produces H_2O pollutants and solid waste. Global H_2 production adds 2.5% to

the global emissions [42]. SRM discharges 9000-10,620.6g of CO_2 with few grams of other effluences into the air per every 1kg of H_2; combination of SRM with CCS can significantly overcome this problem, but the process performance reduces from 76% to 68%, and H_2 production expense increases from $1.26/kg to $1.88/kg (according to the production cost in the year 2020) [31, 39, 42, 43, 82, 84, 85].

$$CH_4 + H_2O_{(s)} \leftrightarrow 3H_2 + CO \ (\Delta H^0_{298K} = +206.2\ ^{kJ}/_{mol}) \quad (1)$$

$$CH_4 + 2H_2O_{(s)} \leftrightarrow 4H_2 + CO_2 \ (\Delta H^0_{298K} = +165\ ^{kJ}/_{mol}) \quad (2)$$

$$CO + H_2O_{(s)} \leftrightarrow H_2 + CO_2 \ (\Delta H^0_{298K} = -41.2\ ^{kJ}/_{mol}) \quad (3)$$

All other technologies for the conversion of CH_4 to H_2 are being used on a very small scale or are still in the development phase.

Methane Decomposition or Catalytic Methane Decomposition (CMD)

CMD (Equation 4) involves the breaking or cracking of CH_4 into its components (C and H_2) by heating it at a very high temperature (1200^0C). CMD is of great interest for getting clean and pure H_2. If CMD occurs in the absence of O_2, and only two components (H_2 and $C_{(s)}$) are produced, then CMD is a kind of de-carbonization process and is also called CH_4 pyrolysis [79]. The H_2 produced through CH_4 pyrolysis is known as turquoise H_2 [36]. If unconverted CH_4 is detected in the product stream, a gas separation facility is also needed to get good quality H_2 [86]. CMD or CH_4 pyrolysis helps to get rid of traditional SRM's two high energy cost measures, including: preventing the occurrence of WGSR, and CO_2 removal step [87]. The obstacle to not commercializing this technology yet, is its highly endothermic nature, because thermal decomposition of CH_4 requires almost 1200^0C temperature, without using any catalyst [88]. For breaking CH_4, solar-thermal and plasma-based techniques are also being studied. This technology also has the problem of deactivating catalysts due to coking, in the same manner as discussed in the DRM technology section of the paper [50, 89]. Besides the endothermic nature, this is another challenge associated with CMD technology.

$$CH_4 \longrightarrow C_{(s)} + 2H_2 \ (\Delta H^0_{298K} = +74.8\ ^{kj}/_{mol}) \quad (4)$$

Steam-CO_2 bi-reforming of CH_4 (SCRM)

SCRM (Equation 5) of CH_4 is a process in which CH_4, $H_2O_{(s)}$, and CO_2 are used as reactants to produce syngas [90]. This process allows us to produce syngas with the desired H_2/CO ratio by adjusting $CH_4/H_2O_{(s)}/CO_2$ feed ratio. Combining SRM and DRM for producing syngas gives another benefit of preventing catalyst deactivation from coking, as the oxidants ($H_2O_{(s)}$ and CO_2), which are used as the feed, are enough to remove the deposited $C_{(s)}$ by gasification.

$$2CH_4 + H_2O_{(s)} + CO_2 \longrightarrow 3CO + 5H_2 \quad (5)$$

Partial Oxidation of Methane (POM)

POM (Equation 6) is an exothermic process in which CH_4 reacts with a limited amount of O_2 to produce syngas [91]. This process yields H_2 rich fuel because the produced H_2/CO ratio is 2.0 [91]. POM is not a single step reaction process. POM goes to completion in the multiple steps, given in (Equations 7-9) [91]. In the first step, 25% of the CH_4 in the reaction feed ($CH_4 + \frac{1}{2}O_2$) is combusted (Equation 7). The rest of the 75% CH_4 reacts with the combustion products to produce syngas (Equations 8-9).

$$CH_4 + \frac{1}{2}O_2 \longrightarrow CO + 2H_2 \ (\Delta H^0_{298K} = -36 \text{kJmol}^{-1}) \quad (6)$$

$$2CH_4 + O_2 \longrightarrow 1.5CH_4 + 0.5CO_2 + H_2O_{(s)} \quad (7)$$

$$0.5CO_2 + 0.5CH_4 \longrightarrow CO + H_2 \quad (8)$$

$$CH_4 + H_2O_{(s)} \longrightarrow CO + 3H_2 \quad (9)$$

Tri-reforming of Methane (TRM)

TRM (Equation 10) is the combination of SRM (Equation 1), DRM (Equation 11) and POM (Equation 6) [92]. In the TRM process, CH_4, CO_2 or flue gases, $H_2O_{(s)}$, and O_2 are used as reactants to produce H_2 and CO [92]. TRM is highly advantageous to obtain syngas with the desired H_2/CO ratio by controlling the molar ratio of the reactants. Less energy is required to process TRM, because the reaction (POM) with exothermic nature is part of the process, and the catalyst's stability against coking also enhanced in TRM, as the oxidants (CO_2, $H_2O_{(s)}$, and O_2), present in the upstream of the process, can help to remove the deposited $C_{(s)}$ by oxidation [93].

$$3CH_4 + 0.5O_2 + H_2O_{(s)} + CO_2 \longrightarrow 4CO + 7H_2 \quad (10)$$

Dry Reforming of Methane (DRM)

DRM (Equation 11) is the use of CH_4 and CO_2 for producing syngas with H_2/CO ratio of 1:1 [6, 94]. This reaction was first introduced by Fischer and Tropsch in the 1920s. Later on, DRM got the attention of the researchers for two reasons: one is the use of two potential greenhouse gases (CH_4 and CO_2), and the second is the production of clean and valuable fuel (H_2). DRM exploits two harmful gases (CH_4 and CO_2), and gives syngas, therefore, the development and implementation of this technology on a large scale will be a great initiative for the mitigation of the greenhouse gases (CH_4 and CO_2) from the atmosphere, and for getting clean energy (H_2). It can also be thought of as the technology with zero emission for getting environmentally sound energy, as the output in an ideal situation is H_2 (nature-friendly energy carrier) and CO (less toxic than CO_2 for the eco-system) only.

Syngas itself can be used for different applications, the most important of which is its conversion into liquid HCs by the Fischer-Tropsch method [95].

Concise on Challenges, Thermodynamics, Kinetics, and Equilibrium of DRM Process

Despite being one of the most investigated topics since the year 2000 and having very positive potential for the environment and energy sectors, there are still challenges that need to be addressed for the installation of this technology on the industrial level. At least 19 reactions (Equations 11, 4, and 12-28) are involved in the DRM process, the most important of which is the direct reaction between CH_4 and CO_2 (Equation 11), which is a highly endothermic reaction. The molecular structure of CH_4 and CO_2 makes them highly stable and chemically inactive compounds. The energy needed to dissociate C─H and C═O is ~430kJ/mol and ~750kJ/mol, respectively [96]. Direct decomposition of CH_4 (Equation 4) and CO_2 (Equation 12) is possible at temperature 1200^0C and 2000^0C, respectively [88, 97]. These parameters suggest that DRM is a highly endothermic process. So, the endothermic nature is one of the problems of DRM.

The occurrence of undesired side reactions during DRM process is the other setback that compels some solutions. According to Equation (11), H_2/CO ratio must be 1, but it is never equal to 1 because of reverse water gas shift reaction (RWGSR) [76, 94, 98]. In the RWGSR (Equation 13), H_2 reacts with CO_2, and gives CO and H_2O [99], due to which H_2 yield reduces and H_2/CO ratio becomes less than unity. An additional constituent (H_2O) is added to the products, which makes the splitting process of H_2 from other product components more expensive and complicated. RWGSR is not the

only reaction that must be avoided to get the desired H_2/CO ratio. Several other side reactions, including CH_4 decomposition (Equation 4), Boudouard reaction (Equation 14), CO_2 hydrogenation (Equation 15), CO hydrogenation (Equation 16), CO_2 hydrogenation (Equation 17), reverse methanation of CO_2 (Equation 18) and the reactions given in Equations 19-28 are difficult to control during the whole process [100-102]. Especially, reactions with an exothermic nature or negative enthalpy value are more difficult to deal with. The use of feedstock (CH_4 and CO_2), greater than the stoichiometric concentration, decreases H_2 and CO production, but it is one of the key reasons for the occurrence of undesired reactions along with the main reaction of the DRM process. To have a total and exact number of possible chemical reactions and resulting chemical species in a C/H/O system is a very complex and difficult task.

$$CH_4 + CO_2 \longrightarrow 2H_2 + 2CO \ (\Delta H^0_{298K} = +247.3\ {}^{kJ}/_{mol}) \quad (11)$$

$$CO_2 \longrightarrow \frac{1}{2}O_2 + CO \ (\Delta H^0_{298K} = +283\ {}^{kj}/_{mol}) \quad (12)$$

$$CO_2 + H_2 \leftrightarrow CO + H_2O \ (\Delta H^0_{298K} = +42.1\ {}^{kJ}/_{mol}) \quad (13)$$

$$2CO \leftrightarrow C + CO_2 \ (\Delta H^0_{298K} = -172\ {}^{kj}/_{mol}) \quad (14)$$

$$CO_2 + 2H_2 \leftrightarrow C + 2H_2O \ (\Delta H^0_{298K} = -90\ {}^{kJ}/_{mol}) \quad (15)$$

$$CO + H_2 \longrightarrow C + H_2O \ (\Delta H^0_{298K} = -131\ {}^{kJ}/_{mol}) \quad (16)$$

$$CO_2 + 3H_2 \longrightarrow CH_3OH + H_2O \ (\Delta H^0_{298K} = -49\ {}^{kJ}/_{mol}) \quad (17)$$

$$2H_2O + CH_4 \longrightarrow CO_2 + 4H_2 \ (\Delta H^0_{298K} = +247.3\ {}^{kJ}/_{mol}) \quad (18)$$

$$2CH_4 + CO_2 \leftrightarrow C_2H_6 + CO + H_2O \ (\Delta H^0_{298K} = +106\ {}^{kJ}/_{mol}) \quad (19)$$

$$2CH_4 + 2CO_2 \leftrightarrow C_2H_4 + 2CO + 2H_2O \ (\Delta H^0_{298K} = +284\ {}^{kJ}/_{mol}) \quad (20)$$

$$C_2H_6 \leftrightarrow C_2H_4 + H_2 \ (\Delta H^0_{298K} = +136\ {}^{kj}/_{mol}) \quad (21)$$

$$CO + 2H_2 \leftrightarrow CH_3OH \ (\Delta H^0_{298K} = -90.6\ {}^{kJ}/_{mol}) \quad (22)$$

$$CH_3OCH_3 + CO_2 \leftrightarrow 3CO + 3H_2 \ (\Delta H^0_{298K} = +258.4\ {}^{kJ}/_{mol}) \quad (23)$$

$$3H_2O + CH_3OCH_3 \leftrightarrow 2CO_2 + 6H_2 \ (\Delta H^0_{298K} = +136\ {}^{kJ}/_{mol}) \quad (24)$$

$$CH_3OCH_3 + H_2O \leftrightarrow 2CO + 4H_2 \ (\Delta H^0_{298K} = +204.8\ {}^{kJ}/_{mol}) \quad (25)$$

$$2CH_3OH \leftrightarrow CH_3OCH_3 + H_2O \ (\Delta H^0_{298K} = -37\ ^{kJ}/_{mol}) \quad (26)$$

$$CO_2 + 4H_2 \leftrightarrow CH_4 + 2H_2O \ (\Delta H^0_{298K} = -165\ ^{kJ}/_{mol}) \quad (27)$$

$$CO + 3H_2 \leftrightarrow CH_4 + H_2O \ (\Delta H^0_{298K} = -206.2\ ^{kJ}/_{mol}) \quad (28)$$

Reaction parameters are very important to monitor and control for the required results from DRM. Applying slightly different conditions can lead to a completely different output. DRM is thermodynamically favorable at pressure 1atm and temperature above 913K [103, 104]. Maximum feed (CH_4 and CO_2) conversion at a constant temperature can be achieved by applying low pressures [94]. At constant pressure, CH_4 conversion can be enhanced by increasing CO_2/CH_4 feed ratio and also the temperature up to 1000K, but using high pressures suppresses this conversion [94, 100, 101, 105]. Using high pressures for the same value of CO_2/CH_4 feed ratio increases temperature limitation value for the $C_{(s)}$ accumulation and MC formation on the surface of the catalyst [94, 102]. Constant pressure and decreasing value of CO_2/CH_4 feed ratio also cause to increase this temperature limitation value [94]. It means more energy is needed to prevent $C_{(s)}$ formation/accumulation and MC formation on the surface of the catalyst. High pressure and high CO_2/CH_4 feed ratio favor the RWGSR [94, 100]. An increased value of CO_2/CH_4 feed ratio has a negative impact on H_2 yield due to which H_2/CO ratio in the product stream becomes less than 1 [94, 100, 101]. Temperature is another key variable to control the DRM process. CH_4 conversion is more prominent at a temperature below 973K but is not obvious when the temperature is above 973K [100, 101]. Temperature greater than 873K or in the range 1273-1473K, reduction in CO_2/CH_4 feed ratio, and catalyst surface (free of $C_{(s)}$) favor CO_2 conversion [94, 101, 105, 106]. High temperature increases CO production more significantly when CO_2/CH_4 is below 1, but when CO_2/CH_4 feed ratio is greater than 1, CO production declines [100, 101]. H_2/CO ratio reduces with rising temperature, pressure, and CO_2/CH_4 feed ratio [100, 101, 106]. At a fixed temperature and fixed CO_2/CH_4 feed ratio, H_2/CO can be enhanced by increasing pressure [100]. The duration of the DRM process depends on the rate-limiting step. Not only the molar ratio of the substrates but also the natural logarithmic value of the equilibrium constant (ln(K)) of a chemical reaction decides its capability to take place, during DRM process [101, 106]. When ln(K) has a value of more than 1, the molar ratio of the raw materials has no effect on the direction of the reaction, but the reverse is the case when ln(K) value is nearly equal to 1 [76, 106]. The chemical reactions given in Equations

(4, 19-21 and 23-25) have a very high negative value of ln(K), therefore, a very high temperature is good for these reactions to proceed in the forward direction [101]. The value of ln(K) for the chemical reactions given in Equations (14-17, 22, 26-28) is highly positive so, these reactions can easily turn up at low temperatures, but proceed in the backward direction when the temperature is very high [101].

Being a reaction (DRM) with a very high positive enthalpy value (+247.3kJ/mol), a catalyst is mandatory for its economic feasibility. A good catalyst is low priced, readily accessible, reduces the energy demand for the reaction, and sustains the activity/stability/product-selectivity for a very long period. A catalyst with these characteristics for DRM is still an objective that has not yet been achieved. The objective for developing a catalyst for CH_4 reforming/decomposition is difficult in two ways: firstly, the catalyst should reduce the reaction's activation energy requirement and must not be inactive swiftly due to the accretion of product $C_{(s)}$, and secondly, the catalyst regeneration step should not affect the de-carbonization nature of the process.

Rapid deactivation of the catalyst due to metal sintering and deposition of produced $C_{(s)}$ on the active sites of the catalyst is another problem in DRM [76, 94, 101]. This is the biggest reason for not commercializing this technology yet. When using CH_4/CO_2 in stoichiometric concentration at the temperature 557^0C-700^0C, $C_{(s)}$ production is the consequence of CH_4 decomposition (Equation 4) and Boudouard reaction (Equation 14) [6, 94, 102]. The accumulation of the product $C_{(s)}$ on the catalyst surface causes blockage of the active sites of the catalyst or encapsulation of the whole catalyst, which reduces the activity of the catalyst and eventually makes it stop functioning. $C_{(s)}$ deposition rises in a direct proportion with the pressure but decreases with increasing temperature and CO_2/CH_4 feed ratio [100, 101]. At a fixed pressure, $C_{(s)}$ deposition reduces with increasing temperature [101]. $C_{(s)}$ production and accumulation can also cause the reactor tube to be plugged. The small size of the metal particles, catalyst support (that is basic in nature) with high surface area, good metal dispersion on the support, and better O mobility of the catalyst surface decrease the $C_{(s)}$ production/accumulation rate [6, 45, 107]. To avoid $C_{(s)}$ fouling, DRM must be performed at a temperature greater than the temperature limiting value [94]. The RWGSR (Equation 13) and Boudouard reaction (Equation 14) can be avoided by applying a temperature higher than 820^0C, because these two reactions cannot occur above this temperature [94, 105]. But this temperature may lead to the problem of metal sintering. Excessive temperature is responsible for the metal

sintering problem, and the reactions given in Equations (4 and 14-16) are the reason for $C_{(s)}$ production, during DRM process [6, 76, 94, 101]. Metal sintering causes metal nucleation, which decreases the catalyst's surface area available for the reaction and also ruins the pore structure [76]. Eventually, the catalyst becomes inactive.

CMD and DRM are the two technologies that researchers are working on because the advantage of mitigating the two most dangerous greenhouse gases is associated with the development of these two technologies. These technologies can help to achieve the goal of H_2 production with minimum to zero C emissions.

Catalyst regeneration is not a simple task, the selection of the catalyst reconditioning method is based on different parameters of the reactor in operation. Metal sintering makes catalyst regeneration sometimes impossible [76]. Nevertheless, in the context of $C_{(s)}$ deposition, regeneration of the catalyst is comparatively more feasible. The reaction of the amassed $C_{(s)}$ with O_2 and $H_2O_{(s)}$, can be used for reconditioning the catalyst, but the consequent components on the reaction of $C_{(s)}$ with O_2 (Equation 29) and $H_2O_{(s)}$ (Equation 30) are CO_2 and CO (an indirect greenhouse gas), respectively, and the catalyst recovery through O_2 is exothermic, and by $H_2O_{(s)}$ is endothermic in nature [108-110]. These types of issues leave a question mark on the non-polluting and cost-effective characteristics of SRM, DRM, and CMD technology and eventually hinder their large-scale usage. The consumption of CO_2 as the reviving agent for catalyst or using the reverse Boudouard reaction (Equation 31) is beneficial for the environment and for retaining the non-contaminating facet of SRM, DRM, and CMD as it involves the usage of a greenhouse gas (CO_2) and producing only CO, which is not as dangerous as CO_2 for the climate [111].

Catalyst Regeneration Methods:

$$C_{(s)} + O_2 \leftrightarrow CO_2 \ (\Delta H^0_{1073K} = -394.7\ {}^{kj}/_{mol}) \quad (29)$$

$$C_{(s)} + H_2O \leftrightarrow CO + H_2 \ (\Delta H^0_{1073K} = +135.9\ {}^{kj}/_{mol}) \quad (30)$$

$$C_{(s)} + CO_2 \leftrightarrow 2CO \ (\Delta H^0_{1073K} = +171\ {}^{kj}/_{mol}) \quad (31)$$

Metal Carbide as an Active Catalyst for DRM

DRM is a surface catalytic reaction. In surface catalysis, the reactant molecules adsorb onto the surface of the catalyst before they react with the catalyst to form the intermediate/product species.

Rate determining step (RDS) in DRM is the reaction between C^* (C species adsorbed on active sites present on the surface of the catalyst, $*=$ active site) and O^* (O species adsorbed on active sites present on the surface of the catalyst) to form CO (Equation 65), because this reaction is the slowest in the process [112]. Operating temperature affects the RDS, changing this temperature may also change the RDS [113].

All the catalysts investigated to date for CH_4 reforming reactions suffer from metal sintering and $C_{(s)}$ fouling. This is because the catalysts that have been tested so far catalyze the $C_{(s)}$ formation reactions. Deactivation of the catalyst because of $C_{(s)}$ producing reactions can be delayed by using oxidants (CO_2, $H_2O_{(s)}$ or O_2) during the catalytic process but cannot be avoided [94, 114]. The excess use of oxidants results in the production of syngas with a very high H_2/CO or CO_2/CO ratio, which is not suitable for industrial applications [114, 115]. The discovery of a readily available and cost-effective catalyst, which can show good activity/stability/product-selectivity for the focal reactions along with satisfactory resistance against coking and metal sintering, can help to commercialize H_2 production technologies like CMD and DRM, which are environmentally/socially feasible. Various catalysts have been studied in the past for CH_4 reforming reactions. These include noble TM-based catalysts, non-noble TM-based catalysts, spinels, and perovskites, etc. [45, 76, 116-119]. Although, noble metals (Ru, Rh, Pd, Ir, and Pt) have shown the best coking resistance, thermal stability and activity for DRM and CMD [115], the use of nickel-based (Ni-based) catalysts is economically more justified. Therefore, Ni-based catalysts were investigated the most [116, 120, 121]. But Ni-based catalysts catalyze $C_{(s)}$ formation reactions, which results in the $C_{(s)}$ production followed by $C_{(s)}$ accretion on the surface of the catalyst. The deposition of $C_{(s)}$ on the surface of the catalyst results in the blockage of the catalyst's active sites, and ultimately MC formation on the surface of the catalyst [94, 114]. So, Ni is not a catalyst to be used for DRM and CMD on an industrial scale. Synthesizing method/process-conditions, precursor, promoter, support, operating conditions, and the type of reactor used for the reaction have a big influence on the activity/stability/product-selectivity of the catalyst in DRM and CMD.

MCs have better coking resistance than Ni-based catalysts [122] and are very similar to noble metals for surface catalysis [57, 123], and the methods used for their synthesis are highly cost-effective [123]. They have a very high tendency to react with oxides, and they are S tolerant. S can be present in NG and biogas, the two major sources of DRM feed (CH_4 and CO_2) [124]. Due to all the

characteristics mentioned above, researchers started to pay attention to the use of TMCs as catalysts for DRM and CMD. Another reason for their consideration as catalysts, especially for the reactions with feed containing oxides, is their lowest deactivation rate due to oxidation. The order of potency of different oxidants to oxidize MCs is $O_2 > H_2O_{(s)} \cong CO_2$.

When a MC is used as a catalyst for DRM, oxidation, caused by CO_2 reduction, changes MC into metal oxide (MO_2) (Equation 32), but CH_4 converts MO_2 again into MC (Equation 33). In this way, there is oxidation and subsequent reduction/re-carburization of the MO_2. This is called oxidation-reduction or oxidation-re-carburization cycle, or simply redox cycle (Figure 2[115, 125-130]) [125]. A schematic of the redox cycle of Mo_2C catalyst in DRM reaction, is presented in (Figure 2[115, 125-130]).

$$\beta - Mo_2C + 5CO_2 \longrightarrow 2MoO_2 + 6CO \quad (32)$$

$$2MoO_2 + 5CH_4 \longrightarrow \beta - Mo_2C + 4CO + 10H_2 \quad (33)$$

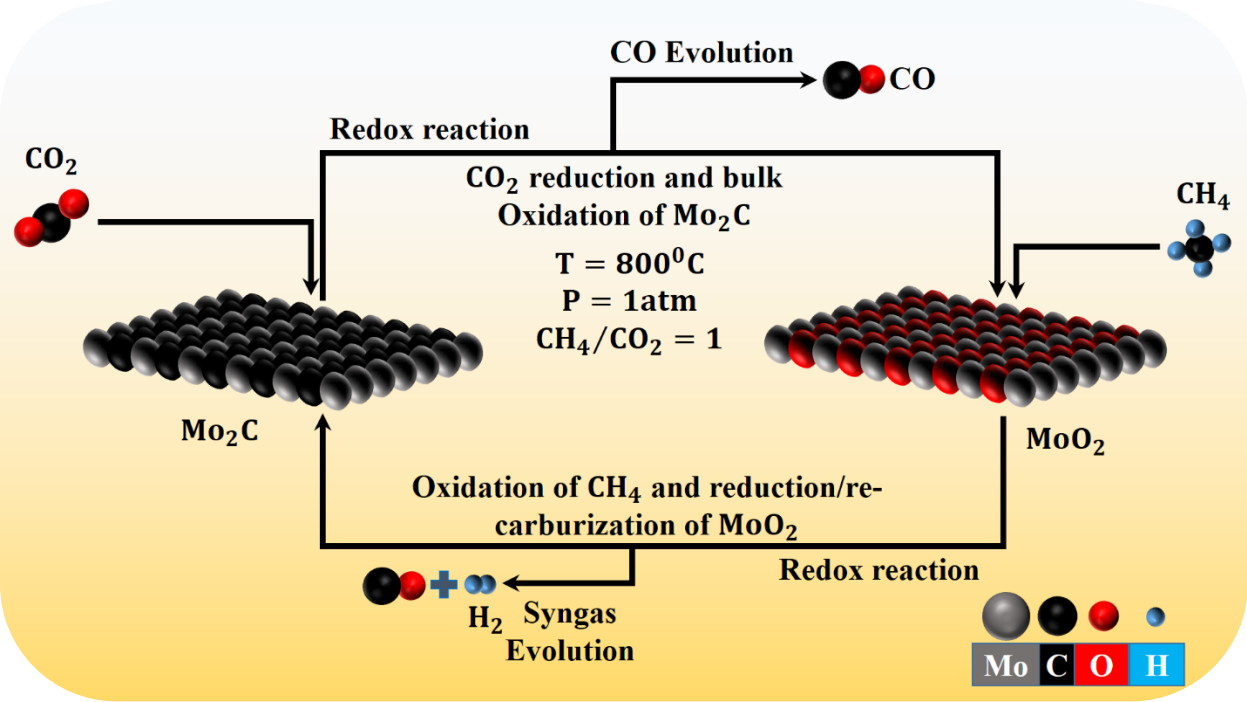

Figure 2. Schematic of the redox cycle of Mo_2C catalyst in DRM reaction. Developed based on [115, 125-130].

Mechanism of DRM Reaction over a TM Catalyst

There are two types of mechanisms that have been suggested for catalytic DRM [115, 131]. The first type is called Eley-Rideal or Langmuir-Rideal or noble metal type mechanism[132]. It is based on the principle of chemisorption [132]. DRM over a pure metal catalyst (mono-functional or bi-functional), obeys this type of mechanism [131, 133-135]. Schematic of the Eley-Rideal mechanism of metal catalytic DRM, when the metal catalyst used for DRM reaction is mono-functional (an unsupported, or supported metal catalyst but catalyst support does not take part in the chemical reaction), is presented in Figure 3[131-137]. If a mono-functional metal catalyst is used for DRM, CH_4 adsorbs on the metal site, and decomposes into H_2 and surface adsorbed C species or C^* [136, 137]. C^* species then react directly with CO_2 to produce CO [136, 137].

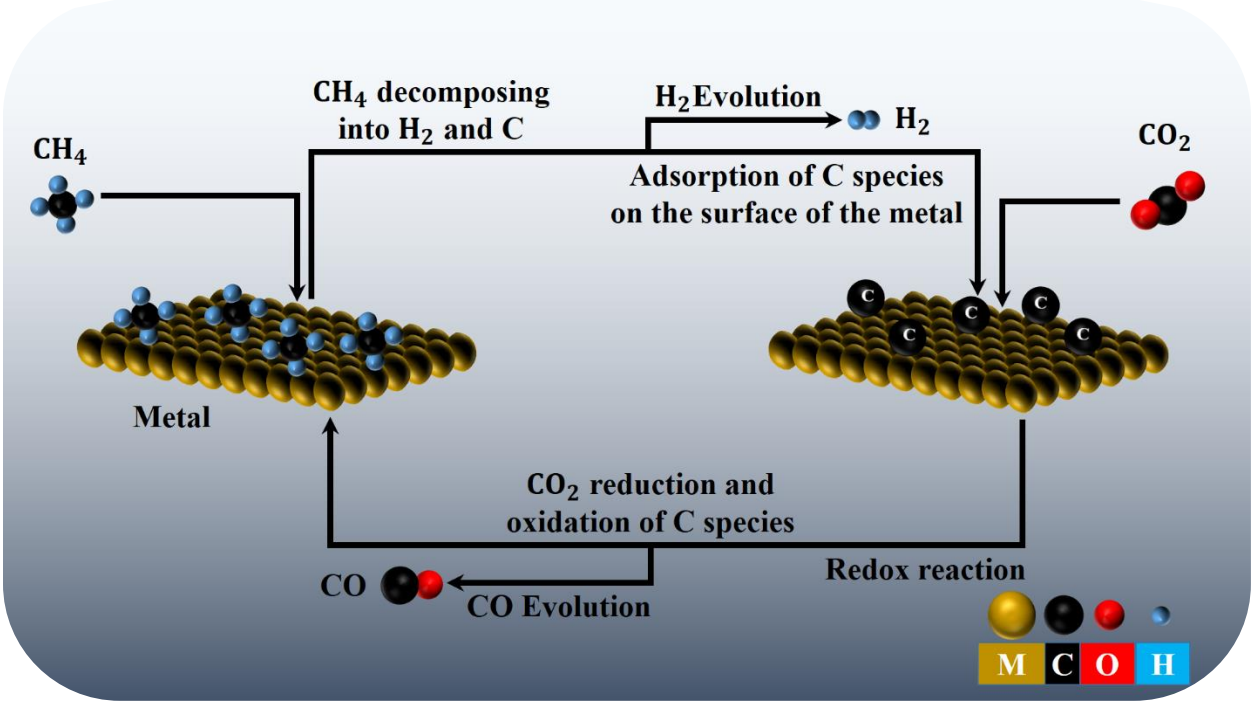

Figure 3. Schematic of the mechanism of DRM reaction over a mono-functional TM catalyst. Developed based on [131-137].

Schematic of the Eley-Rideal mechanism of metal catalytic DRM, when the metal catalyst used for DRM reaction is bi-functional (a supported metal catalyst and catalyst support also participates in the chemical reaction), is presented in Figure 4[131-137]. In the case of a bi-functional metal catalyst, CH_4 adsorbs on the metal surface and dissociates into H^* (H species adsorbed on active sites present on the surface of the catalyst) and $CH^*_{x,x=1-3}$ (CH_x species adsorbed on active sites

present on the surface of the catalyst) species [131, 133, 135]. On the other hand, CO_2 adsorbs on metal surface or the catalyst-support interface, and its decomposition gives CO and O^* or surface OH groups [131, 133]. In the end, $CH_{x,x=1-3}$ species react with O^* or surface OH groups to yield H_2 and CO [131, 133, 135].

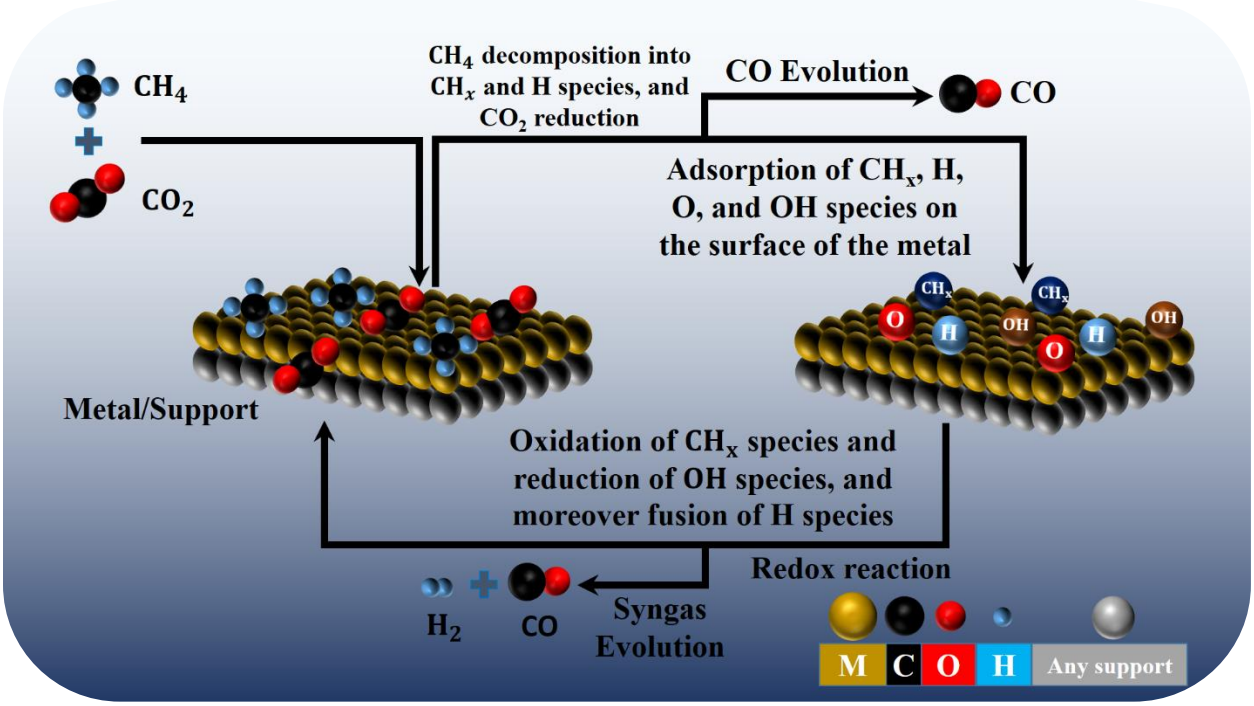

Figure 4. Schematic of the mechanism of DRM reaction over a bi-functional TM catalyst. Developed based on [131-137].

Metal is important for the activation/dissociation of both the chemical compounds (CH_4 and CO_2), but support (that is acidic or basic, but not neutral in nature) merely facilitates CO_2 activation/dissociation [131, 133, 134, 136, 137]. So, metal acts as an active site for CH_4 and CO_2 decomposition, but support (acidic or basic in nature) acts as an active site for CO_2 decomposition only. Active sites are extremely important for converting reactants into intermediate species. Intermediate species react to give the ultimate desired product/products. In the case of acidic catalyst support, CO is the result of the decomposition of formate species [133, 134]. These formate species are formed by the hydrogenation of the CO_2 and adsorbed on the surface of the catalyst support [133]. In the case of basic catalyst support, the decomposition of oxycarbonates is the reason for CO formation [131, 138]. Equations 34-57 illustrate the elementary reactions involved, in the formation

of intermediate species and desired products, in the noble metal type mechanism of TM catalytic DRM, [139, 140].

$$CH_4^* + * \longrightarrow CH_3^* + H^* \quad (34)$$

$$CH_3^* + * \longrightarrow CH_2^* + H^* \quad (35)$$

$$CH_2^* + * \longrightarrow CH^* + H^* \quad (36)$$

$$CH^* + * \longrightarrow C^* + H^* \quad (37)$$

$$CO_2^* + * \longrightarrow CO^* + O^* \quad (38)$$

$$CO_2^* + H^* \longrightarrow COOH^* + * \quad (39)$$

$$COOH^* + * \longrightarrow CO^* + OH^* \quad (40)$$

$$CO_2^* + H^* \longrightarrow HCOO^* + * \quad (41)$$

$$HCOO^* + * \longrightarrow CHO^* + O^* \quad (42)$$

$$CHO^* + * \longrightarrow CO^* + H^* \quad (43)$$

$$CH^* + O^* \longrightarrow CHO^* + * \quad (44)$$

$$CH^* + O^* \longrightarrow COH^* + * \quad (45)$$

$$CHO^* \longrightarrow CO^* + H^* \quad (46)$$

$$CH^* + OH^* \longrightarrow CHOH^* + * \quad (47)$$

$$CHOH^* + * \longrightarrow COH^* + H^* \quad (48)$$

$$C^* + O^* \longrightarrow CO^* + * \quad (49)$$

$$C^* + OH^* \longrightarrow COOH^* + * \quad (50)$$

$$COOH^* + * \longrightarrow CO^* + H^* \quad (51)$$

$$O^* + H^* \longrightarrow OH^* \quad (52)$$

$$OH^* + H^* \longrightarrow H_2O^* \quad (53)$$

$$H_2O^* \longrightarrow H_2O_{(s)} \quad (54)$$

$$H^* + H^* \longrightarrow H_2^* \quad (55)$$

$$H_2^* \longrightarrow H_{2(g)} \quad (56)$$

$$CO^* \longrightarrow CO_{(g)} \quad (57)$$

The second type of proposed mechanism for catalytic DRM is called oxidation-reduction or oxidation-re-carburization, or simply redox mechanism [115, 125]. This mechanism was especially

proposed for DRM over a MC catalyst by Claridge et al. [115]. This mechanism is described in the next section.

Mechanism of DRM Reaction over a Metal Carbide Catalyst

Syngas production through DRM over a MC catalyst follows two types of mechanisms: noble metal type mechanism, and/or redox mechanism [115, 135, 141-143]. These mechanisms for DRM over a MC catalyst were proposed by Claridge et al. [115]. Schematic of the noble metal type mechanism of metal-carbide catalytic DRM is presented in Figure 5[115, 125, 141, 144]. When following the noble metal type mechanism (Equations 58-60) (Figure 5[115, 125, 141, 144]), MC acts as an active site for CO_2 activation/dissociation only, because MCs are highly oxyphilic in nature [135, 145-147]. CO_2 adsorbs on the MC surface, and then CO_2 decomposition yields CO and O^* (Equation 58). O^* species cause the partial oxidation of the MC catalyst, converting the MC phase into metal oxycarbidic (MC—O) phase (Equation 59) [135, 144, 146, 148, 149]. MC—O phase now acts as an active site for CH_4 activation/decomposition [135, 144, 150]. CH_4 adsorbs on MC—O sites and dissociates into $CH^*_{x,x=1-3}$ and H^* species [115, 135, 150]. Desorption of intermediate $CH^*_{x,x=1-3}$ and H^* species gives CO and H_2 (Equation 60) [149]. Replenishing of the MC phase is also the result of CH_4 dissociative adsorption (Equation 60) and is very crucial to keep the TMC catalytic DRM process continuous.

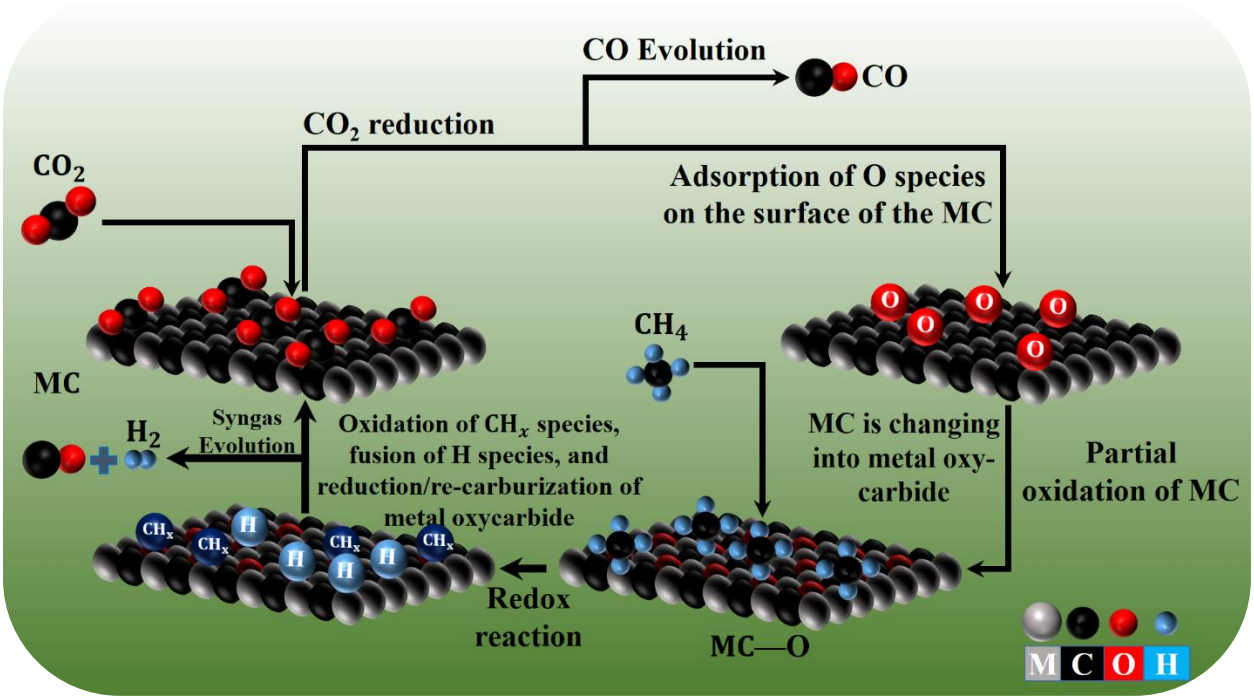

Figure 5. Schematic of the noble metal type mechanism of metal-carbide catalytic DRM reaction. Developed based on [115, 125, 141, 144].

Generation of MC—O phase (with specific oxidation state of metal that is present in the structure) is very important to achieve the desired CH_4 decomposition rate [144]. Determination of the oxidation state of metal in a MC—O structure, at which the maximum CH_4 consumption rate can be obtained, is possible by XANES (X-ray absorption near edge structure) and XPS (X-ray photoelectron spectroscopy) analysis [144]. The oxidation state of Mo in molybdenum oxycarbide (Mo_2CO_x) should be +4 to achieve the maximum CH_4 dissociation rate, and any change in this value affects CH_4 decomposition rate in DRM process [144]. DFT (density functional theory) calculations performed by Kurlov et al. [144] have disclosed the fact that C—H breakage in CH_4 is the RDS for DRM reaction. The temperature at which O containing compound (like CO_2) is introduced into the reaction plays an important role in the generation of an active MC—O phase. According to Hwu et al. [151], the MC—O phase generated at 600K and 900K is inert and active in nature, respectively. CO_2 sometimes causes bulk oxidation of the metal present in the MC structure and generates MO_2 (Equation 32). Bulk oxidation causes permanent deactivation of the MC catalyst. DRM over a supported (highly dispersed) MC catalyst follows noble metal type mechanism, and there is no C exchange between MC and CH_4 [135]. The noble metal type mechanism of DRM has a positive

impact on the stability of the MC catalyst. In DRM over supported MC catalyst, CH_4 dissociation is the RDS [135].

$$CO_2 \rightarrow CO + O^* \quad (58)$$

$$Mo_2C + O^* \longrightarrow Mo_2C{-}O \quad (59)$$

$$CH_4 + Mo_2C{-}O \longrightarrow Mo_2C + 2CO + 2H_2 \quad (60)$$

A schematic of the redox mechanism of metal-carbide catalytic DRM is presented in Figures 6 & 7[115, 125, 141, 144]. In the redox mechanism (Figures 6 & 7[115, 125, 141, 144]), CO_2 adsorbs on the catalyst surface (MC surface). CO_2 decomposes or reduces to produce CO and O^* species (Equation 58). Now produced O^* species can follow one of the two proposed schemes to react with the catalyst [115, 125]. Schematic of the first proposed scheme of the redox mechanism of metal-carbide catalytic DRM is presented in Figure 6[115, 125, 141, 144]. The first scheme (Equations 61-63) (Figure 6[115, 125, 141, 144]) is that O^* species generate only CO by oxidizing surface C of the MC (Equation 61) [115, 147, 152, 153]. This oxidation reaction leaves MC with C vacancies in its structure (Equation 61) [152, 153]. CH_4 now adsorbs on this left behind-catalyst surface and dissociates into C^* species and H_2 (Equation 62) [153]. C^* species, generated by CH_4 dissociation, regenerate the catalyst by filling up the C vacancies (Equation 63) [147, 153]. So, in this explained first scheme of the redox mechanism, the catalyst was first oxidized by O^* species to produce CO, but then there was replication or re-carburization of the catalyst by C^* species, obtained from CH_4 decomposition. That's why it is called oxidation-reduction or oxidation-re-carburization or simply the redox cycle mechanism.

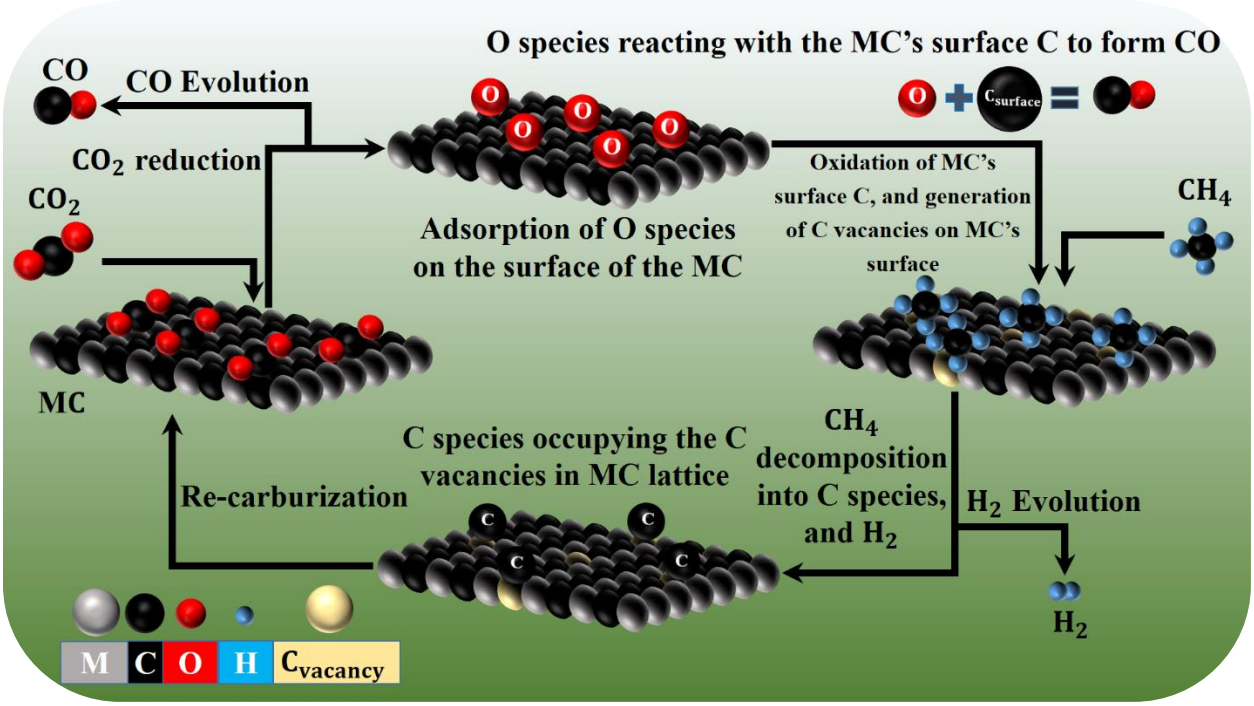

Figure 6. Schematic of the (scheme 1) redox mechanism of metal-carbide catalytic DRM reaction. Developed based on [115, 125, 141, 144].

The schematic of the second proposed scheme of the redox mechanism of metal-carbide catalytic DRM is presented in Figure 7[115, 125, 141, 144]. In the second proposed scheme (Equations 64, 33) (Figure 7[115, 125, 141, 144]), the O* species not only react with C of the MC to produce CO but also cause the bulk oxidation of the metal present in the MC structure (Equation 64) [125, 147, 152]. In this way, MC is converted into MO_2 [125, 147, 152]. Now CH_4 adsorbs on MO_2 [147], and CH_4 decomposition gives H_2, and also converts MO_2 again into MC (Equation 33), by reduction/re-carburization reaction [125, 147]. So, due to oxidation and subsequent reduction/re-carburization of the catalyst, it is called the redox cycle (Figure 6-7[115, 125, 141, 144]).

$$Mo_2C + O^* \longrightarrow [Mo \cdots Mo] + 2CO \quad (61)$$

$$CH_4 \longrightarrow C^* + 2H_2 \quad (62)$$

$$[Mo \cdots Mo] + C^* \longrightarrow Mo_2C \quad (63)$$

$$[Mo \cdots Mo] + 4O^* \longrightarrow 2MoO_2 \quad (64)$$

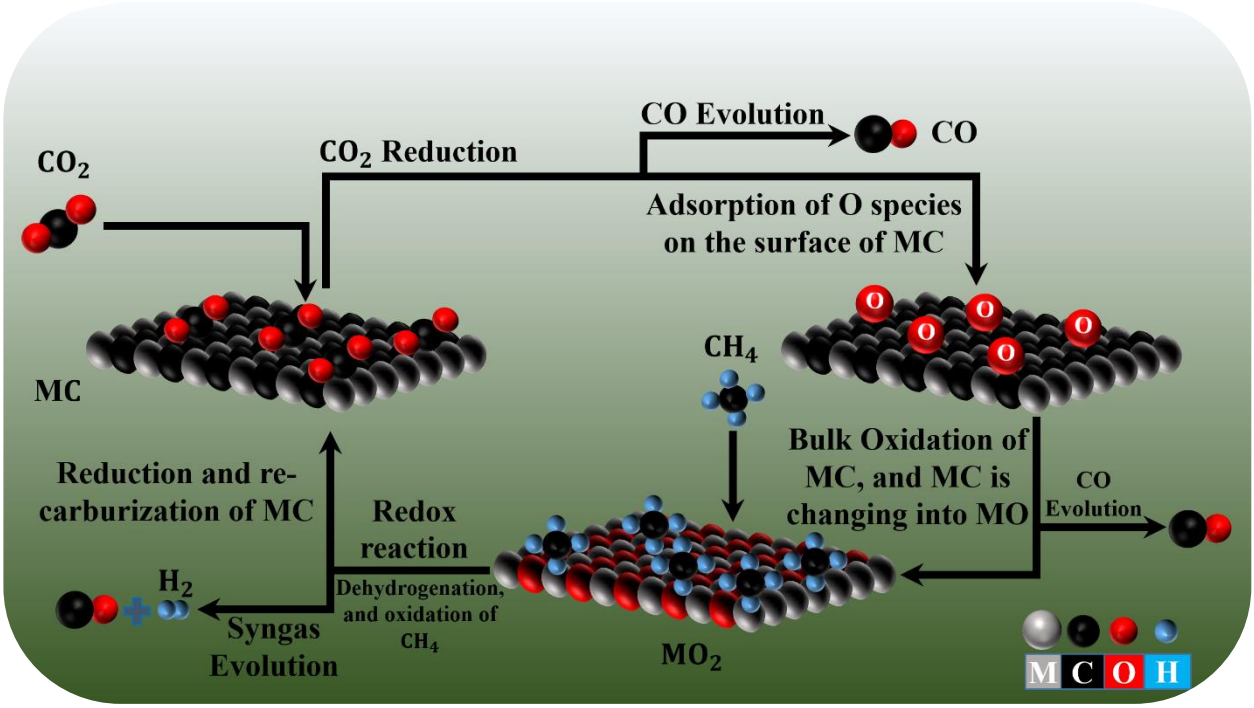

Figure 7. Schematic of the (scheme 2) redox mechanism of metal-carbide catalytic DRM reaction. Developed based on [115, 125, 141, 144].

DRM over unsupported carbide catalysts follow the redox mechanism [135]. The redox mechanism depends upon the C exchange between MC and CH_4. This C exchange is not facile. According to LaMont et al. [143, 153], this C exchange occurs at temperatures above 550^0C, and is the RDS. The presence of intermediate O^* species or an oxidant is plausible for this C exchange [147, 150, 152]. The partial oxidation of MC by O^* gives MC—O (Equation 59) (Figure 5[115, 125, 141, 144]), while the bulk oxidation of the MC results in the conversion of MC into MO_2 (Equation 64) (Figure 7[115, 125, 141, 144]). Re-carburization of MC—O by CH_4 dissociative adsorption (Equation 60) to get the original MC is possible but not an easy process, while the re-carburization of MO_2 by CH_4 dissociative adsorption (Equation 33) for regenerating the MC is almost impossible during DRM. The irreversible bulk oxidation makes MC catalyst permanently inactive for DRM. In this mechanism, there is always also the chance of combination of C^* and O^* to form CO (Equation 65). Such a scenario is ideal for a MC catalyst to maintain its activity/stability in DRM.

$$O^* + C^* \longrightarrow CO \qquad (65)$$

The redox cycle of Mo_2C (Figure 2[115, 125-130]) catalyst in DRM, makes it one of the best choices amongst MCs [125]. According to Darujati et al. [154], when using a stoichiometric feed ratio for DRM at a high mass transfer rate, O^* will fill the C vacancy (Equation 64). In the case when this C vacancy is filled by C^* (Equation 63), there is also a chance that CO_2 adsorbs on C filled site and extracts the C to produce CO (Equation 66).

$$CO_2 + Mo_2(C) \rightleftharpoons [Mo \cdots Mo] + 2CO \quad (66)$$

When DRM over a MC catalyst follows the redox mechanism and there is not enough CH_4 for direct re-carburization of MO_2 to MC (Equation 33), H_2 may also participate in the regeneration of MC. However, the reduction of MO_2 to MC by H_2 is slightly different from that of the proposed MO_2 reduction to MC by CH_4. H_2 helps to reduce MO_2 to metal (Equation 67), and then CH_4 carburizes metal to MC (Equation 68) [155]. Zhang et al. [130] proposed that in DRM over Ni-Mo_2C catalyst with a very high Ni/Mo molar ratio, Ni also participates in the redox cycle. Ni reacts with Mo and produces a $MoNi_4$ alloy phase (Equation 69). These $NiMo_4$ alloy species are then carburized to Ni and Mo_2C by CH_4 (Equation 70). The C^* species can also take part in the redox cycle by re-carburizing MO_2 to MC (Equation 71), in the presence of H_2 [155].

$$MoO_2 + 2H_2 \longrightarrow Mo + 2H_2O \quad (67)$$
$$2Mo + CH_4 \longrightarrow \beta{-}Mo_2C + 2H_2 \quad (68)$$
$$4Ni + Mo \longrightarrow MoNi_4 \quad (69)$$
$$2MoNi_4 + CH_4 \longrightarrow Mo_2C + 2H_2 + 8Ni \quad (70)$$
$$2MoO_2 + 5C^* \longrightarrow \beta{-}Mo_2C + 4CO \quad (71)$$

Besides the main DRM reaction in the reactor, many other reactions take place as well [75, 94, 98, 100-102, 122, 156]. The major side reaction that reduces the H_2 or H_2/CO yield is RWGSR (Equation 13) [75, 94, 156]. The Mo_2C also catalyzes RWGSR (Equation 13) and reduces the yield of the DRM reaction [122, 156]. The RWGSR (Equation 13) is beneficial for the oxidative removal of the $C_{(s)}$ deposited on the catalyst surface during the DRM reaction [157].

Molybdenum Carbide (Mo_2C)

DRM over a MC catalyst is a surface catalytic reaction [115]. A summary of the catalytic performance of simple (un-promoted and unsupported) Mo_xC and other TMCs (excluding WC) for

DRM reaction is provided in Table 1. Due to the resemblance in the surface catalytic action of MCs and noble metals [57], Claridge et al. [115] investigated the catalytic role of Mo_2C for DRM. Claridge et al. [115] synthesized pure β-Mo_2C and Mo_2C/Al_2O_3 catalysts by temperature-programmed reduction (TPR) method. The catalytic behavior of both the MC catalysts was examined, and compared with that of some noble metals, for DRM at similar conditions. The discovered catalytic activity order for DRM was: 5wt%$Ru/Al_2/O_3$>Mo_2C≈5wt%$Ir/Al_2/O_3$>5wt% $Rh/Al_2/O_3$. The resistance offered by Mo_2C and noble metals to coke formation was found to be identical in DRM.

Table 1: Summary of the performance of simple (un-promoted and unsupported) MoxC and other TMCs (excluding WC) catalysts for DRM reaction.

Active Site	Support	SM, RT	App	Synthesis Conditions	Reaction Conditions	Feed Comp.	Max Con [%]	Selectivity [%]	Comment	Refs
β-Mo_2C	–	SM: TPR RT: −	DRM 1997	–	P: 1bar / T: 1120K GHSV: $2.8\times10^3h^{-1}$ Flow: − TOS: 144h	CH_4: 1 CO_2: 1	CH_4: 92.4 CO_2: −	H_2: − CO: 92.5 H_2/CO: 93.0	β-Mo_2C catalyst gets deactivated in DRM reaction at atmospheric pressure due to bulk oxidation.	[114]
β-Mo_2C	–	SM: TPR RT: −	DRM 1997	–	P: 8.3bar / T: 1120K GHSV: $2.8\times10^3h^{-1}$ Flow: − TOS: 144h	CH_4: 1 CO_2: 1	CH_4: 62.5 CO_2: −	H_2: − CO: 69.5 H_2/CO: 78.0	The activity of β-Mo_2C catalyst in DRM reaction remains unchanged at high pressure.	[114]
β-Mo_2C	–	SM: TPR RT: LMR	DRM 1998	P: – / T: 1000-1150K TR: 1K/min CH_4/H_2: 20%v/v (Flow: –) TC: −	P: 1bar / T: 1220K GHSV: $2.87\times10^3h^{-1}$ Flow: − TOS: 28h	CH_4: 1 CO_2: 1	CH_4: 98.8 CO_2: 95.9	H_2: − CO: 92.6 H_2/CO: 94.0	β-Mo_2C is not stable for DRM at atmospheric pressure. The β-Mo_2C activity increases with increasing temperature and decreasing GHSV. The β-Mo_2C shows the activity and resistance against coking, the same as noble metal catalysts for DRM.	[115]
β-Mo_2C	–	SM: TPR RT: LMR	DRM 1998	P: − / T: 1000-1150K TR: 1K/min CH_4/H_2: 20%v/v Flow: − TC: −	P: 8.3bar T: 1220K GHSV: $2.87\times10^3h^{-1}$ Flow: − TOS: 72h	CH_4: 1 CO_2: 1	CH_4: 83.3 CO_2: 89.9	H_2: − CO: 86.5 H_2/CO: 88.0	The catalytic performance of the β-Mo_2C catalyst is more unwavering at high pressure than at ambient pressure for DRM reaction.	[115]
β-Mo_2C	–	SM: TPR RT: LMR	DRM 1998	P: – / T: 1023-1223K TR: 1K/min CH_4/H_2: 20%v/v Flow: 150ml/min TC: –	P: 8bar T: 1220K GHSV: $2.2\times10^3h^{-1}$ Flow: − TOS: 150h	CH_4: 1 CO_2: 1	CH_4: 90.0 CO_2: 90.0	H_2: − CO: 90.0 H_2/CO: −	β-Mo_2C is the most stable catalyst for DRM reaction, amongst the carbides of group-V and VI transition metals.	[158]
Mo_2C	–	SM: TPR RT: FBR	DRM 2002	P: – / T: − TR: − H_2/C_2H_6: 11.6%v/v Flow: 55ml/min TC: –	P: 1atm T: 850^0C GHSV: $5040cm^3g^{-1}h^{-1}$ Flow: − TOS: −	CH_4:CO_2= 1.16	CH_4: 89.5 CO_2: 99.9	H_2: − CO: 89.4 H_2/CO: 101.0	The catalytic activity of Mo_2C for DRM reaction increases with increasing temperature. Using H_2/C_2H_6 mixture as carburizing gas in TPR of MoO_3 gives a very active Mo_2C catalyst for DRM reaction.	[159]
Mo_2C	–	SM: TPR RT: PBR	DRM 2003	P: – / T: 675^0C TR: 2^0C/min CH_4/H_2: 20%v/v Flow: 300sccm TC: –	P: 8.3bar T: 850^0C GHSV: 2800-3200h^{-1} Flow: − TOS: 72h	CH_4: 1 CO_2: 1	CH_4: 84.5 CO_2: −	H_2: − CO: − H_2/CO: 75.0	H_2 treatment affects the crystallite size, surface area, and C content in Mo_2C. Mo_2C synthesized by the SD process is more active but less stable than Mo_2C synthesized by the TPR process.	[143]
Mo_2C	–	SM: SD RT: PBR		P: – / T: 800^0C TR: 10^0C/min CH_4: 100% Flow: 50sccm TC: –			CH_4: 86.3 CO_2: −	H_2: − CO: − H_2/CO: 72.5		

Mo_2C	–	SM: − RT: PBR	DRM 2004	−	P: 1-8.3bar T: 850-1000^{0}C GHSV: 2900-30000h^{-1} G: 0.08-0.43mol/cm^{2}h Flow: – TOS: −	CH_4: 1 CO_2: 1	CH_4: − CO_2: −	H_2: − CO: − H_2/CO: −	The low mass transfer rate of produced gases from the surface of the catalyst is the reason for the increased stability of Mo_2C in DRM reaction at high pressure. Deactivation of the Mo_2C catalyst in DRM reaction can be avoided by using mass transfer limited conditions. [160]
Mo_2C	–	SM: TPR RT: −	DRM 2007	P: – / T: 973K TR: 1K/min CH_4/H_2: 20%v/v (Flow: –) TC: 3h	P: – / T: 1123K GHSV: − Flow: − TOS: 6h	CH_4: 1 CO_2: 1	CH_4: 60.0 CO_2: 77.0	H_2: − CO: − H_2/CO: −	Nitridation of oxide precursor at 973K for 3h before TPR helps in synthesizing a more active/stable Mo_2C catalyst for DRM reaction. [126]
Mo_2C	–	SM: TPR RT: FBR	DRM 2010	P: – / T: 973K TR: 1K/min CH_4/H_2: 20vol% CH_4 Flow: − TC: 2h	P: 1atm T: 1073K GHSV: 14000h^{-1} Flow: − TOS: 35h	CH_4: 1 CO_2: 1	CH_4: 35.0 CO_2: 65.0	H_2: 45.0 CO: 98.0 H_2/CO: −	In DRM reaction at atmospheric pressure, the Mo_2C catalyst oxidized to MoO_2 and permanently becomes inactive. [125]
α-MoC_{1-x} β-Mo_2C α-Mo_2C+ β-Mo_2C	– – –	SM: CTR RT: −	DRM 2017	P: – / T: 350-900^{0}C TR: 10^{0}C/min Ar or H_2: 1 Flow: 50ml/min TC: 1h	P: 1atm T: − GHSV: − WHSV: 6000cm^{3}g^{-1}h^{-1} Flow: 20ml/min TOS: 12h	CH_4: 1 CO_2: 1 Ar: 2	CH_4: 87.0 CO_2: 94.0 CH_4: 67.0 CO_2: 80.0 CH_4: 87.0 CO_2: 94.0	H_2: 82.0 CO: − H_2: 70.0 CO: − H_2: 82.0 CO: −	The α-MoC_{1-x} is the most active and stable catalyst for DRM reaction. [155]
β-Mo_2C	−	SM: TD RT: FBR	DRM 2020	P: – / T: 900^{0}C TR: 5^{0}C/min N_2: 1 (Flow: –) CT: 2h	P: – / T: 850^{0}C GHSV: − Flow: 30cm^3/min TOS: −	CH_4: 1 CO_2: 1	CH_4: 100.0 CO_2: 80.0	H_2: − CO: − H_2/CO: 65.0	Mo_2C synthesized by using xerogel Mo blue as a precursor has good potential as a catalyst for DRM reaction. [161]
VC	–	SM: TPR RT: LMR	DRM 1998	T: 1023-1223K TR: 1K/min CH_4/H_2: 20%v/v Flow: 150ml/min TC: –	P: 8bar T: 1220K GHSV: 1.8×10^{3}h^{-1} Flow: − TOS: 26h	CH_4: 1 CO_2: 1	CH_4: 70.0 CO_2: 90.0	H_2: – CO: 90.0 H_2/CO: 100.0	VC has good catalytic characteristics for DRM reaction, but its activity and stability decline with time due to oxidation of the carbide phase. [158]
NbC	–	SM: TPR RT: LMR	DRM 1998	T: 1023-1223K TR: 1K/min CH_4/H_2: 20%v/v Flow: 150ml/min TC: −	P: 8bar T: 1220K GHSV: 1.2×10^{3}h^{-1} Flow: – TOS: 21h	CH_4: 1 CO_2: 1	CH_4: 65.0 CO_2: 90.0	H_2: – CO: 90.0 H_2/CO: 80.0	NbC catalyst has the most resistance against oxidation than all other carbides of the group-V transition metals in the DRM reaction. Activity and stability of NbC catalyst for DRM reaction increases with increasing temperature. [158]
TaC	–	SM: TPR RT: LMR	DRM 1998	T: 1023-1223K TR: 1K/min CH_4/H_2: 20%v/v Flow: 150ml/min TC: –	P: 8bar T: 1220K GHSV: 1.6×10^{3}h^{-1} Flow: – TOS: 5h	CH_4: 1 CO_2: 1	CH_4: 50.0 CO_2: 87.0	H_2: − CO: 90.0 H_2/CO: 110.0	TaC is the least stable catalyst among the carbides of group-V and VI transition metals for DRM reaction. [158]
MX_{ene} (m-V_2CT_x)	–	SM: AE RT: FBR	DRM 2020	T: RT Acid: HF (48-50%) Substrate/Etchant: 1g/20ml SS: 200RPM	P: 1atm T: 800^{0}C GHSV: 4800mlg^{-1}h^{-1} Flow: −	CH_4: 1 CO_2: 1	CH_4: 78.0 CO_2: 82.0	H_2: – CO: – H_2/CO: 90.0	m-V_2CT_x is more active/stable/selective catalyst than its parent MAX phase and conventional VC, for DRM reaction. [162]

		ST: 92h	TOS: 96h

Note: SM: Synthesizing Method; TPR/TPC: Temperature Programmed Reduction/Temperature Programmed Carburization; SD: Solution-derived; CTR: Carbo-thermal Reduction; TD: Thermal Decomposition; AE: Acid Etching.

RT: Reactor Type; LMR: Labcon Micro-reactor; FBR: Fixed Bed Reactor; PBR: Packed Bed Reactor.

TC: Carburizing Time; SS: Stirring Speed; ST: Stirring Time; TOS: Time on Stream.

Brungs et al. [158] compared the catalytic potential of the carbides of group-V (VC, NbC, and TaC) and VI (Mo_2C and WC) TMs for DRM. All the carbides were synthesized by the TPR method, but face-centered cubic (fcc) (Figure 1 (b)[54]) and hexagonal close-packed (hcp) structure (Figure 1 (c)[54]) was observed for the carbides of group-V and VI TMs, respectively. The β-Mo_2C was found to be the catalyst with the maximum surface area ($91m^2/g$). The catalytic role of all the carbides was examined for DRM, at the same temperature (1220K), pressure (8bar), and CH_4/CO_2 ratio (1:1), but different gas-hour space velocity (GHSV). The carbides of group-V TMs became inactive over time. TaC was the first to be dysfunctional followed by NbC and VC (Figure 8 (a, b, and c)[158]). On the other hand, β-Mo_2C (Figure 8 (d)[158]) and α-WC (carbides of group-VI TMs) were found to be persistent in their catalytic role for 5 days. The stability order of the carbides in catalyzing DRM was found as $Mo_2C \approx WC > VC > NbC > TaC$. The conversion of the carbide phase to the oxide phase (due to oxidation, caused by CO_2) was the reason for the early deactivation of the carbides of group-V TMs, in DRM. This type of carbide catalyst deactivation usually occurs when the applied pressure for DRM is atmospheric. Thermodynamic calculations of the work confirmed that the Gibbs free energy for the re-carburization of the oxides of Mo_2C, WC, and VC catalyst in DRM reaction becomes negative at the same temperature (850K to 900K) (Figure 9 (a-1)[158]). So, these carbide catalysts must show similar stability for catalyzing the DRM. However, the difference in the shape of the crystal structure of the carbides of group-V and VI TMs was declared as the reason for the difference in the stability time in DRM. High temperature improves the activity and stability of NbC catalyst for DRM [158]. In DRM over Mo_2C catalyst, morphological changes take place [128]. Bulk Mo_2C catalyst has a very small surface area [157]. So, a small number of Mo_2C active sites are available for catalyzing any reaction [157]. In DRM reaction over Mo_2C catalyst, H_2/CO ratio less than 1 indicates the occurrence of RWGSR (Equation 13), or oxidation of the deposited $C_{(s)}$ by CO_2 (Equation 31), or CO_2 activation on Mo_2C (Equation 32) [126, 143]. Metal (Mo) sintering decreases the surface area of the Mo_2C [143].

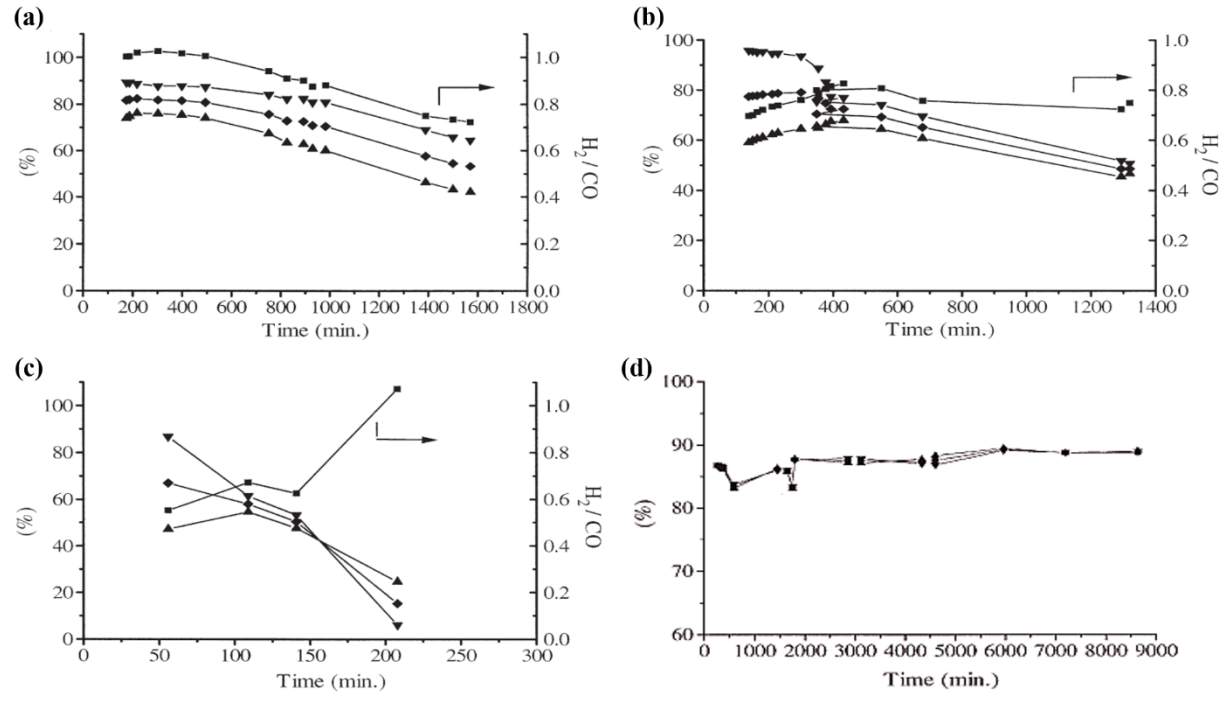

Figure 8. DRM over the group-V & VI TMCs at T = 1220K, P = 2bar, and CO_2/CH_4 = 1. (a) VC (GHSV = $4.4\times10^5 h^{-1}$), (b) NbC (GHSV = $4.4\times10^5 h^{-1}$), (c) TaC (GHSV = $4.4\times10^5 h^{-1}$) and (d) Mo_2C (GHSV = $4.4\times10^5 h^{-1}$). ▲, CH_4 conversion; ▼, CO_2 conversion; and ●, CO yield. Reproduced from [158].

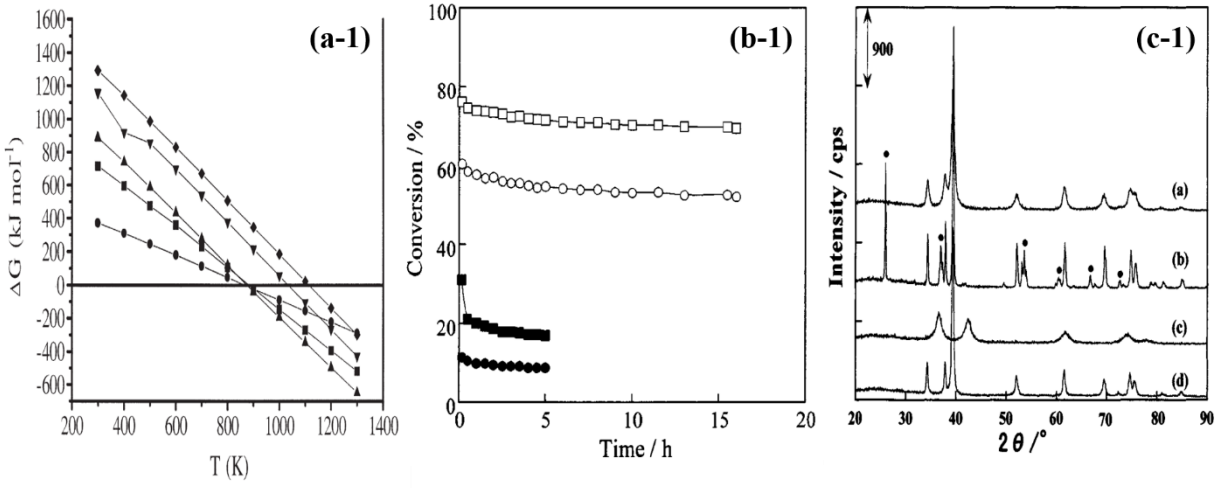

Figure 9. (a-1) Calculated Gibbs free energy for general reaction, ■, Mo_2C; ●, WC; ▲, VC; ▼, NbC and ♦, TaC. Reproduced from [158]. (b-1) Conversion of CH_4 and CO_2 at T = 1123K, P = 1atm and CO_2/CH_4 = 1 over Mo_2C (●, CH_4; ■, CO_2) and α-MoC_{1-x} (○, CH_4; □, CO_2) catalyst. (c-1) XRD

pattern of Mo_2C, (a) before DRM (b) after DRM; and MoC_{1-x}, (c) before DRM (d) after DRM; (●) MoO_2. Reproduced from [142].

Effect of Crystalline Structure and Phase

TMCs have spatial structures categorized into three main types: fcc, hcp, and simple hexagonal stacking (hex). Carbides of group V and VI TMs have different geometrical structures, even after using the same method for synthesizing them [158]. The carbides of group-V and VI TMs have fcc (Figure 1 (b)[54]) and hcp (Figure 1 (c)[54]) crystal structure shape, respectively [158]. Regardless of having the negative Gibbs free energy (required for the re-carburization of the oxides of group-V and VI TMs in DRM reaction) at the same temperature (Figure 9 (a-1)[158]), carbide catalysts of group-V TMs are less stable than that of group-VI TMs [158]. The cause of early deactivation of the carbide catalysts of group-V TMs in DRM reaction is the irreversible oxidation of the carbide phase [158]. While carbide catalysts of group-VI TMs remain stable in DRM reaction due to the redox cycle (Figure 2[115, 125-130]) [158]. The only explanation for this difference in the catalytic stability of carbides of group-V and VI TMs in DRM reaction is the different crystal structure shape [158]. In the case of molybdenum carbide, the varying atomic arrangements result in the presence of four distinct lattice structures: α-MoC_{1-x}, characterized by an fcc structure (Figure 1 (a)[54]), β-Mo_2C, exhibiting a hcp arrangement (Figure 1 (c)[54]), and γ-MoC and η-MoC, showcasing a simple hex configuration (Figure 1 (d)[54]).

Different phases of Mo_xC_y (the value of x and y varies, depending upon the phase of the Mo carbide molecule) show dissimilar catalytic activity/stability in increasing the rate of CH_4 reforming reaction. The β-Mo_2C is a more active and stable phase than α-MoC_{1-x} for catalyzing CH_4 reforming reaction [142, 163]. The α-MoC_{1-x} has a particle size smaller and also better dispersion than β-Mo_2C [126, 142]. Initially, the supported α-MoC_{1-x} shows catalytic activity three times higher than that of β-Mo_2C (Figure 9 (b-1)[142]), for DRM reaction, but this activity reduces to 2/3 in a very short period (Figure 9 (b-1)[142]) [126, 142]. β-Mo_2C and MoO_2 show almost similar catalytic activity for DRM reaction [126]. The α-MoC_{1-x} catalyst does not undergo a phase change in CH_4/H_2 atmosphere [155]. But in DRM reaction or under CH_4/CO_2 environment α-Mo_2C is converted to β-Mo_2C over time, while β-Mo_2C does not undergo a phase change but oxidizes to MoO_2 (Figure 9 (c-1)[142]) [142, 155, 163]. In DRM reaction over an α-MoC_{1-x} catalyst, CO_2 oxidizes α-MoC_{1-x} to MoO_2 (Equation 72), and then CH_4 re-carburizes MoO_2 to form β-Mo_2C (Equation 33) [155]. This

is how α-MoC_{1-x} catalyst undergoes a phase transformation in DRM reaction. α-MoC_{1-x} also undergoes a structural change from fcc (Figure 1 (a)[54]) to hcp (Figure 1 (c)[54]) [126]. The α-MoC_{1-x} shows better oxidation resistance than β-Mo_2C in DRM reaction [126, 142]. In DRM reaction over β-Mo_2C or mixed-phase (β-Mo_2C+ α-MoC_{1-x}) catalyst, oxidation or formation of MoO_2 is the reason for the catalyst deactivation [155]. For DRM reaction over α-MoC_{1-x} and β-Mo_2C catalyst, noble-metal type mechanism (Figure 5[115, 125, 141, 144]) and redox mechanism (Figure 6-7[115, 125, 141, 144]) dominate, respectively [155]. The β-Mo_2C catalyst with hcp crystal structure (Figure 1 (c)[54]) is less active/stable than α-MoC_{1-x} with fcc crystal structure (Figure 1 (a)[54]), for DRM reaction (Figure 9 (b-1)[142]) [142, 155]. In DRM reaction over Mo_xC_x catalyst, CO_2 conversion is always higher than CH_4 (Figure 9 (b-1)[142]) due to RWGSR but α-MoC_{1-x} shows better resistance against RWGSR [126, 142, 164]. The α-MoC_{1-x} and β-Mo_2C catalysts show better substrate conversion and turn-over frequency (TOF) for DRM reaction, respectively [126, 142]. In DRM reaction over α-MoC_{1-x} catalyst CH_4 dissociation is much better (Figure 9 (b-1)[142]), and establishment of redox cycle (Figure 2[115, 125-130]) is easier. The η-Mo_3C_2 is the most stable and active phase for CH_4 reforming reaction [163]. Oshikawa et al. [163] regarded η-Mo_3C_2 as the active species for CH_4 reforming reaction.

$$\alpha\text{-}MoC_{1-x} + (3-x)CO_2 \rightarrow MoO_2 + 2(2-x)CO \quad (72)$$

Mo_2C-nb (molybdenum carbide nanobelts) structurally remains intact in the DRM reaction, but the oxidation of the carbide phase causes deactivation [165]. In DRM over MC catalysts, metal-oxycarbide species regenerate the carbide phase and restore the catalytic activity, but in DRM over Mo_2C-nb, $Mo_2O_xC_y$ species do not participate in the carburization process [165].

Effect of Promotor

The active sites in TMC catalysts play a key role in catalyzing DRM reaction. The exposed Mo atoms in the Mo_2C catalyst act as active sites [126]. Mo_2C catalysts with very high Mo mole% get deactivated in DRM due to coking (Figure 10 (A-C)[166]) [166]. The surface area and stability of a catalyst directly affect its performance for catalyzing a chemical reaction. Mole% of Mo in Mo_2C catalyst affects its surface area as well for catalyzing DRM reaction [166, 167]. The surface area of the Mo_2C catalyst decreases with increasing Mo content [166, 167]. To get a Mo_2C catalyst with the maximum possible surface area, Mo must be added in optimal mole concentration. Temperature

required for the carburization of molybdenum oxide (MoO_x) with very high Mo mole% is also very high [166]. The stability of Mo_2C catalyst in an oxidative environment is a major concern. The catalytic activity and stability of Mo_2C for DRM reaction increases by increasing and decreasing Mo content, respectively [167]. The oxidant (CO_2) used as a substrate for the DRM reaction oxidizes the Mo_2C catalyst and converts the MC phase (Mo_2C) into the metal oxide phase (MoO_2) (Figure 10 (D)[168]) [114, 115, 125, 127, 158, 166, 169-171]. One of the major reasons for this is that the MCs prefer to react with oxides, this is also the explanation for higher CO_2 conversion than CH_4 in DRM reaction over MC catalysts [128, 129]. The addition of another metal as a promoter in the Mo_2C structure has significantly improved its resistance against oxidation [125, 127, 129, 166, 170]. A summary of the effect of adding different promoters on the catalytic performance of Mo_xC catalysts for DRM reaction is provided in Table 2.

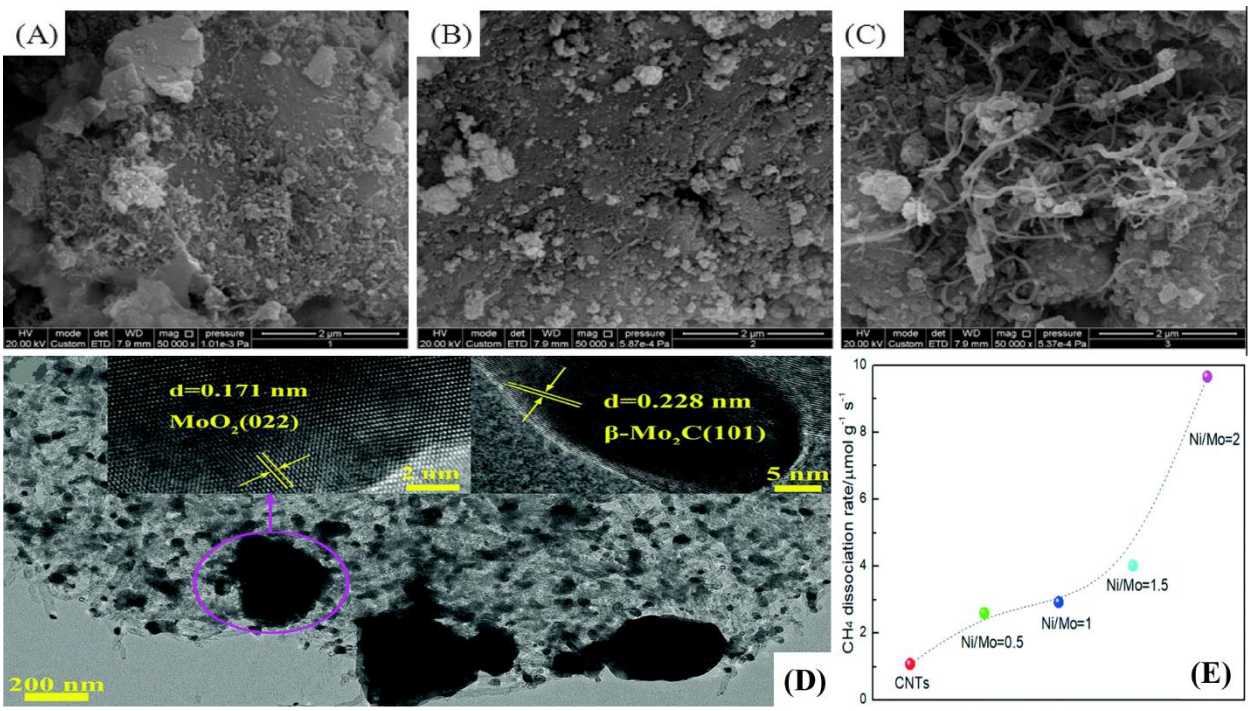

Figure 10. (A-C) SEM images of the surface of Ni-Mo_2C/Al_2O_3 catalysts with different Mo mol%, spent in DRM at T = 800^0C, P = 1atm, CO_2/CH_4 = 1 and GHSV: 12000ml/h-g_{cat}, showing that the catalysts with high Mo mol% have more C filaments deposited on the surface. (A) 0mol%Mo; (B) 5mol%Mo and (C) 10mol%Mo. Reproduced from [166]. (D) TEM image of β-Mo_2C used in DRM at P = 1atm, CO_2/CH_4 = 1 and WHSV: 18000$cm^3g^{-1}h^{-1}$. The inset shows the β-Mo_2C (101) crystal lattice. The inset shows the MoO_2 (022) crystal lattice. Reproduced from [168]. (E) CH_4 dissociation

rate obtained from CH_4 –TPSR study at T = 850^0C and P = 1atm over Ni-Mo_2C catalysts with different Ni/Mo ratios. Reproduced from [130].

Table 2: Summary of the effect of using different promoters on the catalytic performance of MoxC-based catalysts for DRM reaction.

Active Site	Support	SM, RT	App	Synthesis Conditions	Reaction Conditions	Feed Comp.	Max Con [%]	Selectivity [%]	Comment	Refs
Ni-Mo_2C Co-Mo_2C	– –	SM: TPR RT: −	DRM 2009	P: – / T: 700^{0}C TR: 1^{0}C/min CH_4/H_2: 20%v/v Flow: 100ml/min TC: 2h	P: 1bar / T: 850^{0}C GHSV: 3800h^{-1} Flow: 40ml/min TOS: 2h	CH_4: 1 CO_2: 1	CH_4: 89.2 CO_2: − CH_4: 89.8 CO_2: −	H_2: − CO: − H_2/CO: − H_2: − CO: − H_2/CO: −	Ni-Mo_2C with a Ni/Mo atomic ratio 0.2 is the most active and stable catalyst for DRM reaction. Co-Mo_2C with a Co/Mo atomic ratio of 0.4 is the most active/stable catalyst for DRM reaction.	[172]
Ni-Mo_2C	–	SM: TPR RT: FBR	DRM 2010	P: –/ T: 973K TR: 1K/min CH_4/H_2: 20vol% CH_4 Flow: − TC: 2h	P: 1atm / T: 1073K GHSV: 14000h^{-1} Flow: − TOS: 35h	CH_4: 1 CO_2: 1	CH_4: 98.0 CO_2: 95.0	H_2: 45.0 CO: 78.0 H_2/CO: −	Ni as a promoter in Mo_2C helps in reducing the temperature, required for the carburization of carbide catalyst precursor. Ni as a promoter in the Mo_2C catalyst establishes the redox cycle and prevents the deactivation of the Mo_2C catalyst due to oxidation in the DRM reaction.	[125]
Ni-Mo_2C	–	SM: TPR RT: −	DRM 2011	P: – /T: 973K TR: 1K/min CH_4/H_2: 20/80 Flow: 66.7ml/min TC: 1h	P: 1atm / T: 973K GHSV: − Flow: − TOS: 6h	CH_4: CO2<0.1	CH_4: 73.0 CO_2: 100.0	H_2: − CO: − H_2/CO: −	Carburizing temperature, Ni/Mo molar ratio, and CH_4/CO_2 feed ratio are the important factors to be considered for desired CH_4 conversion and H_2 yield in DRM reaction over Ni-Mo_2C catalyst.	[164]
Ni-Mo_2C	–	SM: In-situ TPR RT: FBR	DRM 2011	P: – /T: 800^{0}C TR: 5^{0}C/min CH_4/CO_2: 1 Flow: − TC: −	P: 1atm / T: 800^{0}C GHSV: − W/F: 0.6gscm^{-3} Flow: − TOS: 35h	CH_4: 1 CO_2: 1	CH_4: 82.0 CO_2: 93.0	H_2: 44.0 CO: − H_2/CO: 54.0	Ni-Mo_2C catalyst can be synthesized in-situ and is similar in activity/stability to Ni-Mo_2C synthesized by TPR method and using CH_4/H_2 gas mixture for the carburization of Ni-MoO_x, but is more active/stable than Mo_2C, for DRM reaction.	[129]
Ni-Mo_2C	–	SM: TPR RT: FBR	DRM 2012	P: – / T: 700^{0}C TR: 1^{0}C/min CH_4/H_2: 20vol% CH_4 Flow: − TC: 2h	P: 1atm /T: 800^{0}C GHSV: − W/F: 0.3gscm^{-3} Flow: − TOS: 20h	CH_4: 1 CO_2: 1	CH_4: 80.0 CO_2: 90.0	H_2: 45.0 CO: − H_2/CO: 50.0	The amount of Ni content in the Ni-Mo_2C catalyst significantly affects its performance for DRM reaction. Ni-Mo_2C with Ni/Mo=1/2 shows the best performance. Very low and high Ni content leads to the deactivation of Mo_2C by bulk oxidation and coking in DRM, respectively.	[127]
Ni-Mo_2C	–	SM: TPR RT: FBR	DRM 2013	P: – /T: 700^{0}C TR: 1^{0}C/min CH_4/H_2: 20vol% CH_4 Flow: − TC: 2h	P: 1atm /T: − GHSV: − W/F: 0.24gscm^{-3} Flow: 30ml/min TOS: 20h	CH_4: 1 CO_2: 1	CH_4: 55.0 CO_2: 69.0	H_2: 38.0 CO: − H_2/CO: −	Ni-MoO_x species, obtained by the CP method, are easy to carburize and give highly active/stable Ni-Mo_2C catalyst for DRM reaction.	[173]
Ni-Mo_2C	–	SM: TPR RT: −	DRM 2016	P: – /T: 700^{0}C TR: 1^{0}C/min CH_4/H_2: 20%v/v Flow: 50sccm TC: 2h	P: − / T: 950^{0}C GHSV: − Flow: 120sccm TOS: 300mins	CH_4: − CO_2: −	CH_4: 70.0 CO_2: 100.0	H_2: − CO: − H_2/CO: 90.0	In DRM reaction over Ni-Mo_2C catalyst, H_2/CO product ratio decreases with increasing CO_2 in the feed.	[174]
Ni-Mo_2C	–	SM: TPR RT: −	DRM 2016	P: – /T: 700^{0}C TR: 1^{0}C/min	P: 1atm / T: 800^{0}C GHSV: −	CH_4: 1 CO_2: 1	CH_4: 80.0 CO_2: 90.0	H_2: 85.0 CO: −	The Ni/Mo molar ratio in Ni-Mo_2C catalyst significantly affects its performance for DRM reaction.	[128]

				CH_4/H_2: 40%v/v Flow: 150ml/min TC: 2h	WHSV: 6000scch^{-1}g^{-1} Flow: 120ml/min TOS: 12h			H_2/CO: −	WC has better oxidation resistance and is a more stable catalyst than Mo_2C, for DRM reaction.	
Ni-Mo_2C	–	SM: TPR RT: −	DRM 2020	P: – / T: 850^{0}C TR: 2.5^{0}C/min CH_4/H_2: 20%v/v W/F: 0.0556ghL^{-1} TC: 2h	P: 1atm / T: 800^{0}C GHSV: – Flow: – TOS: 20h	CH_4: 1 CO_2: 1	CH_4: 65.0 CO_2: 80.0	H_2: 80.0 CO: − H_2/CO: 75.0	Ni-Mo_2C catalyst exhibits maximum stability in DRM reaction when using CH_4/CO_2 molar ratio greater than 1.	[175]

Due to showing highly effective performance for CH_4 dissociation (Figure 10 (E)[130]), Ni is the most important metal to be considered as a promoter for Mo_2C catalyst, to improve Mo_2C's activity/stability for catalyzing DRM reaction. In DRM reaction over Ni-Mo_2C catalyst, Ni promotes CH_4 conversion (Figure 11 (a)[127]), while the presence of Mo is beneficial for the oxidative removal of produced $C_{(s)}$ content because Mo_2C catalyzes RWGSR (Equation 13) as well [157, 170]. Ni-Mo_2C is more active/stable than Mo_2C, for catalyzing DRM reaction (Figure 11 (a-d)[127]) [127]. To differentiate between the role of Ni and Mo_2C, for catalyzing DRM reaction, Shi et al. [127] synthesized three Ni-Mo_2C catalysts with Ni/Mo molar ratios of 1/3, 1/2 and 1/1. The effect of increasing Ni content was found to be positive on the carburization process (during catalyst synthesizing), re-carburization of MoO_2 (during DRM reaction), and CH_4 conversion (Figure 11 (a)[127]), but negative on the catalyst's specific surface area. The Ni-Mo_2C catalyst with a Ni/Mo molar ratio of 1/2 was found to be the most active and stable catalyst for DRM (Figure 11 (a-d)[127]), and 1/2>Ni/Mo molar ratio>1/2 in Ni-Mo_2C reduced the activity and stability of Ni-Mo_2C catalyst for DRM (Figure 11 (a-d)[127]). Whatever the Ni/Mo molar ratio is in Ni-Mo_2C, Mo_2C undergoes a phase transformation while the Ni phase remains stable. Conversion of Mo_2C to MoO_2, and coking were the reason for the early deactivation of Ni-Mo_2C catalysts with Ni/Mo ratios of 1/3 and 1/1, respectively. Deactivation of Ni-Mo_2C catalyst with Ni/Mo ratio of 1/1 due to $C_{(s)}$ deposition, pointed out that high Ni content promotes CH_4 activation/dissociation that ultimately increases $C_{(s)}$ production/deposition rate [122, 127, 164]. This is also the reason that in DRM over Ni-Mo_2C catalyst with a very high Ni/Mo molar ratio, CH_4 conversion increases with decreasing temperature and vice versa [164]. Duan et al. [166] investigated Ni-Mo_2C/Al_2O_3 catalyst for catalyzing DRM reaction and found Ni helpful and crucial for CH_4 dissociation, reducing temperature requirement for carburizing/re-carburizing MoO_2, establishing redox cycle of Mo_2C, and preventing deactivation of Mo_2C due to oxidation.

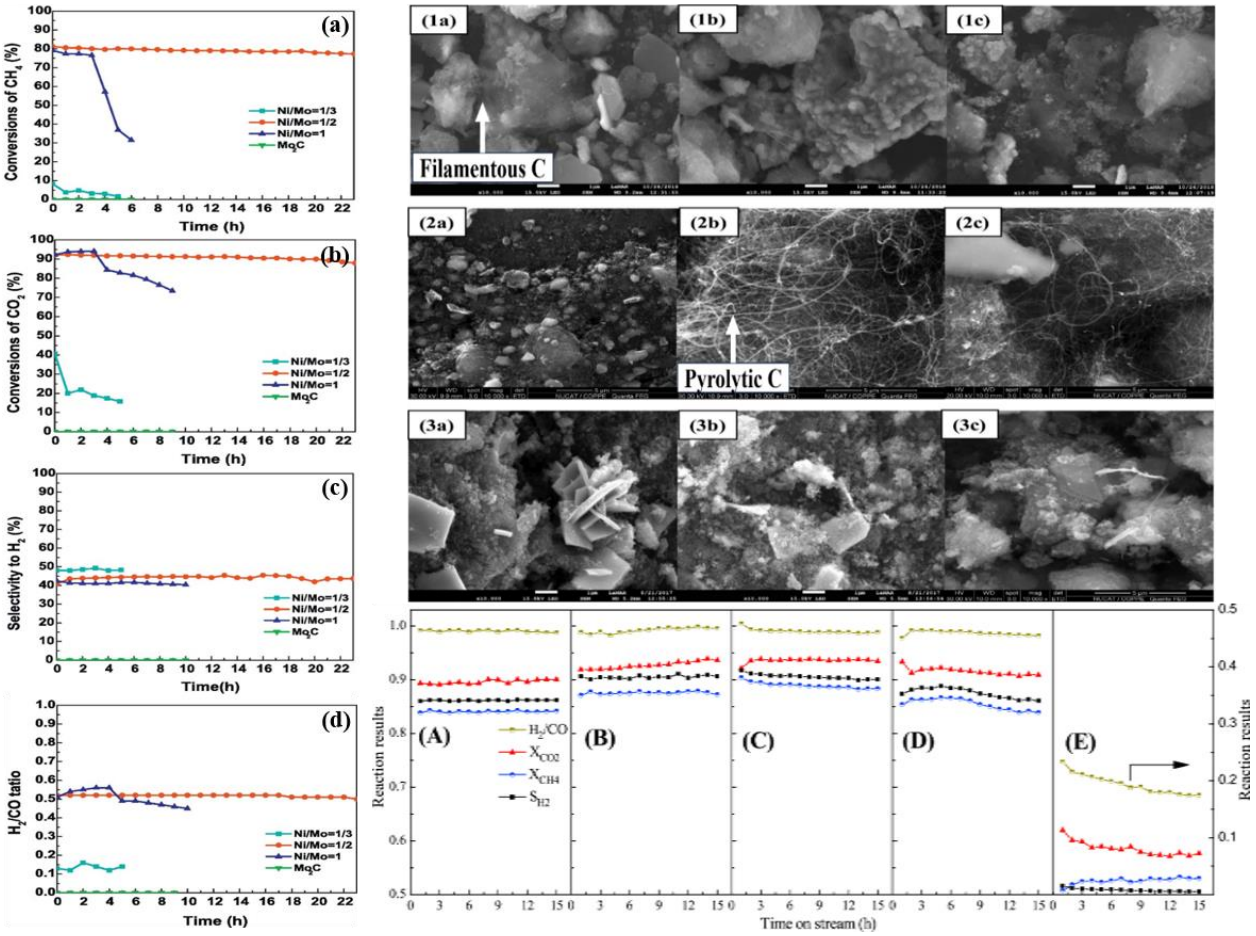

Figure 11. (a-d**)** Lifetime and activity study of Ni–Mo_2C catalysts, with different Ni/Mo molar ratio in CH_4/CO_2 reforming at T = 800^0C, P =1atm, CH_4/CO_2 = 1:1 and W/F: 0.3gscm^{-3}. (a) conversion of CH_4, (b) conversion of CO_2, (c) selectivity to H_2 and (d) H_2/CO ratio. Reproduced from [127]. SEM images of the supported Ni-Mo_2C catalysts with different Ni/Mo molar ratios after 20h of DRM reaction at T = 800^0C, P = 1atm and CH_4/CO_2 ratio = 1. (1a) $Ni/Mo = 0.2$, SiO_2, (1b) $Ni/Mo = 0.3$, SiO_2, (1c) $Ni/Mo = 0.4$, SiO_2; (2a) $Ni/Mo = 0.2$, Al_2O_3 (2b) $Ni/Mo = 0.3$, Al_2O_3, (2c) $Ni/Mo = 0.4$, Al_2O_3; and (3a) $Ni/Mo = 0.2$, SiC, (3b) $Ni/Mo = 0.3$, SiC, (3c) $Ni/Mo = 0.4$, SiC. Reproduced from [124]. (A-E) DRM at T = 800^0C and P = 1atm, CH_4/CO_2 =1:1 and GHSV: 12000ml/h-g_{cat}, over Ni-Mo_2C catalysts with different Mo mole%. (A) 0mole% Mo; (B) 3mole% Mo; (C) 5mole% Mo; (D) 10mole% Mo; and (E) 0mole% Ni. Reproduced from [166].

In Ni-Mo_2C catalyst, the Ni/Mo ratio must be highly appropriate for establishing the redox cycle, or in simple words to create a balance between the oxidation of Mo_2C and re-carburization of MoO_x during DRM reaction. The promoter must be added in a proportion that it can act as an agent to

enhance CH_4 conversion in balance with that of CO_2 conversion, and to improve the stability time of the MC catalyst in DRM reaction. In DRM reaction over Ni-Mo_2C catalyst, Ni-MoO_xC_y are the active species to enhance CH_4 conversion, and very high Ni/Mo molar ratio in Ni-Mo_2C transforms Ni-MoO_xC_y to Ni, β-Mo_2C and η-Mo_2C, and as a result CH_4 conversion and H_2 formation reduces [164]. The very high content of the promoter (that promotes CH_4 dissociation) can cause the MC catalyst to lose its functionality due to coking or $C_{(s)}$ deposition in DRM reaction [122, 127, 128]. In DRM reaction over supported Ni-Mo_2C catalysts, the excessive $C_{(s)}$ produced due to CH_4 dissociation, diffuses into the support, blocks the pores, and reduces the area of the support with time [122]. Zhang et al. [130] observed almost a similar effect of increasing Ni/Mo molar ratio in their study of DRM reaction over Ni-Mo_2C/CNTs catalyst. At similar conditions, Mo_2C (with zero Ni content) shows very small or no activity for DRM reaction (Figure 11 (a-d)[127]) [127-129]. So, Mo_2C must work in synergy with Ni to perform best in catalyzing the DRM reaction [127-129]. Using DRM feed (CH_4/CO_2) molar ratio of less than 1 deactivates Ni-Mo_2C easily due to oxidation [175]. The specific surface area of the Ni-Mo_2C catalyst increases but particle size decreases, with increasing Ni/Mo molar ratio [128, 130]. Small particle size and high Ni/Mo molar ratio favor CH_4 dissociation (Figure 11 (a-d)[127]) but not the redox cycle [128, 130]. A very low Ni/Mo molar ratio is good for CO_2 dissociation (Figure 11 (a-d)[127]), and also for keeping the β-Mo_2C particle size small in Ni-Mo_2C catalyst [128, 130]. An optimized Ni/Mo atomic ratio in Ni-Mo_2C catalyst to catalyze DRM reaction is 1/2 [127]. But according to Cheng et al. [172], a Ni-Mo_2C catalyst with a Ni/Mo atomic ratio of 0.2 is the most active and stable catalyst for the conversion of CH_4 in DRM reaction. Increasing the Ni/Mo atomic ratio beyond 0.2, results in decreasing the activity and surface area of the Ni-Mo_2C catalyst for CH_4 conversion in DRM reaction [172]. A higher CO_2 conversion than CH_4 indicates the occurrence of RWGSR in parallel with DRM reaction in the stream [166]. In DRM reaction over promoted Mo_2C catalysts, oxidation, and metal sintering are the reasons for the catalyst deactivation [128]. Silva et al. [124] found that Ni/Mo atomic ratio in Ni-Mo_2C shows little or no effect on the performance of SiC as a support but $2<Ni/M\leq3$ improves the role of Al_2O_3 as a support. A very high Ni/Mo atomic ratio increases the rate of CH_4 activation/dissociation (Figure 11 (a-d)[127]) but also results in the deposition of pyrolytic and filamentous C on the catalyst surface (Figure 11 (1a-3c)[124]).

Guo et al. [125] conducted a study to compare the catalytic potential of Mo_2C and Ni-Mo_2C for DRM reaction at atmospheric pressure. The oxidation-reduction cycle of Mo_2C, for DRM reaction

over both the catalysts, was also investigated. XRD analysis of freshly synthesized both the catalysts divulged that presence of Ni helps in the carburization process for synthesizing Mo_2C, because Ni made carburization of catalyst precursor (MoO_x) possible at 923K than at 973K in synthesizing Ni-Mo_2C. Without Ni, MoO_x cannot be carburized completely to Mo_2C [122]. XRD study results of both the spent catalysts showed that Ni helps in the regeneration of the Mo_2C catalyst as well in DRM reaction because redox cycle was only observed in DRM reaction over Ni-Mo_2C catalyst. Mo_2C catalyst became inactive after 5h because it was oxidized to MoO_2, but the Ni-Mo_2C catalyst remained active/stable for the whole time on the stream (TOS) due to the establishment of the oxidation-re-carburization cycle. The Ni-Mo_2C catalyst showed much better CH_4/CO_2 conversion and H_2/CO selectivity than Mo_2C catalyst, for DRM reaction. So, Ni as a promoter can help Mo_2C catalyst to catalyze DRM reaction with unwavering stability even at low pressure. In Investigating the effect of Mo mole % (ranged between 0-10mol %) on the catalytic activity of Ni-Mo_2C/Al_2O_3 for DRM reaction, the authors reported that Ni-Mo_2C/Al_2O_3 catalyst with Mo mole% of 3 is the most active catalyst (Figure 11 (A-E)[166]) [166].

Zhang et al. [129] further highlighted the importance of the presence of Ni for the carburization process by synthesizing in-situ Mo_2C and Ni-Mo_2C catalysts. Ni-MoO_x can be carburized under the flow of a CH_4/CO_2 gas mixture, but to carburize MoO_3, it is compulsory to use CH_4/H_2 mixture [129]. So, only Ni-Mo_2C catalyst can be synthesized in-situ and is effective for DRM reaction [129]. When using Ni-Mo_2C catalyst for DRM reaction, the MoO_x re-carburization rate is higher than CO_2 dissociation, and that is why the redox cycle of Ni-Mo_2C is easily established, and Ni-Mo_2C shows more stability than Mo_2C [129]. The Ni/Mo atomic ratio in Ni-Mo_2C catalyst is also important to be considered. It is not only concerned with the performance of the Ni-Mo_2C catalyst itself but also with the function catalyst support as well.

Ce is another promoter that can enhance the catalytic activity and stability of Mo_2C for DRM reaction. Dispersion of active sites is better in Ce-Mo_2C/γ-Al_2O_3 than in Mo_2C/γ-Al_2O_3. In Ce-Mo_2C/γ-Al_2O_3 catalyst, Ce exists in the form of Ce_2O_3 [176]. In DRM reaction over Ce-Mo_2C/γ-Al_2O_3 catalyst, CH_4 rapidly exchanges C with Mo_2C because CO_2 dissociation changes Ce_2O_3 to CeO_2 [176]. The redox nature of Ce prevents the oxidation of Mo_2C and makes it a stable catalyst for DRM reaction [167, 176]. Introducing CO with DRM feed helps in making Ce-Mo_2C/γ-Al_2O_3 even more stable [167, 176]. Darujati et al. [154] proposed the mechanism for DRM reaction over

the Ce-Mo_2C catalyst (Equations 73-75). CH_4 dissociation left C species on the Mo_2C adsorption site (■) (Equation 73). CO_2 dissociation left O on the Ce adsorption site (◆) (Equation 74). The adsorbed C and O react to produce CO and leave their respective adsorption sites (Equation 75). Ce and K as promoters do not affect the surface area of Mo_2C/γ-Al_2O_3 [167]. Increasing the weight% (wt%) of Ce does not significantly change the ability of Ce-Mo_2C/γ-Al_2O_3 catalyst for CH_4 conversion in DRM reaction [167]. The surface area of K-Mo_2C/γ-Al_2O_3 catalyst decreases over time in DRM reaction due to sintering, and increased wt.% of K negatively impacts the CH_4 conversion. The order of impregnation/calcination of Mo_2C and promoter in/on to γ-Al_2O_3 support is a factor that affects the stability [167]. This is important when using high wt.% of Mo_2C, and Ce as a promoter, but not in the case of K and Zr as promoters [167]. The impregnation and calcination of Ce in/on to γ-Al_2O_3 support followed by the impregnation of Mo_2C gives the most stable Ce-Mo_2C/γ-Al_2O_3 catalyst for DRM reaction [167].

$$CH_4 \rightleftharpoons (■)C + 2H_2 \quad (73)$$

$$CO_2 \rightleftharpoons O(◆) + CO \quad (74)$$

$$(■)C + O(◆) \longrightarrow CO + (■) + (◆) \quad (75)$$

In addition to Ni and Ce, the effect of Co as a promoter for improving the catalytic function of Mo_2C for DRM reaction has also been investigated. Using Co as a promoter for Mo_2C/ZrO_2 catalyst improves oxidation/coking resistance of Mo_2C in DRM reaction [157]. Co also helps in suppressing RWGSR (Equation 13) [157]. Increasing the Co/Mo atomic ratio from 0.1-0.4 in Co-Mo_2C positively impacts its catalytic activity and stability for DRM reaction, and Co-Mo_2C with Co/Mo atomic ratio 0.4 is the most active and stable catalyst for CH_4 dissociation [172]. Ni and Co as promoters do not enhance the functionality of Mo_2C catalyst for CO_2 conversion in DRM reaction, but Bi as a promoter does [177].

Effect of Support

Support has been proven very important in enhancing thermal stability/lifetime, and the surface area of the catalyst available for the reaction [157, 178]. Support allows the high dispersion of the active species [157, 176]. In this way, more reactants come in contact with the active sites of the catalyst during the reaction. As a result, the rate of the surface-catalyzed reaction increases, and TOF also increases [142, 157]. Besides having some unwanted impact on DRM reaction, metal oxide supports

have shown very good results in reducing the coke production and preventing sintering of the active metal phase of the catalyst in DRM reaction [178-185]. Metal oxide supports which are basic in nature, reduce coking by the gasification of deposited $C_{(s)}$ [179]. A summary of the effect of using different supports on the performance of simple and promoted Mo_xC-based catalysts, for DRM reaction, is provided in Table 3. Metal oxide support also enhances the stability time of Mo_2C for DRM [171]. Overall, Al_2O_3, and ZrO_2, are the most popular metal oxide supports used. SiO_2 and CNTs are the other common supports. Brungs et al. [171] examined the stability of Mo_2C catalyst supported over several metal oxide supports, for DRM reaction. The discovered stability order was $Mo_2C/Al_2O_3>Mo_2C/SiO_2>Mo_2C/ZrO_2>Mo_2C/TiO_2$. Catalyst stability is not related to the surface area of the support but with the amount of catalyst loaded and distribution of the active species on the support [171]. Supported Mo_2C catalysts have better activity, and resistance against oxidation/coking in DRM reaction [177]. Treacy et al. [177] examined the resistivity of the supports to coking. Different supported Mo_2C catalysts prevent coking in DRM reaction in the order $Mo_2C/ZrO_2>Mo_2C/Al_2O_3>Mo_2C/SiO_2$ [177]. The amount of $C_{(s)}$ deposits on the Mo_2C/ZrO_2 catalyst is insignificant in comparison with the amount of $C_{(s)}$ deposits on the $Mo2C/Al_2O_3$ catalyst in the DRM reaction [177]. In DRM reaction over $NiZr/ZrO_2$, produced C migrates to the catalyst/support interface and forms ZrC. The formation of ZrC mitigates the coking effect and helps in the regeneration of the active sites for CH_4 activation. ZrC itself helps in CO_2 dissociation [186].

Table 3: Summary of the effect of using different supports on the catalytic performance of simple and promoted MoxC-based catalysts for DRM.

Active Site	Support	SM, RT	App	Synthesis Conditions	Reaction Conditions	Feed Comp.	Max Con [%]	Selectivity [%]	Comment	Refs
β-Mo_2C	Al_2O_3	SM: TPR RT: −	DRM 1997	–	P: 8.3bar / T: 1120K GHSV: $2.8\times10^3h^{-1}$ Flow: − TOS: 144h	CH_4: 1 CO_2: 1	CH_4: 65.2 CO_2: −	H_2: − CO: 70.1 H_2/CO: 81.0	β-Mo_2C/Al_2O_3 catalyst remains active and stable in DRM reaction at high pressure for the whole time on stream.	[114]
Mo_2C	Al_2O_3	SM: TPR RT: LMR	DRM 1998	P: – / T: 1000-1150K TR: 1K/min CH_4/H_2: 20%v/v (Flow: –) TC: −	P: 1bar /T: 1120K GHSV: $2.87\times10^3h^{-1}$ Flow: − TOS: 28h	CH_4: 1 CO_2: 1	CH_4: 92.6 CO_2: 92.4	H_2: − CO: 92.5 H_2/CO: 95.0	Mo_2C/Al_2O_3 exhibits catalytic performance, stability, and behavior same as β-Mo_2C for DRM reaction at similar conditions.	[115]
Mo_2C	Al_2O_3	SM: TPR RT: LMR	DRM 1998	P: – / T: 1000-1150K TR: 1K/min CH_4/H_2: 20%v/v CH_4/H_2 flow: − TC: −	P: 8.3bar T: 1120K GHSV: $2.87\times10^3h^{-1}$ Flow: − TOS: 72h	CH_4: 1 CO_2: 1	CH_4: 65.1 CO_2: 80.7	H_2: − CO: 73.1 H_2/CO: 81.0	Mo_2C/Al_2O_3 catalyst depicts consistent action at high pressure, in DRM reaction.	[115]
Mo_2C	SiO2		DRM 2000	P: – / T: 900K TR: 1K/min C_2H_6/H_2: 10%v/v	P: 8bar T: 1220K GHSV: $2.6\times10^3h^{-1}$	CH_4: 1 CO_2: 1	CH_4: 91.0 CO_2: 86.0	H_2: − CO: 89.0 H_2/CO: 95.0	The Mo2C catalyst supported on Al_2O_3 is the most stable catalyst for DRM reaction.	[171]
Mo_2C	γ- Al_2O_3			Flow: − TC: −	Flow: − TOS: 11-40h		CH_4: 89.0 CO_2: 86.0	H_2: − CO: 87.0 H_2/CO: 97.0		
Mo_2C	TiO_2	SM: TPR RT: LMR					CH_4: 31.0 CO_2: 27.0	H_2: − CO: 29.0 H_2/CO: −		
Mo_2C	ZrO_2						CH_4: 90.0 CO_2: 93.0	H_2: − CO: 92.0 H_2/CO: 96.0		
β-Mo_2C	ZrO_2		DRM 2000	P: 1atm / T: 973K TR: 1K/min CH_4/H_2: 20%v/v	P: 1atm T: 1123K GHSV: −	CH_4: 1 CO_2: 1	CH_4: 18.0 CO_2: 31.0	H_2: − CO: − H_2/CO: −	CH_4/CO_2 conversion and TOF for syngas are better in DRM reaction over α-MoC_{1-x} and β-Mo_2C catalysts, respectively. But when supported over ZrO_2, this difference is minimized.	[142]
α-MoC_{1-x}	−	SM: TPR RT: −		Flow: − TC: 3h	Flow: 40cm^3/min TOS: 12h		CH_4: 19.0 CO_2: 33.0	H_2: − CO: − H_2/CO: −		
Mo_2C	TiO_2	SM: TPR RT: FBR	DRM 2002	P: – / T: – TR: – H_2/C_2H_6: 11.6%v/v Flow: 55ml/min TC: –	P: 1atm T: 850^{0}C GHSV: 5040$cm^3g^{-1}h^{-1}$ Flow: − TOS: −	CH_4:CO_2= 1.16	CH_4: 70.1 CO_2: 88.7	H_2: − CO: 77.8 H_2/CO: 90.0	TiO_2 enhances the catalytic activity of Mo_2C for DRM reaction.	[159]
Mo_2C	α- Al_2O_3	SM: − RT: PBR	DRM	−	P: − T: 1050^{0}C	CH_4:CO_2> 1	CH_4: − CO_2: −	H_2: − CO: −	Sulfur affects the catalytic activity of Mo_2C for DRM reaction.	[187]

			DRCO 2004		GHSV: 5000h^{-1} Flow: − TOS: 1.5h	CH_4:CO_2= variable	CH_4: − CO_2: −	H_2/CO: 110 H_2: − CO: − H_2/CO: 175	The effect of sulfur can be minimized by increasing the reaction temperature.	
Mo_2C Mo_2C Mo_2C Mo_2C	− Al_2O_3 ZrO_2 SiO2	SM: TPR RT: PFR	DRM 2004	P: – / T: 750^{0}C TR: 1K/min CH_4/H_2: 20%v/v Flow: − TC: −	P: − T: 950^{0}C GHSV: − Flow: − TOS: 20h	$CH_4/CO_2/N_2$: 50/50/5 $cm^{-1}min^{-1}$	CH_4: − CO_2: 48.0 CH_4: − CO_2: 63.0 CH_4: − CO_2: 48.0 CH_4: − CO_2: 18.0	H_2: − CO: − H_2: − CO: − H_2: − CO: − H_2: − CO: −	Mo_2C/Al_2O_3 and Mo_2C/ZrO_2 have better activity and coking resistance in DRM reaction, respectively. The activity of the Mo_2C/SiO_2 catalyst is medicore for DRM reaction.	[177]
Mo_2C	ZrO_2	SM: TPR RT: −	DRM 2014	P: – / T: 750^{0}C TR: 3^{0}C/min CH_4/H_2: − Flow: 8/32ml/min TC: 3h	P: 1atm T: 850^{0}C GHSV: $4.8\times10^3 mlh^{-1}g^{-1}$ Flow: − TOS: 4h	CH_4: 1 CO_2: 1	CH_4: 37.56 CO_2: 52.09	H_2: 24.80 CO: 39.39 H_2/CO: 61.0	Increasing the percentage loading of Mo_2C in Mo_2C/ZrO_2 catalyst negatively impacts its catalytic role for DRM reaction.	[157]
Mo_2C	Al_2O_3	SM: TPR RT: −	DRM 2016	P: – / T: – TR: 1^{0}C/min CH_4/H_2: – Flow: 100ml/min TC: –	P: 1atm / T: 850^{0}C GHSV: 18l/g.h Flow: − TOS: 12h	CH_4: 1 CO_2: 1	CH_4: 91.45 CO_2: 95.0	H_2: 58.0 CO: − H_2/CO: 85.0	Varying carburization conditions for the same precursor yield MCs with diverse compositions, resulting in distinct catalytic roles in the DRM reaction. Mo_2C catalyst with high Mo content, but less excessive C content is more stable for DRM reaction.	[169]
Mo_2C	CNTs	SM: − RT: −	DRM 2017	−	P: 1atm / T: 850^{0}C GHSV: − WHSV: 18000$cm^3g^{-1}h^{-1}$ Flow: − TOS: 24h	CH_4: 1 CO_2: 1	CH_4: 88.0 CO_2: 97.0	H_2: − CO: − H_2/CO: −	Encapsulating Mo_2C inside the CNTs rather than using CNTs as support can improve the stability time of Mo_2C in DRM reaction.	[188]
β-Mo_2C	CNTs	SM: SSR RT: −	DRM 2017	P: 1atm / T: 850^{0}C TR: 10^{0}C/min Ar: 100% Flow: 300ml/min	P: 1atm / T: 850^{0}C GHSV: − WHSV: 18000$cm^3g^{-1}h^{-1}$ Flow: − TOS: 14h	CH_4: 1 CO_2: 1	CH_4: 85.0 CO_2: 93.0	H_2: 82.0 CO: − H_2/CO: −	CNTs can be used as the C source to synthesize β-Mo_2C. β-Mo_2C/CNTs composite synthesized by solid-solid reaction is more active/stable than β-Mo_2C and Ni-β-Mo_2C (synthesized by conventional TPR method).	[168]
Mo_2C	BC	SM: TPR RT: FBR	DRM 2018	P: 1atm / T: 800^{0}C TR: 5^{0}C/min Ar: 100% Flow: 100ml/min TC: −	P: 0.5MPa T: 875^{0}C GHSV: 6000h^{-1} Flow: − TOS: 50h	CH_4: 1 CO_2: 1	CH_4: 97.2 CO_2: 99.0	H_2: − CO: − H_2/CO: 95.0	Mo_2C/BC can be synthesized by the TPR method without using a CH_4/H_2 gas mixture but an inert gas and is a good catalyst for DRM reaction.	[189]
β-Mo_2C	C	SM: CHR RT: FBR	DRM 2020	P: – / T: 800^{0}C TR: 5^{0}C/min H_2/N_2: 10vol% Flow: – TC: 30min	P: 8bar / T: 800^{0}C GHSV: − Flow: − TOS: −	CH_4: 4 CO_2: 3 N_2: 3	CH_4: − CO_2: −	H_2: − CO: − H_2/CO: 70.0	$Mo_2O_xC_y$ species highly rich in oxygen increase the rate of RWGSR and reduce the H_2/CO yield in DRM reaction.	[190]

Mo_2C-nb Mo_2C	– SiO_2	SM: TPR RT: FBR	DRM 2022	P: 1atm / T: 800^0C TR: 2^0C/min CH_4/H_2: 20/80vol% Flow: – TC: 1h	P: 8bar T: 730^0C GHSV: – Flow: 10ml/min TOS: 36h	CH_4: 4 CO_2: 2 N_2: 4 CH_4: 4 CO_2: 3 N_2: 3	CH_4: 60.0 CO_2: – CH_4: 55.0 CO_2: –	H_2: CO: – H_2/CO: 90.0 H_2: – CO: – H_2/CO: 70.0	Mo_2C-nb structurally remains intact in DRM reaction. Mo_2C/SiO_2 has more resistance against oxidation than Mo_2C, in DRM reaction.	[165]
Mo_2C Mo_2C Ni-Mo_2C	– Al_2O_3 Al_2O_3	SM: TPR RT: CSTR	DRM 2001	P: – / T: 1073K TR: 4K/min $CH_4/H_2/N_2$: 10/10/80 Flow: $3lh^{-1}$ TC: –	P: – / T: – GHSV: – Flow: 6l/h TOS: –	CH_4: 10 CO_2: 10 N_2: 80	CH_4/CO_2: 490 CH_4/CO_2: 140 CH_4/CO_2: 130	H_2: 22.9 CO: – H_2/CO: – H_2: 63.7 CO: – H_2/CO: – H_2: 66.3 CO: – H_2/CO: –	CH_4 conversion and H_2 selectivity of DRM reaction over Mo_2C catalyst can be increased, by using Al_2O_3 as support and Ni as a promoter for Mo_2C catalyst.	[122]
Mo_2C Ce-Mo_2C	γ-Al_2O_3	SM: TPR RT: –	DRM 2005	P: – /T: 675^0C TR: – CH_4/H_2: 20%v/v Flow: – TC: 2h	P: 1bar / T: 900^0C GHSV: $3800h^{-1}$ G: 0.37mol/cm^2/h Flow: – TOS: 7h	CH_4: 1 CO_2: 1	CH_4: 100 CO_2: – CH_4: 98.0 CO_2: –	H_2: – CO: – H_2/CO: – H_2: – CO: – H_2/CO: –	γ-Al_2O_3 is the best support for Mo_2C catalyst amongst γ-Al_2O_3, ZrO_2 and MgO, for DRM reaction. Ce is the best promoter for Mo_2C/γ-Al_2O_3. The order of impregnation/calcination of promoter and Mo_2C catalyst in/on γ-Al_2O_3 support affects the stability.	[167]
Ce-Mo_2C	Al_2O_3	SM: TPR RT: PBR	DRM 2006	P: – / T: 675^0C TR: – CH_4/H_2: 20%v/v CH_4/H_2 flow: – TC: 2h	P: – / T: 900^0C GHSV: $26000h^{-1}$ Flow: – TOS: –	CH_4: 1 CO_2: 1	CH_4: – CO_2: –	H_2: – CO: – H_2/CO: –	Ce as a promoter helps in preventing the oxidation of Mo_2C catalyst in DRM reaction.	[154]
Ni-Mo_2C	SBA-15	SM: TPR RT: FBR	DRM 2011	P: 1atm / T: 1073K TR: – CH_4/H_2: 20vol% Flow: – TC: 2h	P: 1atm / T: 1073K GHSV: $8000ml^3h^{-1}g^{-1}$ Flow: – TOS: 180h	CH_4: 1 CO_2: 1	CH_4: 90.0 CO_2: 90.0	H_2: – CO: – H_2/CO: 90.0	SBA-15 as a support increases the stability time of the Ni-MO_2C catalyst for catalyzing the DRM reaction.	[191]
La-Co-Mo_2C	γ-Al_2O_3	SM: TPR RT: FBPFR	DRM 2014	P: – / T: 750^0C TR: 3^0C/min CH_4/H_2: 20/80vol% Flow: 40ml/min TC: 3h	P: 1atm / T: 850^0C GHSV: $4800mlh^{-1}g^{-1}$ Flow: 40ml/min TOS: 20h	CH_4: 33 CO_2: 39 N_2: 28	CH_4: 99.5 CO_2: 94.0	H_2: 74.0 CO: 66.0 H_2/CO: 96.0	La addition in Co-Mo_2C, in the range 1-3wt%, helps in improving its catalytic action/stability in DRM reaction.’	[192]
Co-Mo_2C	ZrO_2	SM: TPR RT: –	DRM 2014	P: – /T: 750^0C TR: 3^0C/min CH_4/H_2: – Flow: 8/32ml/min TC: 3h	P: 1atm / T: 850^0C GHSV: $4.8\times10^3mlh^{-1}g^{-1}$ Flow: – TOS: 4h	CH_4: 1 CO_2: 1	CH_4: 97.50 CO_2: 97.07	H_2: 92.5 CO: 86.9 H_2/CO: 109.0	Co as a promoter, not only enhances the catalytic activity of Mo_2C/ZrO_2 for DRM reaction but also suppresses the side reactions like RWGSR.	[157]
Ni-Mo_2C	– La_2O_3	SM: TPR RT: FBR	DRM 2015	P: – / T: 700^0C TR: 1^0C/min CH_4/H_2: 20vol% CH_4	P: 1atm / T: 800^0C GHSV: 12000mL/gh Flow: –	CH_4: 1 CO_2: 1	CH_4: 80.0 CO_2: 91.0 CH_4: 66.0	H_2: 45.0 CO: – H_2/CO: –	Ni-Mo_2C shows higher activity than Ni-Mo_2C/La_2O_3 catalyst for DRM reaction at a temperature above 750^0C.	[170]

Ni-Mo_2C				CH_4/H_2 flow: − TC: 2h	TOS: 50h		CO_2: 82.0	H_2: 45.0 CO: − H_2/CO: −	Ni-Mo_2C/La_2O_3 is more stable than Ni-Mo_2C in DRM for more than 25h because it prevents the oxidation of Mo_2C.	
Ni-Mo_2C	Al_2O_3	SM: TPR RT: FBR	DRM 2016	P: – /T: 800^0C TR: 5^0C/min CH_4/CO_2: 1 Flow: 30ml/min TC: −	P: 1atm T: 800^0C GHSV: 12000 $mlh^{-1}g^{-1}$ Flow: − TOS: 15h	CH_4: 1 CO_2: 1 N_2: 1	CH_4: 89.4 CO_2: 94.0	H_2: 90.7 CO: 91.2 H_2/CO: 99.0	In-situ synthesized Ni-Mo_2C/Al_2O_3 catalyst is good for DRM. The mole% of Mo in the Ni-Mo_2C catalyst influences its specific surface area and activity for DRM reaction. Coking causes the deactivation of Ni-Mo_2C at very high Mo %. The carburization temperature of Mo_2O increases with Mo mole%	[166]
Mo_2C Ni-Mo_2C	Al_2O_3	SM: TPR RT: –	DRM 2017	P: – / T: 700^0C TR: 1^0C/min CH_4/H_2/Ar: 20/4/76 Flow: 10/40ml/min TC: 2h	P: 1atm T: 850^0C GHSV: $20000h^{-1}$ Flow: – TOS: 300min	CH_4: 1 CO_2: 1 Ar: 8	CH_4: 40.9 CO_2: 51.4 CH_4: 89.9 CO_2: 99.2	H_2: − CO: − H_2/CO: 77.0 H_2: − CO: − H_2/CO: 92.0	Ni as a promoter further improves the activity of Mo_2C/AL_2O_3. The composition of the carburizing gas used in the TPR of the precursor significantly affects the catalytic performance of the synthesized MC, for DRM reaction.	[193]
Ni-Mo_2C	La_2O_3-ZrO_2	SM: TPR RT: FBR	DRM 2018	P: – /T: 1073K TR: 1K/min CH_4/H_2: 20vl% CH_4/H_2 flow: − TC: 2h	P: 1atm T: 1173K GHSV: – Flow: 40ml/min TOS: 100h	CH_4: 1 CO_2: 1	CH_4: 94.0 CO_2: 90.0	H_2: 90.0 CO: 95.0 H_2/CO: 95.0	The Ni-Mo_2C/La_2O_3-ZrO_2 catalyst with 7.5mole% of La_2O_3 is good for DRM reaction at high temperature.	[194]
Ni-Mo_2C	SiO_2	SM: TPR RT: −	DRM 2019	P: – /T: 800^0C TR: 1^0C/min CH_4/H_2: 20%v/v Flow: 20/80ml/min TC: 2h	P: 1atm T: 800^0C GHSV: − Flow: − TOS: 20h	CH_4: 1 CO_2: 1 N_2: 1	CH_4: 67.0 CO_2: 76.5	H_2: 87.5 CO: − H_2/CO: 75.0	The activity of SiO_2 supported Ni-Mo_2C catalyst for DRM reaction escalates with increasing Ni/Mo atomic ratio.	[124]
Ni-Mo_2C	Al_2O_3	SM: TPR RT: −	DRM 2019	P: – /T: 800^0C TR: 1^0C/min CH_4/H_2: 20%v/v Flow: 20/80ml/min TC: 2h	P: 1atm T: 800^0C GHSV: − Flow: − TOS: 20h	CH_4: 1 CO_2: 1 N_2: 1	CH_4: 80.0 CO_2: 90.0	H_2: 87.5 CO: − H_2/CO: 80.0	The Al_2O_3 support improves the functionality of the Ni-Mo_2C catalyst with 2<(Ni/Mo atomic ratio)≤3 for DRM reaction.	[124]
Ni-Mo_2C	SiC	SM: TPR RT: −	DRM 2019	P: − / T: 800^0C TR: 1^0C/min CH_4/H_2: 20%v/v Flow: 20/80ml/min TC: 2h	P: 1atm T: 800^0C GHSV: − Flow: − TOS: 20h	CH_4: 1 CO_2: 1 N_2: 1	CH_4: 87.5 CO_2: 87.5	H_2: 87.5 CO: − H_2/CO: 87.5	SiC support helps Ni-Mo_2C catalyst perform better in DRM regardless of the Ni/Mo atomic ratio in the structure. Ni-Mo_2C/SiC shows more coke resistance than $NiMo_2C/Al_2O_3$. The order of efficiency of different supports in boosting the activity of Ni-Mo_2C for DRM reaction is SiC>Al_2O_3>SiO_2.	[124]
Ni-Mo_2C	SiC	SM: TPR RT: −	DRM 2019	P: – / T: 800^0C TR: 1^0C/min CH_4/H_2: 20%v/v Flow: 20/80ml/min TC: 2h	P: 1atam T: 800^0C GHSV: − Flow: − TOS: 20h	CH_4:CO_2= 0.6	CH_4: 95.0 CO_2: 75.0	H_2: − CO: − H_2/CO: 70.0	Too low DRM feed ratio (CH_4/CO_2) negatively impacts the activity of Ni-Mo_2C/SiC catalysts, especially with low Ni/Mo atomic ratio.	[124]

Ni-Mo_2C	SiC	SM: TPR RT: −	DRM 2019	P: – /T: 800^0C TR: 1^0C/min CH_4/H_2: 20%v/v Flow: 20/80ml/min TC: 2h	P: 1atam T: 800^0C GHSV: − Flow: − TOS: 20h	CH_4:CO_2= 1.5	CH_4: 50.0 CO_2: 90.0	H_2: 80.0 CO: − H_2/CO: −	With a very high DRM feed ratio, the activity of Ni-Mo_2C/SiC first reduces and then becomes stable, regardless of the Ni/Mo atomic ratio in the lattice.	[124]
Ni-Mo_2C	Al_2O_3	SM: TPR RT: −	DRM 2021	P: – / T: 800^0C TR: 1^0C/min CH_4/H_2: 20%v/v Flow: 100ml/min TC: 2h	P: 1atm T: 800^0C GHSV: 420585h^{-1} Flow: − TOS: 20h	CH_4: 1 CO_2: 1	CH_4: 90.0 CO_2: 95.0 CH_4: 80.0 CO_2: 90.0	H_2: − CO: − H_2/CO: 80.0 H_2: − CO: − H_2/CO: 80.0	Unlike the Ni-Mo_2C/Al_2O_3, the catalytic activity of Ni-Mo_2C/SiC for DRM reaction is independent of the temperature used for its synthesis by the TPR process. Ni-Mo_2C with a high (above 0.2) Ni/Mo ratio exhibits good catalytic activity for DRM reaction.	[195]
Ni-Mo_2C	SiC									
Ni-Mo_2C	CNTs	SM: – RT: –	DRM 2021	–	P: 1atm / T: 850^0C GHSV: 60000$cm^3/g^{-1}h^{-1}$ Flow: − TOS: 36h	CH_4: 1 CO_2: 1	CH_4: 73.0 CO_2: 84.0	H_2: – CO: – H_2/CO: 84.0	In DRM reaction over Ni-Mo_2C catalyst with a very high Ni/Mo molar ratio, Ni also participates in the redox cycle.	[130]
β-Mo_2C-Ni	Al_2O_3	SM: MM RT: FBR (DBD)	DRM 2021	T: 700^0C TR: 1-5^0C/min CH_4/H_2: 20vol% Flow: 150ml/min TC: 2h MMT: 60mins	Input Power: 112W T: 470^0C GHSV: − WHSV: 50000ml/g/h Feed flow: 100ml/min TOS: 675mins	CH_4: 1 CO_2: 1 Ar: 8	CH_4: 82.5 CO_2: 84.6	H_2: 92.7 CO: 89.5 H_2/CO: −	β-Mo_2C catalyst improves CO_2 conversion and H_2 and CO selectivity and reduces coking and selectivity of unwanted or higher HCs species in DBD plasma-assisted DRM. Input power in DBD plasma assisted DRM significantly affects the substrates' (CH_4 and CO_2) conversion and catalytic activity of β-Mo_2C.	[2]

Note: SSR: Solid-solid Reaction; CHR: Carbo-hydrothermal Reduction; MM: Mechanical Mixing; PFR: Plug Flow Reactor; CSTR: Continuously Stirred Tank Reactor; FBPFR: Fixed Bed Plug Flow Reactor; MMT: Mechanical Mixing Time.

The reaction of Mo metal with the support generates different in-active species, depending upon the support used for the Mo_2C catalyst [177]. The production of these in-active species results in reducing the amount of active species (Mo_2C) on the surface of the support [177]. This eventually affects the activity of supported MC catalysts for DRM reaction [177]. Although, Mo_2C/ZrO_2 is more stable than Mo_2C/Al_2O_3, but the greater number of Mo_2C particles or active sites on Al_2O_3 support makes the Mo_2C/Al_2O_3 catalyst a better choice in terms of activity, for DRM reaction [177]. The surface area of $Mo_2C/\gamma\text{-}Al_2O_3$ catalyst in DRM reaction remains intact in comparison when using other metal oxide supports [167]. $Mo_2C/\gamma\text{-}Al_2O_3$ is thermally more stable as well [167]. Oxidation is the main reason for the deactivation of $Mo_2C/\gamma\text{-}Al2O_3$ catalyst, stability time against oxidation can be increased by increasing the wt.% of Mo_2C or catalyst bed thickness by dilution [167]. La addition in Co-$Mo_2C/\gamma\text{-}Al_2O_3$ in the range 1-3wt% is beneficial in preventing catalyst deactivation due to oxidation in DRM reaction, and side reactions can also be suppressed which in-turn helps in increasing H_2 yield as well [192].

The $Mo_2C/\gamma\text{-}Al_2O_3$ is active, but Mo_2C/ZrO_2 is the most stable catalyst DRM reaction [167]. The amphoteric nature of ZrO_2 catalyst support is very beneficial in the adsorption and conversion of DRM reactants [157]. The $\alpha\text{-}MoC_{1-x}$ and $\beta\text{-}Mo_2C$ with similar loading over ZrO_2 support are similar in catalytic activity for DRM reaction [142]. The activity of Mo_2C/ZrO_2 catalyst for DRM reaction can be improved by using a promoter or by increasing the reducibility of MoO_x precursor (used for synthesizing Mo_2C by TPR method) [177]. A better interaction between the active metal of the catalyst and the support improves the catalytic action of a supported catalyst [177]. This interaction can be improved by using a low temperature for the calcination of the catalyst [177]. The Mo_2C/ZrO_2 calcined at 400^0C gives 11% more CO_2 conversion in DRM reaction, than a Mo_2C/ZrO_2 catalyst calcined at 600^0C [177]. The dispersion of the Mo_2C catalyst over ZrO_2 support can be increased by pre-heating ZrO_2 support at 400^0C [157]. Unlike the Mo_2C/Al_2O_3 catalyst, increasing the Mo_2C loading percentage in Mo_2C/ZrO_2 negatively impacts the catalytic potential of ZrO_2 itself for DRM reaction [157]. Loading of Mo_2C catalyst over ZrO_2 support, blocks the sites of ZrO_2, which are active for DRM reaction [157]. The Mo_2C/ZrO_2 catalyst with small percentage loading of Mo_2C is more active for DRM reaction because the catalyst and support both participate in the conversion of DRM substrates [157]. But Mo_2C/ZrO_2 catalyst with small and high percentage of Mo_2C loading gives the same DRM reaction yield due to the sintering effect [157]. The ZrO_2 support can reduce the sintering effect to some extent [157]. The formation of MoO_2/CO and amorphous C in DRM

reaction over Mo_2C/ZrO_2 catalyst indicates that the net effect of C containing species has been increased and decreased, respectively [157]. The formation of MoO_2 in DRM reaction over Mo_2C/ZrO_2 catalyst stops further catalysis.

La_2O_3 is another potential support that can be used for Mo_2C catalyst. Zhang et al. [170] compared the catalytic role of Ni-Mo_2C/La_2O_3 with that of unsupported Ni-Mo_2C catalyst for DRM reaction. In both the catalysts, Ni and Mo content were found to be 4.4% and 14.6%, respectively. The obtained size of β-Mo_2C particles was 27nm and 18.5nm for Ni-Mo_2C and Ni-Mo_2C/La_2O_3 catalyst, respectively. Higher DRM substrate conversions were observed over Ni-Mo_2C/La_2O_3 catalyst at the temperature from 650^0C to 750^0C (Figure 12 (a-b)[170]). But above 750^0C, Ni-Mo_2C surpassed Ni-Mo_2C/La_2O_3 catalyst (Figure 12 (a-b)[170]). In terms of stability, Ni-Mo_2C/La_2O_3 catalyst was found to be vastly superior to Ni-Mo_2C for DRM reaction (Figure 12 (c-e)[170]). Conversion of β-Mo_2C to MoO_2 was found to cause Ni-Mo_2C to be inactive earlier than Ni-Mo_2C/La_2O_3. So, La_2O_3 as support was found helpful in preventing the oxidation of β-Mo_2C in the DRM reaction. To improve the stability of ZrO_2 support in Ni-Mo_2C/ZrO_2 catalyst, Tao et al. [194] used different mole% of La_2O_3. In DRM reaction over Ni-Mo_2C/La_2O_3-ZrO_2 catalyst, H_2/CO selectivity is good, but is less than 1 due to RWGSR (Equation 13). The H_2/CO selectivity increases in proportion with the reaction temperature and conversion of DRM substrates because at high temperature the oxidation-re-carburization cycle of Mo_2C becomes more dominant than the RWGSR (Equation 13). The catalytic activity of Ni-Mo_2C/La_2O_3-ZrO_2 for DRM reaction depends upon the surface area and concentration of oxygen vacancies (Vö) on the surface. The catalyst surface area is inversely proportional to the mol% of La_2O_3 in Ni-Mo_2C/La_2O_3-ZrO_2, while the concentration of Vö is directly proportional to the concentration of the c-$La_2Zr_2O_7$ crystal content in Ni-Mo_2C/La_2O_3-ZrO_2. The concentration of c-$La_2Zr_2O_7$ crystal content increases by increasing the La/Zr ratio or mole% of La_2O_3. The c-$La_2Zr_2O_7$ crystal helps in improving the dispersion of the active metal and reducing the activation energy of DRM reactants. Therefore, the mole% of La_2O_3 in Ni-Mo_2C/La_2O_3-ZrO_2 catalyst must be decided in a way that there is a balance between the surface area and concentration of c-$La_2Zr_2O_7$ crystal. The Vö help in the activation of CO_2 and form O_β or O^* species (Equation 76). The O^* species help in the activation of CH_4 (Equation 77). The Ni-Mo_2C/La_2O_3-ZrO_2 catalyst with specific mole% (7.5 mole%) of La_2O_3 is good for DRM reaction at high temperatures. Mesoporous silica molecular sieve (SBA-15) supported Ni-Mo_2C catalyst is more active and stable than a simple and Ni promoted Mo_2C for DRM reaction [191]. But oxidation of Mo_2C to MoO_2, $C_{(s)}$

deposition, and side reactions are still the problems that affect the catalyst performance and H_2/CO yield [191].

$$CO_2 + V\ddot{o} \longrightarrow CO + O^* \quad (76)$$

$$CH_4 + O^* \longrightarrow CO + 2H_2 \quad (77)$$

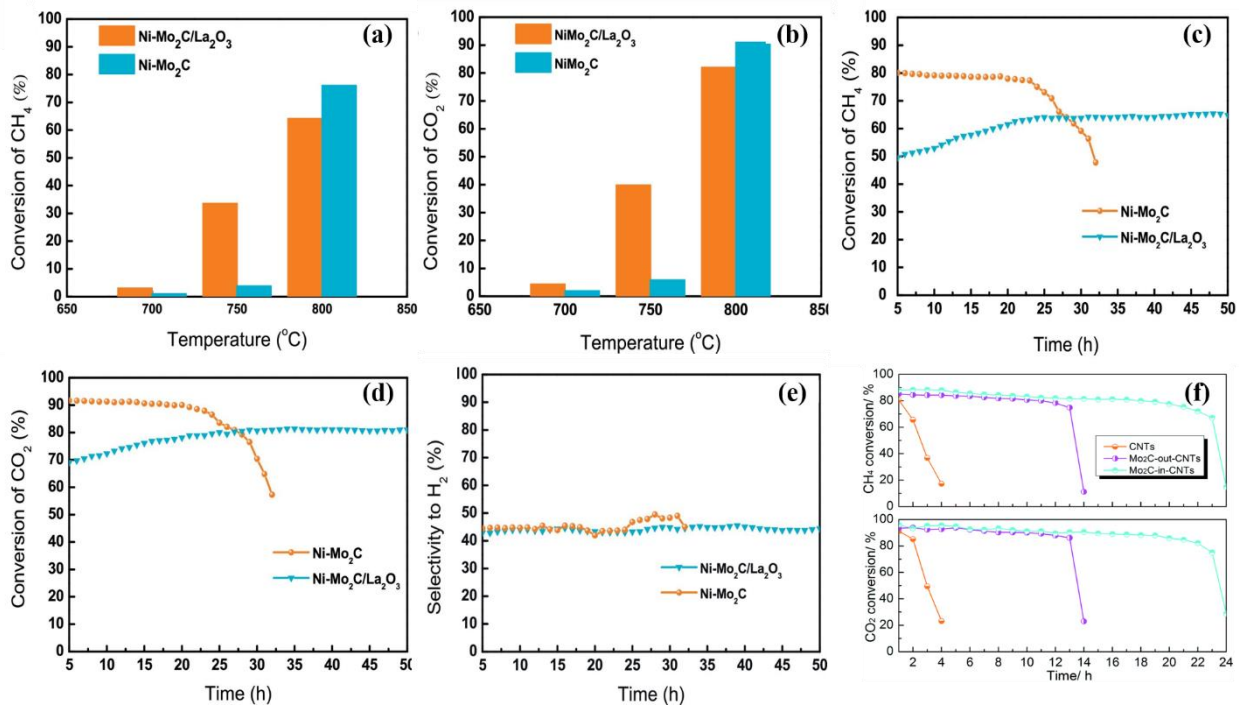

Figure 12. (a-b) Effect of reaction temperature on (a) CH_4 conversion and (b) CO_2 conversion in DRM over Ni-Mo_2C and Ni-Mo_2C/La_2O_3 catalysts, at P = 1atm, CH_4/CO_2 = 1 and F/W = 12000mL/g h. (c-e) Catalytic performance of Ni-Mo_2C and Ni-Mo_2C/La_2O_3 catalysts in DRM at T = 800°C, P = 1atm, CH_4/CO_2 = 1 and F/W = 12000mL/g. Reproduced from [170]. (f) Lifetime study of Mo_2C-out-CNTs and Mo_2C-in-CNTs catalysts in DRM at T = 850°C, P = 1atm, CH_4/CO_2 = 1 and WHSV = 18000$cm^3g^{-1}h^{-1}$). Reproduced from [188].

MgO is another potential support for the Mo_2C catalyst. However, similar to Mo_2C/α-Al_2O_3, oxidation causes catalyst deactivation [167]. Moreover, the Mo_2C/MgO suffers from sintering as well, as the reaction temperature increases [167]. The α-Al_2O_3 and MgO supports are not very effective in increasing the surface area and catalytic activity of Mo_2C for DRM reaction [187].

In DRM over Mo_2C/CeO_2 catalyst, Mo_2C/CeO_2 promotes the formation of CO more than H_2 therefore, H_2/CO is always less than 1 in DRM over Mo_2C/CeO_2 catalyst [142]. TiO_2 also promotes the catalytic role of MCs for DRM reaction [159].

Mo_2C/SiO_2 is more stable than an unsupported Mo_2C catalyst in DRM reaction [165]. According to the experimental work done by Silva et al. [124], the order of efficiency of SiC, Al_2O_3, and SiO_2 supports in upgrading the functionality of Ni-Mo_2C for DRM is SiC>Al_2O_3>SiO_2. The morphology of SBA-15 catalyst support in DRM reaction is immutable [191].

Carbonaceous structures, e.g., carbon nanotubes (CNTs), biochar (BC), and activated carbon (AC) are the other potential supports. Mo_2C/BC catalyst has good potential for DRM reaction and can be synthesized by the TPR method, without using any additional source like CH_4/H_2 gas mixture for carburization. Mo_2C/BC can be synthesized under the flow of an inert gas because the gases released from BC help in the carburization process [189]. Mo_2C/AC is better than Mo_2C/SiO_2 in avoiding RWGSR during DRM reaction [142]. In DRM over supported Mo_2C catalysts, oxidation is the reason for the catalyst deactivation [164, 167]. Encapsulating Mo_2C inside the CNTs rather than using CNTs as a support can help to prevent Mo_2C from oxidation for a longer period, in DRM reaction (Figure 12 (f)[188]) [188]. To improve this time further, a promoter (Ni or Co) can also be used [188]. In DRM reaction over Mo_2C/CNTs CO_2 conversion is always greater than CH_4 conversion (Figure 12 (f)[188]) because CNT_s react directly with CO_2 [188].

To investigate the effect of adding support on the role of Ni-Mo_2C in DRM, Duan et al. [166] prepared in-situ Ni-Mo_2C/Al_2O_3 catalyst and found it highly effective for DRM. Ni as promoter improves the catalytic activity of Mo_2C/Al_2O_3 for DRM reaction [193]. In Ni-Mo_2C/Al_2O_3 catalyst with a very low (0.2) Ni/Mo ratio in the structure, due to the presence of acidic sites on Al_2O_3 support, NiO forms and reacts with Al_2O_3 to form Ni aluminates ($NiAl_2O_4$) (Equation 78) [195]. $NiAl_2O_4$ species are inactive for catalyzing DRM reaction [195]. The formation of $NiAl_2O_4$ leaves Ni-Mo_2C/Al_2O_3 with a very small amount of Ni, which is not enough to dissociate CH_4 at the rate in balance with the CO_2 dissociation and to establish the redox cycle in DRM reaction [195]. Due to these reasons, Ni-Mo_2C/Al_2O_3 catalyst with a low Ni/Mo ratio become inactive in DRM reaction. Ni-Mo_2C/Al_2O_3 with high (0.3 or more) Ni/Mo ratio shows good/stable activity for DRM reaction [195]. High temperature favors the sintering of Ni and the formation of $NiAl_2O_4$ [195]. Therefore,

using low (700^0C-800^0C) temperature in synthesizing Ni-Mo_2C/Al_2O_3 by TPR of the precursor is favorable to prevent Ni sintering and $NiAl_2O_4$ formation, and as a result, the synthesized Ni-Mo_2C/Al_2O_3 can exhibit good catalytic activity for DRM reaction [195]. The catalytic activity of Ni-Mo_2C/SiC in DRM reaction is independent of the carburizing temperature used in its synthesizing process [195]. SiC itself is not an active catalyst for DRM reaction [159].

$$NiO + Al_2O_3 \longrightarrow NiAl_2O_4 \quad (78)$$

Effect of Synthesizing Method

Synthesizing method also needs to be considered for getting a catalyst with desired physicochemical characteristics [196]. MC catalysts are usually synthesized by TPR of the metal oxides (Figure 13[197-199]) [114, 115, 125, 127, 158, 170]. TPR method for synthesizing a MC involves the carbo-thermal reduction (CTR) of a metal precursor (metal salt or metal oxide) at an elevated temperature. A schematic of the TPR method for synthesizing a MC catalyst is presented in Figure 13[197-199].

To synthesize Mo_2C by the TPR method, a Mo precursor (MoO_2, MoO_3, etc.) is reduced under a mixture of C containing gas (CH_4, C_2H_6, C_3H_8, C_4H_{10} etc.) and H_2 [199, 200]. The synthesis of a supported Mo_2C catalyst by the TPR method involves (1) dissolving a Mo salt in water or an aqueous stabilizer ($C_6H_8O_7$ etc.) solution (2) immersing the support material (Al_2O_3 etc.) in it, (3) calcining the impregnated solid in the air, and (4) carburizing finally carburizing the solid [54, 155, 167, 171]. The surface of the Mo_2C, synthesized by the TPR method, is usually contaminated by polymeric C. However, the H_2 treatment helps purify the Mo_2C synthesized by the TPR method.

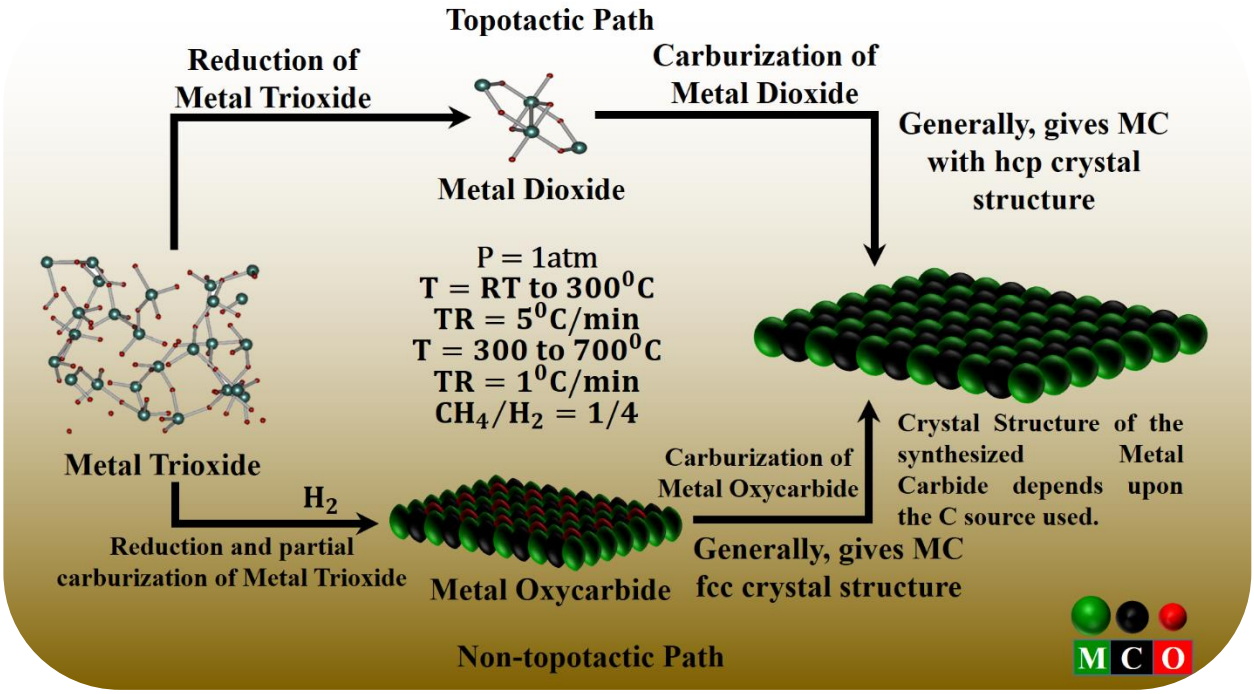

Figure 13. Schematic of the TPR method, for synthesizing a metal carbide catalyst. Developed based on [197-199].

In the synthesis of Mo_2C by the TPR method, the carburization process governs the morphology, specific surface area, and catalytic performance of the end-product. Roohi et al. [169] found temperature, the composition of carburizing gas, and metal content in the metal oxide (the precursor) as the key parameters, that control the carburization process and eventually the amount of C content in the final Mo_2C product. Overindulgence of C content in Mo_2C structure blocks the pores and decreases surface area, which reduces the catalytic activity/stability of the MC.

The process used for preparing the metal oxide (the precursor) also influences the catalytic properties of the MC [201]. The impregnation technique is the most used technique for the synthesis of metal oxides (the precursors) [114, 115, 125, 127, 158, 170]. The precursors, synthesized through impregnation, aggregates with time [201]. So, the end-product lacks in uniform distribution of the functional species on the support [201]. For the better dispersion of active species on the support, Duan et al. [166] used solution-combustion-method for preparing NiMo-Al_2O_3 precursors, and synthesized Ni-Mo_2C/Al_2O_3 catalysts, with different Mo molar%, by in-situ (by using DRM substrates (CH_4/CO_2=1) as the carburizing gas) TPR of NiMo-Al_2O_3 precursors. Duan et al. ratified in-situ synthesized Ni-Mo_2C/Al_2O_3 catalyst efficacious for DRM reaction.

TPR of a precursor (pretreated by flowing a gas over it at a specific temperature and pressure) gives different phases of the MC, depending upon the temperature used for its carburization [163]. Nitriding (flowing NH_3 at atmospheric pressure and 973K temperature) of MoO_x (the precursor) followed by TPR at 1173K and 973K results in the formation of η-Mo_3C_2 and α-Mo_2C, respectively [163]. According to Tsuji et al. [142], nitridation of the MoO_x followed TPR results in the formation of only α-MoC_{1-x} with fcc structure (Figure 1 (a)[54]). Direct TPR of MoO_x gives only β-Mo_2C with hcp structure (Figure 1 (c)[54]) [142]. Nitridation of the metal oxides before TPR helps in synthesizing more active/stable Mo_2C catalysts for DRM reaction [126]. Calcination of catalyst precursor is a very important step in synthesizing a catalyst with desired characteristics. The experimental study of Brungs et al. [171] ratified that calcination of MoO_x precursor for a very long period of time followed by TPR, results in Mo_2C catalyst with very poor stability for DRM reaction [171].

TPR of MoO_x at 973K, 923K and 873K gives only β-Mo_2C [163]. The β-Mo_2C synthesized by carburizing MoO_x at the temperature 923K and 873K gives the highest and least CH_4 conversion, respectively, when used as a catalyst for CH_4 reforming reaction. Ni-Mo_2C catalyst with Ni/Mo mole ratio of 75/25, synthesized by carburization of Ni-MoO_x at low temperature (773K), gives high CH_4 conversion and H_2 yield in DRM reaction [164]. Ni-Mo_2C catalyst, with a small Ni/Mo mole ratio (25/75) and synthesized by carburizing Ni-MoO_x at high temperature (813K), gives a very good H_2 yield with minimum $C_{(s)}$ formation in DRM reaction [164]. Ni-Mo_2C catalyst precursor (Ni-MoO_x) synthesized by the co-precipitation (CP) method can be carburized at a temperature 15^0C less than the temperature required to carburize Ni-MoO_x synthesized by mechanical mixing (MM) [173]. Ni-Mo_2C resulting from the carburization of the Ni-MoO_x (synthesized by CP) shows better dispersion of the Ni particles, and also high catalytic activity for DRM reaction (Figure 14 (A-C)[173]) [173]. The temperature required to carburize Ni-MoO_x (synthesized by CP or MM) is less than the temperature required to carburize MoO_3 [173].

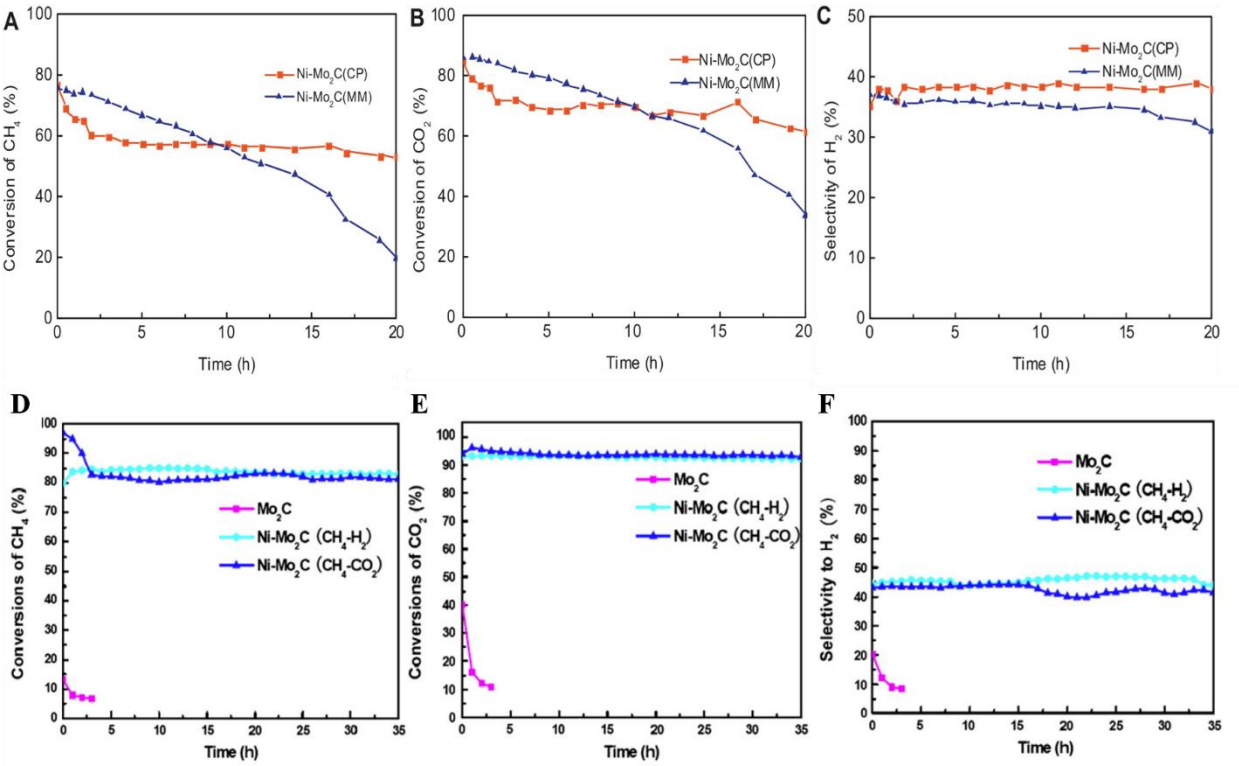

Figure 14. (A-C) Lifetime study of Ni-Mo_2C (synthesized by using a precursor, which itself was synthesized by mechanical mixing (MM)) and Ni-Mo_2C (synthesized by using a precursor, which itself was synthesized by co-precipitation (CP)) catalysts in CH_4/CO_2 reforming at P = 1atm and W/F: 0.24gscm^{-3}. (A) conversion of CH_4, (B) conversion of CO_2, and (C) selectivity to H_2. Reproduced from [173]. (D-F) Activity and stability of Ni-Mo_2C catalysts, synthesized in-situ (using CH_4/CO_2 gas mixture for the carburization of Ni-MoO_x), and by TPR method (using CH_4/H_2 gas mixture for the carburization of Ni-MoO_x) in DRM at T = 850°C, P = 1 atm, CH_4/CO_2 = 1 and W/F = 0.6gscm^{-3}). (D) conversion of CH_4, (E) conversion of CO_2, and (F) selectivity to H_2. Reproduced from [129].

Mo_2C catalyst synthesized by using diluted carburizing CH_4/H_2 gas mixture in the TPR method is more active than Mo_2C synthesized by using pure carburizing CH_4/H_2 gas mixture [193]. Using a C_2H_6/H_2 gas mixture instead of a CH_4/H_2 gas mixture for the carburization of metal oxide lowers the temperature required for the carburization process [171]. Mo_2C synthesized by TPR, and H_2/C_2H_6 mixture as carburizing gas is very active for catalyzing DRM reaction [159]. Ni-Mo_2C catalyst synthesized in-situ (using CH_4/CO_2 gas mixture for the carburization of Ni-MoO_x) and by

TPR method (using CH_4/H_2 gas mixture for the carburization of Ni-MoO_x) show similar activity/stability for DRM reaction (Figure 14 (D-F)[129]) [129].

Roohi et al. [169] synthesized nine Mo_2C/Al_2O_3 catalysts by two-step-impregnation-TPC method. All nine samples were synthesized by using the same precursor (MoO_3/Al_2O_3), but at different conditions (temperature and composition of carburizing gas) for the carburization process. The catalytic role of only three catalysts (with minimum excessive C content) was investigated for DRM reaction. The catalysts were comparable in terms of activity for DRM reaction. Their stability started to decline over time. This loss in stability was the result of the conversion of the carbide phase into the oxide phase at atmospheric pressure. So, the use of different conditions (temperature and composition of carburizing gas) for the carburization of the same precursor did not help in synthesizing a supported MC catalyst with better oxidation resistance in the DRM reaction.

The Mo_2C synthesized by the TPR method and solution-derived (SD) synthesizing method has smaller crystallite size and larger surface area, respectively [143]. The catalysts synthesized by either of the processes have excess C [143]. The excess C from Mo_2C, synthesized by the SD method, can be removed by H_2 treatment [143]. By increasing the temperature and time for H_2 treatment, crystallite size increases and surface area decreases [143]. In Mo_2C, synthesized by TPR, temperature and time for H_2 treatment affect only particle size and surface area, while excess C content remains unchanged [143]. Excess C improves the catalyst's resistance against oxidation in DRM reaction [143]. Regardless of the excess C, Mo_2C synthesized by the SD method is less stable in DRM reaction, but substrate conversions and H_2/CO yield are high [143].

The carbothermal reduction method can be used to synthesize different phases of Mo_2C [155]. The phase of the Mo_xC_y molecule, resulting from the carbothermal reduction process, depends upon the precursor used, the method used for synthesizing the precursor, and the gas used for the reduction of the precursor [155]. The carbothermal reduction process gives only β-Mo_2C regardless of the precursor used when applying H_2 gas for reducing the precursor [155]. While the use of Ar may result in the mixture of α-MoC_{1-x} and β-Mo_2C depending upon the precursor used, and the method used for synthesizing the precursor [155].

Gavrilova et al. [161, 202] synthesized Mo_2C by the thermal decomposition of the xerogel Mo blue. The surface area and phase of the Mo_2C product, synthesized by this method depends upon the

molar ratio of the reducing-agent (ascorbic acid ($C_6H_8O_6$) or hydrochloric acid (HCl)) to Mo source (ammonium heptamolybdate ($(NH_4)_6Mo_7O_{24}\cdot 4H_2O$)) used in synthesizing the precursor (xerogel Mo blue). The thermal decomposition of xerogel Mo blue, synthesized by using the reducing-agent/Mo source ratio of 0.6-1.0, gives β-Mo_2C. This β-Mo_2C has good potential as a catalyst for DRM reaction.

Other than CH_4/H_2 gas mixture, CH_4/CO_2 gas mixture, C_2H_6/H_2 gas mixture, and CNTs can also be used as the C source to synthesize Mo_2C [168]. A precursor with a maximum 60 wt.% Mo content can be carburized by using CNTs as the C source, and it also suggests that lowering the Mo content easier the carburization [168]. Gao et al. [168] synthesized β-Mo_2C/CNTs composite by solid-solid reaction. The specific surface area, pore volume, and dispersion of active species in β-Mo_2C/CNTs decreases directly with increasing Mo content in the precursor, and vice versa for the particle size. However, the catalytic activity and oxidation resistance of β-Mo_2C/CNTs do not follow any such trend. The β-Mo_2C and CNTs individually show no activity for DRM reaction, they both work in synergy for catalyzing DRM reaction, and β-Mo_2C/CNTs with 30wt% Mo content is the most active and stable catalyst for DRM, but its activity decreases over time. The activity/stability of β-Mo_2C/CNTs increases with increasing DRM reaction temperature. However, WHSV (weight-hour space velocity) negatively impacts the stability of β-Mo_2C/CNTs. The β-Mo_2C/CNTs is more active/stable than β-Mo_2C and Ni-β-Mo_2C (synthesized by conventional TPR method), for DRM reaction.

Kurlov et al. used delaminated MoO_3 sheets and C spheres as Mo source and C source, respectively, to synthesize β-Mo_2C/C by carbothermal hydrogen reduction (CHR) method [190]. The synthesized β-Mo_2C/C showed two different morphologies: nano particles and nanorods. In the DRM reaction, β-Mo_2C/C was oxidized to $Mo_2C_xO_y$ in a very short time. The $Mo_2C_xO_y$ species formed by the oxidation of β-Mo_2C/C nanorods were highly rich in O elements, and these species significantly reduced the H_2/CO ratio by increasing the rate of RWGSR.

There are various methods other than the TPR for synthesizing the Mo_2C, but the catalytic potential of Mo_2C synthesized by these methods, for CH_4 reforming reactions, has not been explored yet. Using MoO_x-amine hybrid precursor helps synthesize the Mo_2C with crystallinity, structural forms (1D, 2D, or 3D), and size of interest [203]. Different amines can be used for forming the MoO_x-

amine hybrid precursors, including aniline, dopamine, glycine, dodecyl amine, imidazole, 4-Cl-o-phenylenediamine, 1,6-hexanediamine, and 1,2-dodecanamine [203-206]. The amine molecules serve as the sources of C, reducing agents, and structure-guiding agents [204]. MoO_x-amine hybrid precursors are the precipitates, formed during the chemical reaction between the Mo-salts and amine molecules in an acidic environment. These MoO_x-amine hybrid precursors grow anisotropically. The pyrolysis of MoO_x-amine hybrid precursors results in the synthesis of Mo_2C. The Mo:amine ratio and the pyrolysis temperature influence the crystallinity and structural form of the final carbide product [203, 205]. The $\mathrm{Mo:amine} < 1.5$ and $\mathrm{Mo:amine} = 2$ give β-Mo_2C and α-MoC_{1-x}, respectively [203]. The properties of the amine molecules also affect the final carbide product [203]. Koizumi et al. [207] heated a mixture of MoO_3 and xylene at 790^0C and 1atm under $\mathrm{Ar/H_2} = 85/15$ mixture for 1h and synthesized the interconnected Mo_2C nanoflakes (5-15nm) with 3D origami-like structures by chemical vapor deposition (CVD). Mondal et al. [208] synthesized Mo_2C particles (sized 5-15nm) incorporated on carbon nanosheets by the calcination of a dried mixture containing $C_6H_{12}O_6$, $(NH_4)_6[Mo_7O_{24}]\cdot 4H_2O$, and $(NH_4)_2CO_3$, under the N_2 atmosphere.

High-energy mechanical ball milling method helps in synthesizing the MCs powder with size micron or submicron [209-212]. The process involves the milling of a mixture containing M source powder (could be pure M as well) and C source powder (could be pure C or graphite as well). Different milling techniques, including planetary mills and abrasive mills, can be utilized [213-215]. Although, high-energy mechanical ball milling is an effective method for synthesizing nanostructured MCs [209, 210], but contamination, long milling time (usually more than 12h), high energy consumption, and the production of relatively small amounts of the powders are the drawbacks of this simple technique. It is also very important to perform the milling process under an inert atmosphere to prevent the oxidation of Ms. The high-energy mechanical milling mechanically activates the substrates which in turn induces the chemical reaction between the substrates, and the process is then termed as mechano-chemical (MC) method. High-energy mechanical ball milling may also be considered a preliminary step for further processing, such as synthesis in molten salt, arc plasma etc. [216].

A highly cost-effective and widely used method for synthesizing the MCs is molten salt synthesis (MSS) [217]. In this method, reactants are first mixed with salt (usually a mixture of two or more salts is used) and then dissolved in it at a high temperature. In this method, molten salt acts as a

solvent to serve the chemical reactions between the reactants while controlling the characteristics (particle size and shape) of the final product [217]. Yang et al. [217] synthesized Mo2C (with a particle size of 0.5–1.0 um) contaminated with Mo metal. In their study, they used a mechano-chemical method to synthesize Mo2C. Firstly, Mo and C powders were mechanically activated under an argon atmosphere using a high-energy planetary mill (10 mm hardened steel ball, ball-to-powder ratio: 5:1, and rotational speed 1200 rpm). After milling, the mechanically activated powder was mixed with a KCl and NaCl ($\text{molar ratio} = 1:1$) mixture (60wt%) and heated at 1000^0C for 1h. The reaction product was then allowed to be cold down to room temperature in the air. To obtain the final product (free of salt impurities) the product was boiled several times in water. Hu et al. [218] impregnated carbon fiber paper (CFP) with nickel ions, and mixed MoO_3 with C black and salt (NaCl and KCl) particles. After this, combined impregnated CFP and mixture (containing MoO_3/C-black/NaCl/KCl), and finally heated it at 1000^0C for 309h to synthesize CFP supported Ni doped Mo_2C. Ge et al. [219] used Mo as a cathode, Pt as an anode, and C as a counter electrode to synthesize Mo_2C, and called the process as electrochemical method. A salt mixture (containing LiCl, NaCl, and Na_2O_3) was used to serve the chemical reaction between Mo and C at 900^0C. Chen et al. [220] combined MSS and the electroreduction method to synthesize the Mo_2C with a lamellar structure. During the process, a cathode (a Mo foil) and an anode (S_nO_2) were immersed in a crucible filled with a $CaCl_2$ and CaO mixture, and finally was heated up to 850^0C for 5h under the CO_2 atmosphere. Salts to be used in the MSS method of MCs must be heated in air and Ar at 200^0C-400^0C to remove the moisture and O_2, respectively. Although the synthesis of MCs using the MSS method requires a low processing temperature, the oxidation of M powders during the process leads to an impure final product. This drawback has made the method less popular among researchers.

Effect of Reaction Conditions

DRM reaction over a MC catalyst is examined in the temperature range of 1120K to 1220K [115, 124, 125, 127, 158, 166, 169-171]. The catalytic activity of all (simple, promoted and supported) β-Mo_2C for DRM reaction increases with increasing temperature (Figure 12 (a-b)[170]) [115, 156, 159, 166, 170, 189, 193]. High temperature is good to keep Mo_2C stable/active in DRM reaction because high temperature is beneficial for the carburization/re-carburization process which in turn helps in the regeneration of Mo_2C, but metal sintering limits the highest temperature that can be applied [159, 160, 167]. Low temperature is advantageous for oxidation reaction and leads to the deactivation of Mo_2C due to oxidation in DRM reaction [160]. Low temperature also accords $C_{(s)}$

formation in DRM reaction over Mo_2C catalyst [156]. The temperature for DRM reaction over a MC catalyst must be moderate (normally applied 800^0) to establish the redox cycle or to keep the catalyst active/stable for the whole TOS. The percentage conversion of DRM substrates over a MC catalyst decreases with decreasing temperature and vice versa (Figure 12 (a-b)[170]) [160]. A low temperature value (usually 800^0C or 1173K) at which the CH_4 and CO_2 conversion remain constant over time, is good for DRM reaction over MC catalysts [160]. However, the temperature at which the conversions decline over time is called deactivation temperature [160]. At this temperature, the oxidation of MC catalyst starts, and proceeding the reaction without increasing the temperature eventually results in the permanent deactivation of the catalyst [160]. The deactivation temperature of the Mo_2C catalyst in DRM reaction must be very low for a desirable catalytic function, and this can be achieved by decreasing Mo_2C wt.% loading or decreasing pressure or increasing molar feed velocity (G), but at constant GHSV [160]. Duan et al. [166] observed the highest activity of Ni-Mo_2C/Al_2O_3 catalyst for DRM reaction at 800^0C. But Brungs et al. [171] found that very high temperature changes γ-Al_2O_3 to α-Al_2O_3, which results in compromising the stability time of Mo_2C for DRM.

Not only temperature but the operating pressure also affects the lifetime of the Mo_2C catalyst for DRM reaction [115]. DRM reaction over MC catalysts has been studied in the pressure range 1bar to 8bar [115, 125, 127, 158, 169, 170]. At ambient or atmospheric pressure, DRM substrate (CO_2) oxidizes MC (Mo_2C) and changes the MC phase into the metal oxide (MoO_2) phase (Figure 10 (D)[168]) [115, 122, 169]. The conversion of DRM substrates is always higher at elevated pressure [115, 189]. Claridge et al. [115] studied DRM reaction over β-Mo_2C and $Mo_2C/Al2O_3$ catalysts. At 1 bar, both the catalysts sustained similar activity and stability for 8h. After 8h, their activity started to decline, and they became almost inactive in the next 20h. This happened because at low pressure carbide phase could not remain stable and the MC (Mo_2C) was converted to its respective metal oxide (MoO_2), due to oxidation caused by CO_2. At 8.3bar, homogeneous unwavering activity/stability and no macroscopic $C_{(s)}$ deposition were observed for both the catalysts, for more than 72h on the stream. At low pressure, only bulk oxidation is the reason for the deactivation of the Mo_2C catalyst in the DRM reaction, and no $C_{(s)}$ deposits on the surface of the Mo_2C. In DRM reaction over Mo_2C catalyst at atmospheric pressure, the rate of oxidation of Mo_2C is faster than the re-carburization of MoO_2 [115]. This indicates that Mo_2C molecules at the surface of the catalyst bed are the first to be oxidized [115]. This oxidation front then moves further deep into the catalyst

bed with time due to the difference in the rates of the reactions, involved in the redox cycle of the catalyst in the DRM reaction. At high pressure, the time for which reactants interact with the catalyst changes. This creates a balance between the intensity of the reactions of the oxidation-reduction cycle. So, the change in the residence time of the reactants is the reason for long-term stability of the Mo_2C catalyst in DRM reaction at elevated pressure. York et al. [114] also discovered the same cause for the deactivation of β-Mo_2C and $Mo_2C/Al2O_3$ catalysts in DRM at 1bar pressure. At elevated pressure, no decline was observed in the activity of both catalysts. So, at low pressure, oxidation of the Mo_2C catalyst halts the DRM reaction [114, 115, 122, 125, 127, 156, 169]. DRM at low pressure reduces the specific surface area of the Mo_2C catalyst over time and ultimately ceases its catalytic operation [156]. LaMont et al. [160] proved that the stability of Mo_2C catalyst in DRM reaction at high pressure is neither because of change in the residence time of reactants, nor because increased pressure favors the redox mechanism. But low mass transfer rates of reaction products form the catalyst surface at high pressure makes Mo_2C a stable catalyst for DRM reaction. The high pressure used for DRM reaction over Mo_2C catalyst increases the deactivation temperature of Mo_2C as well [160]. High pressure does not affect the stability ratio (R_s, Equation 79) and DRM substrates' conversions. The kinetics of oxidation and re-carburization reaction can be matched by keeping the R_s above 0.8 [154]. A very high pressure difference between the inlet and outlet of the reactor during DRM reaction over Mo_2C catalyst is the indication of the coke formation in DRM [156].

$$R_s = \frac{P_{H_2} + P_{CO}}{P_{CO_2} + P_{H_2O}} \tag{79}$$

Using a supported Ni-Mo_2C catalyst for DRM at atmospheric pressure can also prevent the oxidation of Mo_2C [170]. Re-carburization of MoO_2 depends upon CH_4 activation. At ambient pressure, the rate of CH_4 dissociation is always smaller than that of CO_2 in DRM over Mo_2C catalyst. So, at low pressure oxidation of Mo_2C is more expeditious than re-carburization of MoO_2.

DRM feed (CH_4/CO_2) ratio also influences the catalyst's function. According to Silva et al. [124], a very low CH_4/CO_2 feed ratio negatively affects the performance of Ni-Mo_2C/SiC, but with a very high DRM feed ratio the activity of this catalyst initially declines but then stabilizes and remains constant. When using stoichiometric DRM feed ratio over Mo_2C catalyst, R_s is zero, oxygen species produced by CO_2 dissociation can easily react with Mo_2C to form MoO_2 (Equation 64), and at $R_s =$

0 coking also occurs at the bottom of the catalyst bed [164, 167, 176]. According to Darujati et al. [176], the reaction between CO_2 and Mo_2C $C_{(surface)}$ is the rate determining step. R_s must be 0.8 or above to prevent Mo_2C from oxidation [176]. Introducing CO with a stoichiometric CH_4/CO_2 ratio gives the R_s of 1.5, which shifts RWGSR equilibrium from CO to H_2, and the oxidation of Mo_2C can be avoided [167, 176]. Increasing G does not increase CH_4 conversion in DRM over Mo_2C catalyst, but increasing R_s value and inverse space velocity (ISV) of CH_4 enhances CH_4 conversion, but the deposition of the produced $C_{(s)}$ (due to CH_4 dissociation) on the catalyst surface can deactivate catalyst [176]. R_s value beyond 3.0 no more prevents the oxidation of Mo_2C, because oxidizing gases can easily react with Mo_2C [167, 176].

GHSV in DRM reaction also has an influence on the activity of MC catalyst [115]. According to Claridge et al. [115], low GHSV improves the activity and stability of Mo_2C catalyst for DRM reaction [115]. The results of the study of Li et al. [189] were also in agreement. But LaMont et al. [160] later proved that GHSV has no effect on the stability of Mo_2C catalyst in DRM reaction. According to Sehested et al. [156], the affinity of $C_{(s)}$ formation in DRM reaction over Mo_2C catalyst at low temperature, can be reduced by adjusting the CH_4/CO_2 ratio in such a way that O/C=1.7 and H/C=0.75 with constant GHSV [156]. Using conditions, such as high temperature, high pressure or increasing G at constant GHSV for DRM reaction can prevent the bulk oxidation of the Mo_2C catalyst.

In addition to temperature and pressure, the presence of impurities particularly sulfur (S) affects catalysis. S adsorbs on the catalyst surface and blocks the active sites. S can also react with the active catalyst species or substrates to form catalytically inactive species. Reaction feed must be S free for a successful catalysis. Sulfur adsorbs on Mo_2C surface and forms inactive CS_2 species by reacting with $C_{(surface)}$, the catalytic activity of Mo_2C for DRM and DRCO (dry reforming coupled with partial oxidation) reaction declines [187]. Once the S adsorption reaches a saturation point, the activity of the Mo_2C catalyst for DRM reaction becomes stable [187]. The effect of S can be minimized by increasing the reaction temperature [187].

Mo_2C as a Catalyst for Plasma-assisted/Non-thermal DRM Reaction

The use of non-thermal plasma (NTP) or di-electric barrier discharge (DBD) plasma can overcome or mitigate the high temperature (1120-1220K) requirement to process DRM. Catalyst deactivation

due to metal sintering in thermal catalytic DRM is also related to applying high thermal energy (1120-1220K) to complete the process, which can also be avoided by using NTP plasma instead of thermal energy to process the reaction because NTP plasma makes DRM possible at low (room) temperature [221].

The electron (e^-) energy required to dissociate CH_4 and CO_2 is 4.5eV and 5.5eV, respectively [222]. DBD plasma generates energy in the range 1-10eV, that is high enough to break C—H and C═O [223]. In contrast to thermal catalytic DRM, CH_4 conversion in DBD plasma-assisted DRM is always higher than CO_2, because of direct decomposition of CH_4 to solid $C_{(s)}$ and H_2 (Equation 81) [221]. The minimum e^- energy for direct CH_4 dissociation to its constituents is 10eV, and DBD plasma is capable of generating this amount of energy [221, 224]. On the other hand, direct dissociation of CO_2 to CO and O (Equation 82), requires a minimum e^- energy of 11.9eV [224]. The imbalance between the conversion of both the DRM substrates (CH_4 and CO_2) creates a disproportion between $C_{(s)}$ production and removal rate. Excessive $C_{(s)}$ production and deposition on the inner walls of the reactor tube cause clogging of the reactor tube and ultimately cease the process. So, an ideal catalyst for DBD plasma-assisted DRM should be the one that can reduce coking by equalizing the $C_{(s)}$ production and removal rate, or in other words: can improve CO_2 dissociation to develop an equilibrium between CH_4 and CO_2 conversion. A MC, because of having a naturally very high affinity towards oxides, is one of the best choices for playing such a catalytic role.

The reactions, e^- impact vibrational excitation and dissociation, are responsible for the conversion of CH_4 to $CH^*_{x,x=1-3}$ ($*=$ excited state) or to $CH_{x,x=1-3}$ and H^* or H_2 (Equation 80), or directly to $C_{(s)}$ and H_2 (Equation 81), depending upon the e^- energy [221, 222, 224-227]. The combination of $CH^*_{x,x=1-3}$ or $CH_{x,x=1-3}$ species leads to the formation of higher HCs. The e^- impact vibrational excitation and dissociation reactions are also responsible for the conversion/dissociation of CO_2 to CO or CO^* and O or O^- (Equation 82) [224]. At least 12 elementary e^- vibrational-excitation/dissociation reactions are possible in DBD plasma-assisted DRM [221, 224-227].

$$CH_4 + e^- \longrightarrow (CH^*_{x,x=1-3} \text{ or } CH_{x,x=1-3}) + (H^* \text{ or } H_2) + e^- \quad (80)$$

$$CH_4 + e^- \longrightarrow C_{(s)} + 2H_2 + e^- \quad (81)$$

$$CO_2 + e^- \longrightarrow (CO^* \text{ or } CO) + O^- \text{or } (O + e^-) \quad (82)$$

Addition of β-Mo_2C into Ni/Al_2O_3 is helpful in weakening the Ni-Al_2O_3 interaction and preventing the formation of $NiAl_2O_4$ species, which are inactive for catalyzing DRM [2, 195]. Treating Mo_2C-Ni/Al_2O_3 catalyst at 500^0C for 1h by flowing 100ml/min 15vol% CH_4/H_2 gas mixture over it, before using it for DRM, induces Ni-Mo_2C interface [2]. Strong Ni-Mo_2C interaction in Mo_2C-Ni/Al_2O_3 results in the formation of Ni_3C species, which in-turn improves Ni dispersion over Al_2O_3 support [2]. In DBD plasma-assisted DRM over Mo_2C-Ni/Al_2O_3 catalyst, CH_4/CO_2 conversion, product (H_2 and CO) selectivity, and H_2/CO ratio are better than DBD plasma-assisted DRM over Ni/Al_2O_3 catalyst (Figure 15 (A-D)[2]) [2]. Improved Ni dispersion over Al_2O_3 support and Ni-Mo_2C interaction are the reasons for the better catalytic activity of Mo_2C-Ni/Al_2O_3 than Ni/Al_2O_3 [2]. Coking resistance and stability of Mo_2C-Ni/Al_2O_3 catalyst is also higher than that of Ni/Al_2O_3 (Figure 15 (E)[2]), in DBD plasma-assisted DRM [2]. This is because the $C_{(s)}$ species (filamentous and graphitic), which are inactive and difficult to oxidize, are produced more in the case of Ni/Al_2O_3 catalyst and deposited on its surface [2]. In the case of Mo_2C-Ni/Al_2O_3 catalyst, amorphous C species, which can easily be oxidized, dominate [2]. Increasing input power from 0-80W in DBD plasma-assisted DRM over Mo_2C-Ni/Al_2O_3 catalyst, decreases CH_4 and CO_2 conversion (Figure 15(F)[2]), but applying input power above 80W positively impacts the reactants' conversion (Figure 15(F)[2]) [2]. CH_4 conversion remains higher than CO_2 in all the cases when using input power 0-120W (Figure 15(F)[2]) [2]. But applying input power above 120W improves the catalytic function of Mo_2C-Ni/Al_2O_3, and CO_2 conversion becomes higher than CH_4 (Figure 15(F)[2]) [2]. To achieve similar substrates' percentage conversions, and to prevent coking the input power and Ni/Mo ratio are very crucial in plasma-assisted DRM over Mo_2C-Ni/Al_2O_3 catalyst.

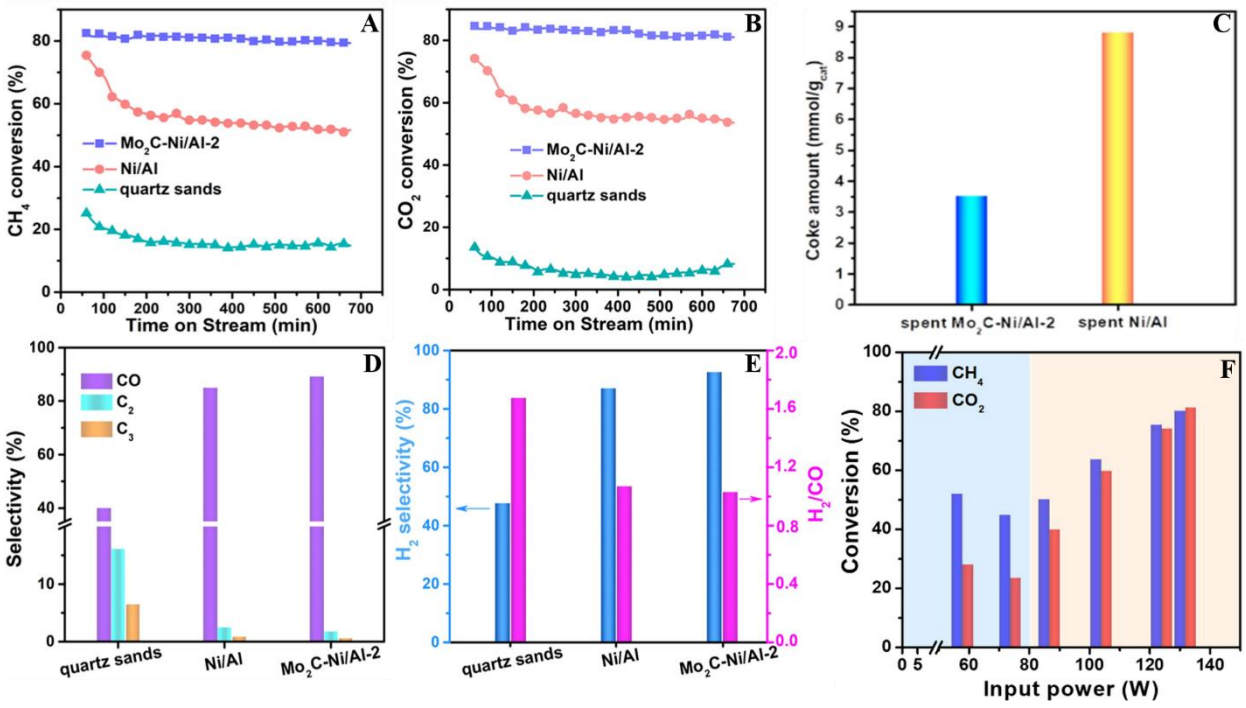

Figure 15. (A-D) Stability performance of Mo_2C-Ni/Al_2O_3 with Ni/Mo = 2, Ni/Al_2O_3 and quartz sands (the blank experiment) in DRM reaction under plasma-catalytic condition. (A) CH_4 conversion; (B) CO_2 conversion; (C) the selectivity of CO, C_2, C_3 products from the gas analysis at reaction time of 675min; (D) the selectivity of H_2 and H_2/CO ratio from the gas analysis at reaction time of 675min. (E) Amount of coke over the spent catalysts from the O_2-TPO analysis Reaction conditions: discharge length = 10mm, input power = 112W, WHSV = 50000mL/g/h, CH_4/CO_2/Ar = 1/1/8, the temperature of catalytic bed was ca. 470°C and there was no additional thermal input. (F) Catalytic performance at different input powers over the Mo_2C-Ni/Al_2O_3 with Ni/Mo = 2 catalyst under plasma-catalysis condition. Reaction conditions: WHSV = 50000mL/g/h, discharge length = 10mm, CH_4/CO_2/Ar = 1/1/8, the temperature of catalytic bed was ca.170–425°C and there was no additional thermal input. Reproduced with the permission from [2].

Mo_2C as Catalyst for Other CH_4 Reforming-based H_2 Production Technologies

Steam Reforming of CH_4 (SRM)

SRM is a highly mature technology in comparison with other H_2 production technologies/methods. However, catalyst deactivation due to coking is still a problem that needs to be addressed. Due to having anti-coking properties, MCs have the potential to be considered for catalyzing SRM reaction. A summary of the performance of TMC-based catalysts for SRM is provided in Table 4. In the case

of an unsupported Mo_2C catalyst, there is only β-Mo_2C phase, and is less active than α-MoC_{1-x} phase for SRM reaction [228]. Using 700^0C temperature in TPR of the Mo_2C catalyst's precursor, results in the synthesis of the most active/stable Mo_2C catalyst for SRM reaction [229]. TPR of Mo_2C catalyst's precursor at a very high temperature (above 700^0C) gives Mo_2C catalyst with a very small specific surface area or a small number of active sites available for catalyzing a reaction like SRM [229]. Mo_2C/Al_2O_3 is more active/stable than unsupported Mo_2C catalyst for SRM reaction because in Mo_2C/Al_2O_3, both the phases: α-MoC_{1-x} and β-Mo_2C coexist, and α-MoC_{1-x} is very active for SRM reaction [229]. In terms of Mo_2C particles supported on zeolite Y, Mo_2C/FAU is not an active catalyst for SRM reaction (Figure 16 (a-d)[228]) [228]. However, the catalytic activity/stability of Ni/FAU for SRM reaction can be improved by adding Mo_2C in its structure (Figure 16 (a-d)[228]). The introduction of Mo_2C in Ni/FAU catalyst structure makes Ni particles smaller, and the dispersion of Ni particles on support is also better in Ni-Mo_2C/FAU. In SRM reaction over Ni-Mo_2C/FAU catalyst, Mo_2C prevents the oxidation and sintering of Ni. Mo_2C reduces the amount of energy required for the activation of SRM reaction substrates and promotes CH_4 conversion, which in turn increases coking. Mo_2C wt.% in Ni-Mo_2C/FAU catalyst must be optimized in a way that there is a balance between $C_{(s)}$ formation and $C_{(s)}$ consumption during SRM reaction. This can be done by increasing the activity of $H_2O_{(s)}$ or increasing the $H_2O_{(s)}/CH_4$ feed ratio.

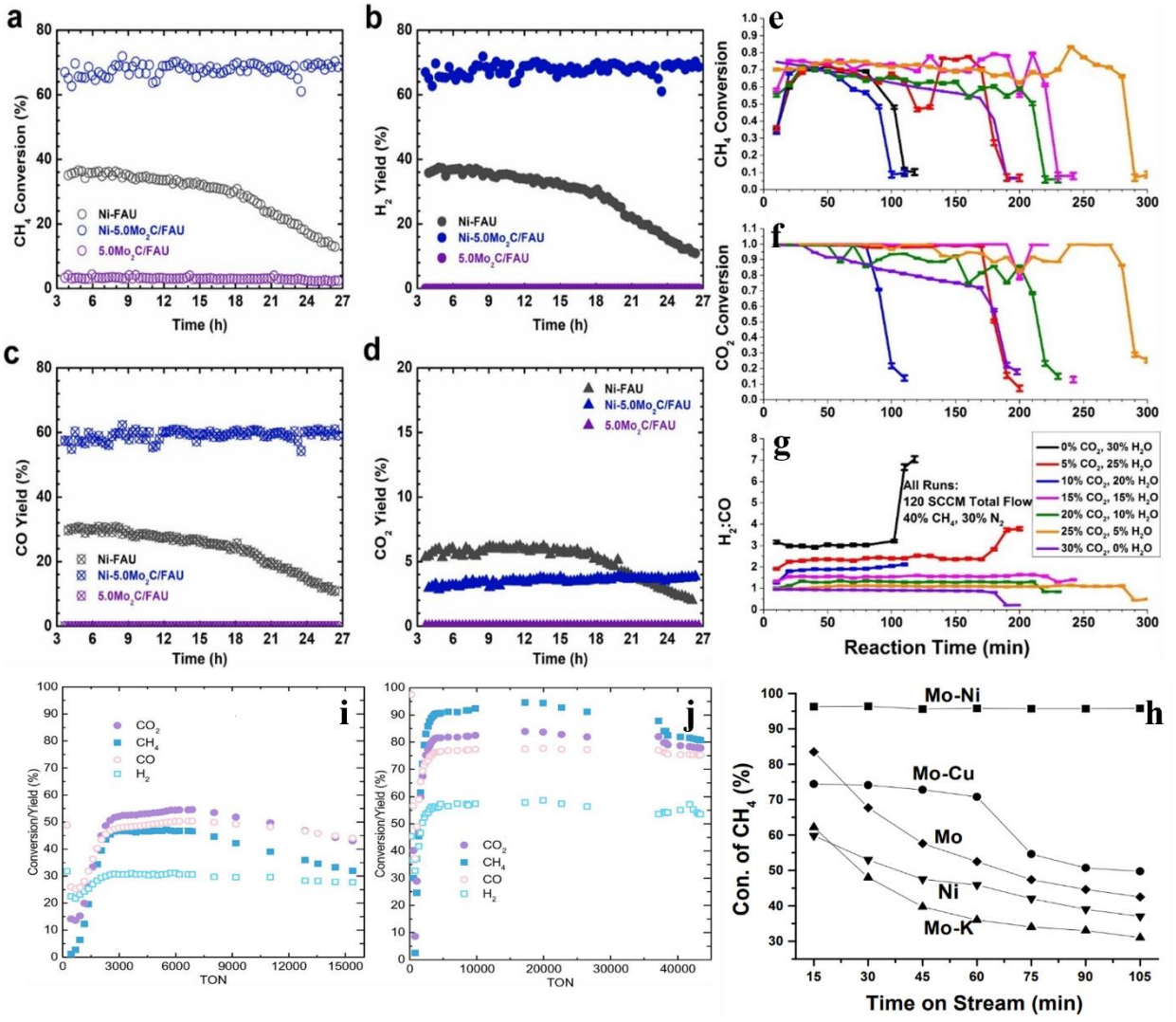

Figure 16. (a-d) Performance test of Ni/FAU, Ni-Mo_2C/FAU with 5wt% Mo, and Mo_2C/FAU with 5wt% Mo in SRM at T = 850°C, P = 1atm, $H_2O_{(s)}/CH_4$ = 1, CH_4 flow = 20.3sccm with 55 mg of catalyst, and bed height of 0.4cm. (a) CH_4 conversion; (b) H_2 yield; (c) CO yield; and (d) CO_2 yield. Reproduced from [228]. (e) CH_4 conversion, (f) CO_2 conversion, and (g) H_2:CO production ratio for various amounts of CO_2 and H_2O oxidants at T = 950^0C, over Ni-Mo_2C catalyst. Error bars represent the 95% confidence interval for each measurement. Reproduced from [174]. (h) Conversion of CH_4 vs. TOS (reaction conditions: T = 1123 K, P = ambient, CH_4/O_2 = 2.05/1 and GHSV = 2 × 105 ml/h-g) over catalysts: Mo–Ni, 0.5% Ni, 35.4% Mo_2C/Al_2O_3; Mo–Cu, 1.4% Cu 35.4% Mo_2C/Al_2O_3; Mo, 35.4% Mo_2C/Al_2O_3; Ni, 0.5% Ni/Al_2O_3; Mo–K, 1.2% K 35.4% Mo_2C/Al_2O_3; mass ratio %). Reproduced from ([230]). (i-j) Catalytic performance of (i) W_xC-NR/γ-

Al_2O_3 and (j) W_xC-NP/γ-Al_2O_3, for DRM reaction at T = 1173K, P = 1atm, CH_4/CO_2 = 1 and flow = 30 $mLmin^{-1}$. Reproduced from [231].

Table 4: Summary of the catalytic performance of TMCs for CH4 reforming reactions (other than DRM).

Active Site	Support	SM, RT	App	Synthesis Conditions	Reaction Conditions	Feed Comp.	Max Con [%]	Selectivity [%]	Comment	Refs
Mo_2C	–	SM: TPR RT: –	SRM 2004	P: – / T: 700^0C TR: 10^0C/min CH_4/H_2: 20%v/v Flow: 4l/h TC: 3h	P: 1atm /T: 700^0C GHSV: – CH_4 flow: 40ml/min $H_2O_{(s)}$ flow: 6.5ml/h TOS: 6h	CH_4: 1 $H_2O_{(s)}$: 4	CH_4: 40.0	H_2: 40.0 CO: – H_2/CO: –	Al_2O_3 supported Mo_2C is more active/stable than unsupported Mo_2C catalyst for SMR reaction. Using 700^0C temperature in TPR of Mo_2C catalyst precursor, results in the most active/stable Mo_2C catalyst for SMR reaction.	[229]
Mo_2C	Al_2O_3						CH_4: 95.0	H_2: 70.0 CO: 25.0 H_2/CO: –		
Ni-Mo_2C	–	SM: TPR RT: –	SRM 2016	P: – / T: 700^0C TR: 1^0C/min CH_4/H_2: 20%v/v Flow: 50sccm TC: 2h	P: – T: 950^0C GHSV: – Flow: 120sccm TOS: 300mins	CH_4: – $H_2O_{(s)}$: –	CH_4: 70.0	H_2: 40.0 CO: – H_2/CO: 300.0	In SMR reaction over Ni-Mo_2C catalyst, H_2/CO product ratio increases with increasing $H_2O_{(s)}$ in the feed.	[174]
Ni-Mo_2C	Zeolite HY	SM: TPR RT: FBR	SRM 2022	P: – / T: 700^0C TR: 1^0C-5^0C/min CH_4/H_2: 15vol% Flow: 85sccm TC: 2h	P: 1atm T: 850^0C GHSV: – CH_4 Flow: 20sccm TOS: 27h	CH_4: 1 $H_2O_{(s)}$: 1	CH_4: 70.0	H_2: 70.0 CO: 70.0 H_2/CO: –	Mo_2C is not an active catalyst for SMR reaction. In SMR reaction over Ni catalyst, Ni sintering, and formation of NiO species cease the catalysis. Ni-Mo_2C catalytic synergism gives a very high H_2/CO yield in SMR reaction.	[228]
α-Mo_2C	–	SM: TPR RT: –	CH_4 Reform 2000	P: – / T: 873-1173K TR: 1K/min CH_4/H_2: 20%v/v Flow: 4l/h TC: 3h	P: – T: 973K GHSV: – Flow: 15ml/min TOS: 7h	CH_4: 1	CH_4: 40.0	H_2: – CO: –	α-Mo_2C changes to β-Mo_2C, when used as a catalyst for CH_4 reforming reaction.	[163]
β-Mo_2C							CH_4: 50.0	H_2: – CO: –	β-Mo_2C synthesized by carburizing at 873K is an active and stable catalyst for CH_4 reforming.	
η-Mo_3C_2							CH_4: 50.0	H_2: – CO: –	η-Mo_3C_2 is the active specie for CH_4 reforming reaction, as it maximizes the CH_4 conversion rate.	
Mo_2C	Al_2O_3	SM: TPR RT: FBR	POM 2003	P: 1atm / T: 1123K TR: 1-10K/min CH_4/H_2: 20vol% Flow: – TC: 2h	P: 1atm T: 1123K GHSV: 2×10^5ml/hg Flow: – TOS: 105min	CH_4:O_2=2.05	CH_4: 84	H_2: 96.0 CO: 96.0	Ni is the best promoter for Mo_2C catalyst to increase the CH_4 conversion in POM.	[230]
Ni-Mo_2C							CH_4: 96	H_2: 61.5 CO: 64.0		
Cu-Mo_2C							CH_4: 74	H_2: 70.0 CO: 73.0		
K-Mo_2C							CH_4: 62	H_2: 41.0 CO: 41.0		
$Co_{0.2}W_{0.8}C_x$	–	SM: TPR RT: –	POM 2009	P: – / T: 900K TR: 1K/min C_2H_6/H_2: 10%v/v Flow: 100ml/min TC: –	P: 4.5bar, 5.5bar T: 830^0C, 850^0C GHSV: 30000mlg^{-1}h^{-1} Flow: – TOS: 100h, 70h	CH_4:O_2=2.7 $CH_4/O_2/N_2$=33/11/44	CH_4: 75.0	H_2: – CO: 93.0	The bulk $Co_{0.2}W_{0.8}C_x$ catalyst is more active than the supported one for POM. Using a combustion catalyst in series with a MC catalyst enhances the stability of the carbide phase in POM.	[232]
$Co_{0.2}W_{0.8}C_x$	Al_2O_3						CH_4: 53.0	H_2/CO: 201.0 H_2: – CO: 85.0 H_2/CO: 201.0		
Ni-Mo_2C	–	SM: TPR RT: –	SCRM 2016	P: – / T: 700^0C TR: 1^0C/min CH_4/H_2: 20%v/v Flow: 50sccm	P: – T: 950^0C GHSV: – Flow: 120sccm	CH_4: – CO_2: – $H_2O_{(s)}$: – N_2: –	CH_4: 70.0 CO_2: 100.0	H_2: – CO: – H_2/CO: 150.0	Ni-Mo_2C is a good catalyst to catalyze SCRM. H_2/CO yield can be increased by increasing $H_2O_{(s)}$ flow in the reactant stream.	[174]

				TC: 2h	TOS: 300mins				Increasing the CO_2 flow in the reactants' stream decreases H_2/CO yield.	
Ni-Mo_2C	ZrO_2	SM: TPC RT: FBR	SCRM 2018	P: – / T: 850^0C TR: 1^0C-5^0C/min H_2/N_2: 10vol% H_2 Flow: – TC: 30mins	P: – T: 700^0C GHSV: 36000ml$g^{-1}h^{-1}$ Flow: 30ml/min TOS: –	CH_4: 1 CO_2: 0.4 $H_2O_{(s)}$: 0.8 N_2: 1	CH_4: 75.0 CO_2: 55.0	H_2: 95.0 CO: 98.0 H_2/CO: –	Ni-Mo_2C catalyst synthesized by the TPR method and glucose as the C source shows very good resistance against coking in SCRM reaction.	[233]
Mo_2C-Ni	ZrO_2	SM: TPR RT: FBR	SCRM 2015	P: – / T: 850^0C TR: 2-5^0C/min CH_4/H_2: 20%v/v Flow: – TC: 30mins	P: – T: 700^0C GHSV: 36000ml$g^{-1}h^{-1}$ Flow: – TOS: 20h	CH_4: 1 CO_2: 0.4 $H_2O_{(s)}$: 0.8 N_2: 1	CH_4: 98.0 CO_2: 80.0	H_2: – CO: – H_2/CO: 200.0	Mo_2C promoted Ni/ZrO_2 catalyst remains stable for a very long period of time in SCRM reaction.	[90]
La-Ni-Mo_2C	Al_2O_3	SM: TPR RT: FBR	TRM 2015	P: – / T: 700^0C TR: 1^0C/min CH_4/H_2: 20vol% Flow: 40ml/min TC: 2.5h	P: – T: 850^0C GHSV: – Flow: 4600mlh^{-1} TOS: –	CH_4: 1 O_2: 0.16 CO_2: 0.39 $H_2O_{(s)}$: 0.30	CH_4: 95.0 CO_2: 85.0	H_2: 95.0 CO: 85.0 H_2/CO: –	La is the best additive to enhance the catalytic activity of Ni-Mo_2C/γ-Al_2O_3 for TRM, especially at low temperature.	[234]
Ni-Mo_2C	Al_2O_3	SM: TPR RT: FBR	TRM 2017	P: – / T: 700^0C TR: 1^0C/min CH_4/H_2: 20vol% Flow: 40cm^3/min TC: 2.5h	P: – T: 850^0C GHSV: – Flow: 4600cm^3h^{-1} TOS: –	CH_4: 1 O_2: 0.16 CO_2: 0.39 $H_2O_{(s)}$: 0.30	CH_4: 93.0 CO_2: 83.0	H_2: 93.0 CO: 83.0 H_2/CO: –	Co-impregnation of Ni and Mo metal into γ-Al_2O_3 support followed by TPR gives the most active Ni-Mo_2C/γ-Al_2O_3 catalyst for TRM.	[235]
Ni-WC	–	SM: Annealing RT: FBR	PCDR 2023	P: – / T: 980^0C TR: 10^0C/min N_2: 100% Flow: – TC: 6h	P: – T: 800^0C GHSV: – Flow: – TOS: –	Pyrolysed Plastic: 1 CO_2: 1	–	H_2: – CO: – H_2/CO: –	Ni-WC catalyst enhances the syngas yield in dry reforming of pyrolyzed plastics. H_2/CO yield depends upon the type of plastic used as feed.	[236]

$H_2O_{(s)}$-CO_2 bi-reforming of CH_4 (SCRM)

SCRM is a technology that helps in producing syngas with desired H_2/CO ratio. MCs have also been investigated for catalyzing SCRM. A summary of the performance of TMC-based catalysts for SCRM is provided in Table 4. Ni-Mo_2C catalyzes SCRM reaction, and the produced H_2/CO ratio depends upon the $H_2O_{(s)}$ and CO_2 flow in the substrates' stream (Figure 16 (e-g)[174]) [174]. Increased $H_2O_{(s)}$ and CO_2 flow impact H_2/CO product ratio positively and negatively, respectively (Figure 16 (e-g)[174]). Oxidation of Mo_2C to MoO_2 primarily causes the deactivation of Ni-Mo_2C catalyst in SCRM reaction, and the time at which the oxidation of Mo_2C starts in SCRM reaction does not follow a certain trend regardless of changing reaction feed composition with a specific pattern. Mo_2C, when used as a promoter, improves the catalytic activity of other supported metal catalysts. Mo_2C promoted Ni/ZrO_2 catalyst is very stable in catalyzing SCRM reaction [90]. Without Mo_2C, sintering of Ni, and coking deactivate Ni/ZrO_2 catalyst in SCRM reaction. The addition of Mo_2C in Ni/ZrO_2 structure does not inhibit the Ni sintering during SCRM reaction but decreases the size of Ni particles, improves the Ni dispersion over ZrO_2 support, enhances Ni-ZrO_2 interaction, prevents the oxidation of Ni, and finally allows only $C_{(s)}$ with whisker structure to be deposited on the catalyst surface. The $C_{(s)}$ with whisker structure does not block the active sites, like $C_{(s)}$ with shell-like structure does. In this way, Mo_2C helps Ni/ZrO_2 catalyst to remain stable for a very long period in SCRM reaction. Mo_2C-Ni/ZrO_2 catalyst with Mo_2C wt.% of 0.5 exhibits the best catalytic performance for SCRM reaction. Using glucose than CH_4/H_2 gas mixture, as the C source, in synthesizing Ni-Mo_2C/ZrO_2 catalyst by TPR method, results in Ni-Mo_2C/ZrO_2 catalyst, which shows excellent coking resistance and activity in SCRM reaction, but gives H_2/CO yield less than unity [233]. Ren et al. [233] attributed increased coking resistance of Ni-Mo_2C/ZrO_2 catalyst in SCRM reaction to small (9.1nm) Ni particles, intensified Ni-Mo_2C interaction, improved Ni-ZrO_2 interaction, and increased CO selectivity.

Partial Oxidation of CH_4 (POM)

POM gives H_2 rich syngas yield. In MC catalysis at low pressure, oxygen species present in the system oxidize MC into MO_2. A summary of the performance of TMC-based catalysts for POM is provided in Table 4. In POM over Mo_2C/Al_2O_3 catalyst, CH_4 conversion decreases over time (Figure 16 (h)[230]) due to oxidation of the carbide phase [230]. Introducing Ni or Cu as a promoter improves the activity/stability of Mo_2C/Al_2O_3 catalyst for the POM (Figure 16 (h)[230]) [230]. This is because Ni and Cu help in the reduction of MoO_3 to MoO_2, and then also in the carburization/re-

carburization of MoO_2 to oxycarbide or Mo_2C (Equation 33) by CH_4 decomposition [230]. The individual role of Ni, Cu, and Mo_2C in CH_4 activation is not worthy (Figure 16 (h)[230]), but the synergetic action of Mo_2C and Ni or Cu helps in CH_4 dissociation (Figure 16 (h)[230]) and increasing H_2/CO yield [230]. Ni is better than Cu as a promoter for Mo_2C (Figure 16 (h)[230]) [230]. Without Ni, CH_4 reduction of MoO_3 results in CO, CO_2 or H_2O, depending upon the reducing temperature [230]. K makes Mo—O bond even stronger in MoO_3 so, it's not a good promoter for Mo_2C [230]. $Co_{0.2}W_{0.8}C_x$ catalyst is more active than Mo_2C for the POM [232]. The catalytic activity/stability of $Co_{0.2}W_{0.8}C_x$ for POM increases with increasing CH_4/O_2 feed ratio and pressure, which in-turn enhances the product selectivity or syngas yield [232]. At low pressure, the carbide phase is oxidized and H_2/CO product ratio declines over time, but CO_2 selectivity increases [232]. The carbide phase increases the rate of the POM reaction. The concentration of $Co_{0.2}W_{0.8}C_x$ phase in $Co_{0.2}W_{0.8}C_x/Al_2O_3$ is not as much as in the bulk phase, therefore, $Co_{0.2}W_{0.8}C_x$ is more active than $Co_{0.2}W_{0.8}C_x/Al_2O_3$ in catalyzing POM reaction.

MCs are very sensitive to O_2. To prevent the oxidation of the MCs with O_2, Xiao et al. [232] proposed a strategy of using a combustion catalyst in the way, before the feed gas ($CH_4 + 1/2\ O_2$) reaches to the oxygen sensitive carbide catalyst inside the reactor. This combustion catalyst could help in completely utilizing the feed O_2 for the combustion of 25% of the feed CH_4 (Equation 7). In this way, only the rest of the CH_4 feed and combustion products (CO_2 + H_2O) would reach the carbide catalyst, and the reaction between MC and O_2 could be prevented, or the oxidation of the carbide phase could be prevented. Xiao et al. [232] proposed the usage of $BaMn_2Al_{10}O_{19}$ as the combustion catalyst.

Not only the catalyst but reactor also influences the kinetics of a chemical reaction, and ultimately the product quality. Using a reactor, made up of carbide material, for the POM reaction results in the formation of unwanted inactive micro and nano species that affect the POM reaction rate and yield [237].

Tri-reforming of CH_4 (TRM)

In TRM, the monitored/regulated use of all oxides ($H_2O_{(s)}$, CO_2, and O_2) is advantageous in producing syngas with desired H_2/CO ratio, and also in preventing the catalyst from deactivation due to coking. A summary of the performance of TMC-based catalysts for TRM is provided in Table

4. Zou et al. [234] examined the catalytic role of Ni-Mo_2C/γ-Al_2O_3 for TRM by adding La, Ce, Co, Mg, and K elements as promoters in its structure. At low temperature, the activity of all other catalysts was found to be very poor except La-Ni-Mo_2C/γ-Al_2O_3. Ce and Co promoted catalysts degraded over time. Mg promoted coking while K disturbed the carburization cycle by making Mo—O stronger and producing MoO_3, and exhibited the worst role in boosting the catalytic action of Mo_2C/γ-Al_2O_3 for TRM [230, 234]. Co-impregnation of Ni and Mo metal into the γ-Al_2O_3 support followed by TPR gives the most active Ni-Mo_2C/γ-Al_2O_3 catalyst for TRM [235]. This is because co-impregnation of Ni and Mo into γ-Al_2O_3 support results in $NiMoO_4$ precursor which is easier to reduce/carburize than MoO_3 and MoO_2, due to the presence of Ni, and Ni helps in the carburization process [235].

With a particular focus on TRM, it is worthwhile to mention that silicon carbide (SiC) can also be potentially used as an effective support for Ni-Mo_2C or Ni catalyst. SiC as a support for Ni catalyst promotes $H_2O_{(s)}$ conversion more than CO_2 conversion in TRM reaction and produces a very high H_2/CO ratio [93]. This is because there is strong metal-support interaction in Ni/SiC catalyst which forms very strong basic sites [93]. Due to the presence of strong basic sites and the strong acidic nature of CO_2, the desorption of CO_2 requires more energy than that of $H_2O_{(s)}$ [93]. Metal-support interaction and particle size in Ni/SiC catalyst depend upon the Ni source used in synthesizing Ni/SiC catalyst [93]. H_2/CO yield in TRM reaction over Ni/β-SiC catalyst can be increased by increasing the H_2O and O_2 flow in the reactant stream [238]. Increasing only the flow of O_2 helps in processing the TRM reaction at optimum temperature/pressure conditions [238]. Gracia-Vargas et al. [239] used Na, K, Mg, and Ca as promoters to improve the catalytic activity/stability of Ni/β-SiC for TRM reaction. Na, Ca, and K negatively affect the catalytic activity/stability of Ni/β-SiC by catalyzing the oxidation of the carbide phase, but Mg-Ni/β-SiC with Ni/Mg molar ratio 1/2 and 1/1 exhibited the best catalytic action for TRM reaction [239]. Ca influenced the basic sites in Ni/β-SiC positively, but the obtained CO_2 conversion rate was not desirable because Ca increased the rate of WGSR (Equation 3) as well [239]. The addition of Mg in the Ni/β-SiC catalyst structure made Ni particles smaller, Mg also improved the basicity and coking resistance of Ni/β-SiC for catalyzing TRM reaction [239]. Mg-Ni/β-SiC catalyst synthesized by impregnating β-SiC support with Mg first and then Ni showed the highest activity and coking resistance in TRM reaction [240]. Reversing the impregnation order blocks the Ni active sites, and also affects Ni-Mg, and metal-support

interaction [240]. In TRM reaction over Mg-Ni/β-SiC catalyst, to obtain the best possible substrate conversion percentage and H_2/CO yield, Ni/Mg molar ratio should be 1/1 [240].

Tungsten Carbide (WC)

Pt like behavior of WC in surface catalysis [57] was the motivation for considering it as an alternative to a noble metal catalyst for DRM reaction. A summary of the performance of simple (un-promoted and unsupported) and supported WC catalysts for DRM reaction is provided in Table 5. Claridge et al. [115] found α-WC catalyst less active than Mo_2C and noble metal catalysts, for DRM reaction, and the sequence of the catalytic activity for DRM reaction is 5wt%$Ru/Al_2/O_3$>Mo_2C≈5wt%$Ir/Al_2/O_3$>5wt%$Rh/Al_2/O_3$>WC. However, the stability and coking resistance of α-WC catalyst for DRM reaction was comparable with that of Mo_2C and noble metal catalysts. Claridge et al. proposed two possible mechanisms for DRM reaction over WC catalyst, exactly similar to the two possible mechanisms of DRM reaction over Mo_2C catalyst. The first type of mechanism is called oxidation-re-carburization or cyclic or redox mechanism (Equations 83-87). According to this mechanism, the first CO_2 adsorbs on the surface of the WC and dissociates into CO and O^* (Equation 83). In the second stage, O^* reacts with the surface carbon ($C_{(surface)}$) of the WC to produce CO and leaves behind a C vacancy (□) on the surface of the WC (Equation 84). This C vacancy is either filled by O^* (the first step towards the deactivation of WC due to oxidation) (Equation 85) or C^* (C generated by CH_4 bond cleavage adsorption (Equation 86), and again giving fresh/intact WC) (Equation 87). From WC, $C_{(surface)}$ plays the most significant role rather than bulk C, for catalyzing DRM reaction, because metallic oxide overlayers are commonly observed rather than pure metallic W, in the post reaction analysis of the WC catalyst. The second type of mechanism is called the noble metal type mechanism (Equations 83, 86 and 88). In this type of mechanism, CO_2 dissociative adsorption gives CO and O^* (Equation 83). After this, CH_4 adsorption and bond cleavage give C^* and H_2 (Equation 86). In the final step, O^* and C^* react to give CO (Equation 88), and it is the most important reaction that distinguishes the noble-metal type mechanism from the redox mechanism. In DRM over WC catalyst, CO_2 conversion is always higher than CH_4 due to RWGSR or due to the reaction between WC and CO_2 (Equation 89), or due to the oxidation of the deposited $C_{(s)}$ by CO_2 (Equation 31) [241]. H_2/CO yield can be increased by increasing CH_4/CO_2 feed ratio [241].

$$CO_2 \longrightarrow CO + O^* \quad (83)$$

$$WC_{(surface)} + O^{*} \longrightarrow W(\square) + CO \quad (84)$$

$$W(\square) + O^{*} \longrightarrow WO \quad (85)$$

$$CH_4 \longrightarrow C^{*} + 2H_2 \quad (86)$$

$$W(\square) + C^{*} \longrightarrow WC \quad (87)$$

$$O^{*} + C^{*} \longrightarrow CO \quad (88)$$

$$WC + CO_2 \longrightarrow W + 2CO \quad (89)$$

Table 5: Summary of the catalytic performance of WxC-based catalysts for DRM reaction.

Active Site	Support	SM, RT	App	Synthesis Conditions	Reaction Conditions	Feed Comp.	Max Con [%]	Selectivity [%]	Comment	Refs
WC	–	SM: TPR RT: –	DRM 1997	–	P: 8.3bar /T: 1120K GHSV: $2.8\times10^{3}h^{-1}$ Flow: – (TOS: 144h)	CH_4: 1 CO_2: 1	CH_4: 62.7 CO_2: –	H_2: – CO: 68.7 H_2/CO: 79.0	WC catalyst remains stable in DRM reaction at elevated pressure.	[114]
α-WC	–	SM: TPR RT: PBR	DRM 1998	P: – / T: 1000-1150K TR: 1K/min CH_4/H_2: 20%v/v (Flow: –) TC: –	P: 1bar / T: 1120K GHSV: $2.87\times10^{3}h^{-1}$ Flow: – TOS: 28h	CH_4: 1 CO_2: 1	CH_4: 92.0 CO_2: 93.1	H_2: – CO: 92.6 H_2/CO: 94.0	α-WC catalyst is slightly less active than Mo_2C and noble metal catalysts for DRM reaction. The coking resistance of α-WC in DRM reaction is similar to that of Mo_2C and noble metal catalysts.	[115]
α-WC	–	SM: TPR RT: PBR	DRM 1998	P: – / T: 1000-1150K TR: 1K/min CH_4/H_2: 20%v/v (Flow: –) TC: –	P: 8.3bar / T: 1120K GHSV: $2.87\times10^{3}h^{-1}$ Flow: – TOS: 72h	CH_4: 1 CO_2: 1	CH_4: 62.7 CO_2: 75.4	H_2: – CO: 68.6 H_2/CO: 79.0	α-WC catalyst is more resistive against oxidation at high pressure, in DRM reaction.	[115]
WC	–	SM: Calcination RT: FBR	DRM 2002	P: – / T: 400-900^{0}C Non-O-containing acyclic compound + Tungsten salt TC: 1-5h	P: 1atm / T: 850^{0}C GHSV: $5040cm^3g^{-1}h^{-1}$ Flow: – TOS: –	CH_4: 1 CO_2: 1	CH_4: 90.0 CO_2: 99.7	H_2: – CO: 86.6 H_2/CO: 101.0	The catalytic activity of WC increases with increasing temperature for the DRM reaction.	[159]
WC	–	SM: TPR RT: –	DRM 2007	P: – / T: 973K TR: 1K/min CH_4/H_2: 20%v/v (Flow:–) TC: 3h	P: – / T: 1123K GHSV: – Flow: – TOS: 6h	CH_4: 1 CO_2: 1	CH_4: 40.0 CO_2: 60.0	H_2: – CO: – H_2/CO: –	Nitridation of oxide precursor at 973K for 3h before TPR helps in synthesizing a more stable WC catalyst for DRM reaction.	[126]
WC	–	SM: – RT: –	DRM 2019	–	P: – / T: 668^{0}C GHSV: – Flow: $50cm^3$/min TOS: 60h	CH_4: 1 CO_2: 1	CH_4: – CO_2: –	H_2: – CO: – H_2/CO: 60.0	The C is produced in DRM reaction over the WC catalyst.	[242]
WC	–	SM: MC RT: –	DRM 2019	P: – / T: – / TR: – Mg/C: – TC: 5-9h	P: – T: 950^{0}C GHSV: –	CH_4: 1 CO_2: 1	CH_4: 18.9 CO_2: –	H_2: – CO: – H_2/CO: 175.0	The nano-WC catalyst synthesized by the PMC method is more active than nano-WC synthesized by the MC method, for DRM reaction.	[242]
WC		SM: PMC RT: –		P: – / T: – / TR: – Mg/C: – TC: 2.15h	Flow: $50cm^3$/min TOS: 60h		CH_4: 26.0 CO_2: –	H_2: – CO: – H_2/CO: 174.0	The activity of the WC catalyst for DRM reaction increases in proportion with increasing temperature and decreasing particle size.	
WC+W_2C	–	SM: PMC RT: –	DRM 2019	P: – / T: – TR: – Mg/C: – TC: 2.15h	P: – / T: 843^{0}C GHSV: – Flow: $50cm^3$/min TOS: 60h	CH_4: 1 CO_2: 1	CH_4: – CO_2: –	H_2: – CO: – H_2/CO: 230.0	WC is an active specie for catalyzing the DRM reaction.	[242]
WC	BC	SM: TPR RT: FBR	DRM 2015	P: – / T: 1000^{0}C TR: 10^{0}C/min N_2: 100% (Flow: –) TC: 3h	P: 0.5MPa / T: 850^{0}C GHSV: $6000h^{-1}$ Flow: – TOS: 500h	CH_4: 1 CO_2: 1	CH_4: 83.0 CO_2: 95.0	H_2: – CO: – H_2/CO: 91.0	Biochar can be used as the C source in synthesizing WC by TPR of tungsten oxide precursor. WC/BC is an active catalyst for DRM reaction.	[241]
W_xC-NR	γ-Al_2O_3	SM: TPR RT: PBR	DRM 2019	P: – T: 1173K TR: 2K/min	P: 1atm T: 1173K GHSV: –	CH_4: 1 CO_2: 1	CH_4: 45.0 CO_2: 55.0	H_2: 30.0 CO: 50.0 H_2/CO: –	The shape and phase of the crystal structure of WC catalyst affect its activity and stability in DRM reaction.	[231]

W_xC-NP				CH_4/H_2: 1:4 (40ml/min) TC: 1h	Flow: 30ml/min TOS: –		CH_4: 92.0 CO_2: 82.0	H_2: 55.0 CO: 75.0 H_2/CO: –		
WC-AC	–		DRM 2019	P: – T: 950^0C	P: 1atm T: 800^0C	CH_4: 1 CO_2: 1	CH_4: 20.0 CO_2: 15.0	H_2: – CO: –	[243]	WC-AC composite support itself has very poor catalytic performance for DRM reaction.
		SM: TPR		TR: 2^0C/min	GHSV: 2400mlg^{-1}h^{-1}			H_2/CO: 280.0		
Co	WC-AC	RT: FBR		H_2: 1 (150ml/min) TC: 2h	Flow: 100ml/min TOS: 700min		CH_4: 95.0 CO_2: 95.0	H_2: – CO: – H_2/CO: 92.0		WC-AC support synthesized by carburizing the precursor under H_2 in the TPR method enhances the catalytic performance of Co metal for DRM.
WC	–	SM: TPC RT: FBR	DRM 2019	P: – T: 800^0C TR: 800^0C/h	P: 1atm / T: 970^0C GHSV: – Flow: 10ml/min (TOS: –)	CH_4: 1 CO_2: 1	CH_4: – CO_2: –	H_2: 49.0 CO: 48.84 H_2/CO: –	[244]	Membrane MCs intensify the direct reaction between CH_4 and CO_2, as catalysts in DRM reaction.
WC		SM: TPC		CH_4/H_2: 60/40 by vol	P: 1atm / T: 900^0C			H_2: 25.0		
	Al_2O_3	RT: MR		CH_4/H_2 flow: 50cm^3/min TC: 2h	GHSV: – Flow: 20ml/min (TOS: –)		CH_4: – CO_2: –	CO: 44.0 H_2/CO: –		
Co_6W_6C	–	SM: – RT: SiO_2-lined	DRM 2004	–	P: 5atm / T: 850^0C GHSV: – WHSV: 11200scch^{-1}g^{-1} Flow: – TOS: 90h	CH_4: 1 CO_2: 1 Ar: 3	CH_4: 82.0 CO_2: 78.0	H_2: – CO: 76.0 H_2/CO: 100.0	[245]	Co_6W_6C shows remarkable activity for DRM reaction at high temperature, and its activity is not affected by C production/deposition.
Co_6W_6C	–	SM: TPR RT: FBR	DRM 2005	P: – / T: 850^0C TR: 15^0C/min CO_2/CO: 0.75 CO_2/CO flow: – TC: 24h	P: 3.4atm / T: 850^0C GHSV: – WHSV: 9000scch^{-1}g^{-1} Flow: – TOS: 100h	CH_4: 1 CO_2: 1	CH_4: 70.0 CO_2: 70.0	H_2: – CO: 55.0 H_2/CO: 173.0	[246]	The Co_6W_6C is an active and stable catalyst for DRM reaction at high temperature. The CO_2/CO ratio in the carburization of the precursor $Co(en)_3WO_4$ plays a key role in synthesizing an active and stable Co_6W_6C catalyst for DRM.
Co-WC	–		DRM 2006	P: 1atm / T: 850^0C TR: 15^0C/min	P: 3.4atm / T: 850^0C GHSV: –	CH_4: 1 CO_2: 1	CH_4: 78.0 CO_2: 70.0	H_2: – CO: 58.0	[247]	A different CO_2/CO ratio is required to synthesize Ni-WC and Co-WC by the TPR method.
		SM: TPR		CO_2/CO: 0.5	WHSV: 9000scch^{-1}g^{-1}			H_2/CO: 165.0		At low temperature, the Ni-WC catalyst is better than Co-WC for DRM reaction.
Ni-WC		RT: FBR		CO_2/CO flow: – TC: 24h	Flow: – TOS: 100h		CH_4: 85.0 CO_2: 78.0	H_2: – CO: 78.0 H_2/CO: 162.0		
Ni-WC	–	SM: TPR RT: –	DRM 2016	P: – / T: 850^0C TR: 1^0C/min CH_4/H_2: 40%v/v (150ml/min) TC: 2h	P: 1atm / T: 800^0C GHSV: – WHSV: 6000scch^{-1}g^{-1} Flow: 120ml/min TOS: 12h	CH_4: 1 CO_2: 1	CH_4: 82.0 CO_2: 90.0	H_2: 85.0 CO: – H_2/CO: –	[128]	The Ni/W molar ratio in Ni-WC significantly affects its performance for DRM reaction. WC has better oxidation resistance and is a more stable catalyst than Mo_2C, for DRM reaction.
Ni-WC	–	SM: TPR RT: –	DRM 2020	P: – / T: 850^0C TR: 2.5^0C/min CH_4/H_2: 20%v/v (Flow :–) W/F: 0.0556ghL^{-1} TC: 2h	P: 1atm / T: 800^0C GHSV: – Flow: – TOS: 20h	CH_4: 1 CO_2: 1	CH_4: 75.0 CO_2: 85.0	H_2: 90.0 CO: – H_2/CO: 80.0	[175]	Ni-WC catalyst exhibits maximum stability in DRM reaction when using CH_4/CO_2 molar ratio less than 1.
Ni-WC	–	SM: Annealing RT: FBR	DRM 2023	P: – / T: 980^0C TR: 10^0C/min	P: – / T: 800^0C GHSV: 5000mlg^{-1}h^{-1}	CH_4: 1 CO_2: 1	CH_4: 75.0 CO_2: 50.0	H_2: – CO: –	[236]	Saccharides are a good source of C for synthesizing MCs.

				N_2: 100% / Flow: – TC: 6h	Flow: – TOS: 16h	Ar: 1	H_2/CO: 85.0	Ni-WC synthesized by using sucrose as the C source is the most active catalyst for DRM reaction.

Effect of Crystalline Structure and Phase

Different crystal structures and different catalytic roles of the carbides of group-V TMs (have fcc crystal structure (Figure 1 (b)[54])) and group-VI TMs (have hexagonal crystal structure (Figure 1 (d)[54])), for DRM reaction, have made the morphology of the MC catalysts very important [158, 231]. The total number of facets, and the number of facets exposed to the reactants of a chemical reaction, of a catalyst, depends upon the crystal structure of the catalyst. WC has a hexagonal (Figure 1 (d)[54]), while carbides of group-V TMs have an fcc crystal structure (Figure 1 (b)[54]), and a hexagonal crystal structure has a smaller number of facets than an fcc crystal structure. Therefore, WC has several numbers of exposed facets less than that of a carbide of group-V TM, to DRM reactants, and therefore, it is more difficult to be oxidized than the carbides of group-V TMs, by DRM reactants. That is the reason why WC shows better oxidation resistance than the carbides of group-V TMs in DRM reaction at similar conditions. WC catalyst does not undergo a structural deformation (particles' sintering) in contrast to Mo_2C catalyst, during DRM reaction [128].

In terms of morphology, Mounfield et al. [231] found that nanoparticle morphology of WC promotes RWGS reaction, which ends up the main DRM reaction with low H_2 selectivity (Figure 16 (i & g)[231]). This could be the result of the presence of H_2 on the carbide surface, when there is high CH_4 conversion. The conversion of DRM substrates is higher in the case of W_xC-NP (tungsten carbide nanoparticles) than in the case of W_xC-NR (tungsten carbide nanorods) as a catalyst (Figure 16 (i & j)[231]). This is due to the difference between the surface areas of the particles of both crystal morphologies. A high CO_2 conversion, high CO selectivity but low H_2 selectivity at high temperature, in DRM over a WC catalyst, give clear manifestation that there is oxidation on the carbide surface or RWGS reaction is also taking place in parallel with DRM reaction [231, 248]. A syngas yield with H_2/CO ratio greater than unity at high temperature indicates that the CH_4 decomposition reaction is ruling the DRM reaction [248]. CH_4 conversion in DRM reaction over WC/SiO_2 catalyst is very poor [159].

The different degree of catalytic activity/stability of different crystal phases of the same MC, for the same reaction, highlights the importance of the crystal phase, for a better catalytic reaction [249]. β-W_2C nanoparticles showed better coke resistance than α-WC nanorods, in the results of the experimental study done by Mounfield et al. [231]. They substantiated this result with the fact that

the presence of a higher number of C vacancies in the lattice of β-W_2C helped in the development of the redox cycle during the DRM reaction, but the redox cycle was not established in the case of the DRM reaction over α-WC catalyst. Grigoryan et al. [242] found nano-WC more active than nano-W_2C, for CH_4 conversion in DRM reaction. In DRM reaction over α-WC or β-W_2C catalyst, CO_2 conversion is always higher than CH_4 due to RWGSR [126].

To improve control over reaction conditions, reaction kinetics, resistance against side reactions, catalyst stability, and H_2 selectivity/yield in DRM, membrane reactor and membrane catalyst is a matter of interest. Gavrilova et al. [244] compared the activity of conventional powdered WC and membrane WC/Al_2O_3 catalysts for DRM reaction. Both the catalysts were not purely WC, but there were also the particles of W and β-W_2C. CH_4 conversion in the case of both catalysts is very low. A very high CH_4 conversion in DRM reaction over membrane WC/Al_2O_3 is due to the H_2O production (Equation 90) or due to the reaction between CH_4 and H_2O (Equation 91). The membrane WC/Al_2O_3 catalyst favors the direct reaction between CH_4 and CO_2, and the direct reaction constant for this case was 30 times higher than the DRM reaction over conventional WC catalyst. No $C_{(s)}$ deposition on the surface of the membrane catalyst also supports the explanation that membrane MC catalysts benefit the direct reaction between CH_4/CO_2. So, membrane MC catalysts intensify the DRM reaction and slightly improve the H_2/CO yield.

$$CH_4 + 3CO_2 \longrightarrow 4CO + 2H_2O \quad (90)$$

$$CH_4 + H_2O \longrightarrow CO + 3H_2 \quad (91)$$

Effect of Promoter

The effect of different promoters in improving the catalytic role of WC for DRM reaction has also been studied, and a promoted WC catalyst performs better than a simple WC catalyst, in catalyzing DRM reaction [245]. A summary of the effect of different promoters on the performance of WC catalysts for DRM reaction is provided in Table 5. Iyer et al. [245] synthesized Co_6W_6C by using cobalt-tungsten eta-carbide precursor. At the temperature of 850^0C, this catalyst was found remarkable in terms of stability and activity for DRM reaction. But at 500^0C, a cut-back in the percentage-conversion of DRM feed was observed. Co increases the $C_{(s)}$ formation. So, Co_6W_6C in the DRM reaction undergoes a phase transformation (Equation 92). The produced $C_{(s)}$ deposits on the surface of the WC, but it does not affect the catalysis. Keeping Co_6W_6C at 850^0C for 24h before

using it as a catalyst for DRM reaction, can improve its catalytic activity [245]. Shao et al. [246] synthesized different Co_6W_6C catalysts by using different CO_2/CO gas mixture ratios for the carburization of the $Co(en)_3WO_4$ precursor. Using a CO_2/CO gas mixture ratio of 0.75 for the carburization of $Co(en)_3WO_4$ precursor gives the most active and stable Co_6W_6C catalyst for DRM reaction. Initially in DRM reaction over Co_6W_6C catalyst, CH_4 conversion is very high. So, there is no balance between the rate of $C_{(s)}$ deposition and removal from the surface of the catalyst. The deposited $C_{(s)}$ converts the Co_6W_6C catalyst into WC and Co (Equation 92), which are more active for DRM reaction. Once the species (WC and Co) are generated, the conversion of DRM reactants becomes steady. At such a steady state, no side reaction takes place, and the activity of the catalyst can be maintained for a very long period of time with no further $C_{(s)}$ deposition on the surface of the catalyst. To achieve this steady state, the temperature must be high enough (850^0C or above) for CH_4 conversion, so that the $C_{(s)}$ can be formed and deposited on the surface of the Co_6W_6C catalyst, and active species (WC and Co) can be generated. On the other hand, the carburization of the $Co(en)_3WO_4$ precursor under the mixture of CO_2/CO gas, synthesizes the Co_6W_6C catalyst with some oxygen on the surface. In DRM reaction over Co_6W_6C catalyst at low temperature, this oxygen reacts with Co_6W_6C and forms $CoWO_4$ species (Equation 93). The $CoWO_4$ species are inactive for DRM reaction. In DRM reaction over Co_6W_6C catalyst at high temperature, there is enough CH_4 conversion and $C_{(s)}$ production to remove oxygen from the surface of the catalyst (Equation 94).

Ni as another promoter, improves the functionality of WC catalyst for CH_4 dissociation in DRM reaction [128]. Shao [247] compared the catalytic activity of Co-WC and Ni-WC for DRM, and concluded that both Co-WC and Ni-WC are good catalysts for DRM reaction but Ni-WC performs well even at low temperature. Co-WC has oxygen species on its surface, which can be removed by flowing CH_4 over it, but this CH_4 treatment is not required for Ni-WC [247]. However, the Ni/W ratio in Ni-WC is a key parameter. A very small Ni/W molar ratio in the Ni-WC catalyst will result in the deactivation of the Ni-WC catalyst due to oxidation in the DRM reaction because WC prefers to react with CO_2. In DRM reaction over Ni-WC catalyst, oxidation of WC is the main reason for the catalyst deactivation [128]. A very large amount of Ni in Ni-WC promotes CH_4 dissociation. The increase in CH_4 conversion results in producing more $C_{(s)}$. This $C_{(s)}$ deposits on the surface of the catalyst, encapsulates or blocks the active sites, and ultimately results in ceasing the catalysis. Moreover, the particle size and surface area of WC decrease by increasing the Ni/W molar ratio. So, the Ni/W molar ratio in the Ni-WC catalyst must be regulated in a way that there is a balance

between CH_4 and CO_2 conversion during the DRM reaction. Ni-WC remains stable when using CH_4/CO_2 molar ratio is less than 1, $CH_4/CO_2>1$ deactivates Ni-WC due to coking [175]. With a similar Ni/M (M = Mo or W) molar ratio, Ni-Mo_2C and Ni-WC have similar specific surface areas. When Ni/M (M = Mo or W) molar ratio in Ni-Mo_2C and Ni-WC is 1/9 or 1/2, their catalytic activity for DRM reaction is similar. Pure WC does not show any catalytic activity for DRM reaction [128]. So, Ni and WC work in synergy to catalyze the DRM reaction [128]. Ni-WC enhances the H_2/CO yield in the pyrolysis combined with dry reforming of plastics [236]. H_2/CO yield depends upon the composition of the plastic used as the substrate.

Ni promoted WC catalyst has better resistance against oxidation than Ni-Mo_2C in DRM reaction [128]. The re-carburization of tungsten oxides is also much easier in comparison with the re-carburization of molybdenum oxides [128]. These two reasons make WC a more stable catalyst than Mo_2C, for DRM reaction [128].

$$Co_6W_6C + 5C \longrightarrow 6WC + 6Co \quad (92)$$

$$Co_6W_6C + (26 - x)O_8 \longrightarrow 6CoWO_4 + xCO + (1 - x)CO_2 \quad (93)$$

$$CoWO_4 + 2CH_4 \longrightarrow Co + WC + C + 4H_2O \quad (94)$$

Effect of Synthesizing Method

The most commonly used method for synthesizing WC catalyst is TPR (Figure 13[197-199]). The synthesis of WC using the TPR method involves the CTR of tungsten precursors. Some other methods, including SD, carbothermal reduction, CHR, and solid-solid reaction can also be used for synthesizing WC. The synthesizing method/conditions greatly affect the catalyst's activity/stability/product selectivity for a chemical reaction. Nanoparticles are considered to have great potential for surface catalysis due to having a very large surface area. Grigoryan et al. [242] synthesized WC and WC+W_2C nano-powders, by using the mechanochemical (MC) method and plasma-mechanochemical (PMC) method. Nano-powders (WC and WC+W_2C) were not pure, because some of the W metal particles were oxidized to WO_2 and WO_3 by air during unloading into the reactor, for synthesizing the carbide phase. However, the free C found in the synthesized samples was less than 1%. WC nano-catalyst synthesized by the PMC method was found to be more active than the one prepared by MC method, for DRM reaction. The $C_{(s)}$ formed during the DRM reaction did not affect the catalytic activity of WC, synthesized by both methods. With decreasing particle

size, the catalytic activity of WC for DRM reaction increases proportionally, and DRM reaction temperature also affects the catalytic activity of WC in a similar way. The nano-powder containing mixture WC+W_2C gave the least CH_4 conversion, this result proved that the active species for catalyzing the DRM reaction are only WC.

The crystal structure and size of the obtained tungsten carbide depend upon the temperature used for the carburization process [241]. In the TPR method, using $CO_2/CO = 0.75$ for the carburization of $Co(en)_3WO_4$ precursor, results in the synthesis of a very active/stable Co_6W_6C catalyst for DRM reaction [246]. In order to synthesize Co-WC and Ni-WC under CO_2/CO flow by TPR process, CO_2/CO must be ≥0.5 and ≥0.75, respectively [247]. In addition to CO_2/CO, carbohydrates can also be used for the carburization process. Wysocka et al. [236] synthesized WC and Ni-WC by using ammonium metatungstate as the W source, nickel nitrate as the Ni source, and saccharides (monosaccharides and disaccharides) as the C source. WC synthesized by using any of the saccharides as the C source was not found active in catalyzing DRM reaction, because all the WC catalysts were oxidized to tungsten oxides. But Ni-WC synthesized by using trehalose (T), fructose (F), glucose (G), or sucrose (S) as the C source, followed the catalytic activity order for DRM reaction as Ni-WC_F>Ni-WC_S>Ni-WC_G>Ni-WC_T. Ni prevented the oxidation of the carbide phase, and only graphitic C was deposited on the catalyst surface during the DRM reaction.

Biochar can be used as the C source for synthesizing WC by TPR of tungsten oxide or precursor [241]. Nitridation of the precursor before TPR helps in synthesizing a very stable WC catalyst for DRM reaction [126].

There are several methods for synthesizing the WC, but the catalytic potential of WC synthesized by all the methods, for CH_4 reforming reactions, has not been studied yet. On commercial scale, submicron-sized WC is synthesized by the carbonization of C-coated-WO_3 with C-black at 1400^0C-1600^0C for 2-10h under the flowing H_2 or Ar atmosphere [250, 251]. This process is known as the precursor method. In this process, first WO_3 is coated with C by cracking a C containing gas (most commonly C_3H_6), and then the C coated WO_3 powder is mixed with C black and heated at 1400^0C-1600^0C for 2-10h under the flowing H_2 or Ar atmosphere [250]. The precursor method is a highly time-expedited process [252]; however, it requires highly pure substrates which makes this method unviable.

The hydrothermal reaction method is relatively a cheaper method to synthesize the WC nano-powders [253]. In this method, metal salt (ammonium metatungstate, or ammonium paratungstate, etc.) aqueous solution is used as the precursor (WO_3) source, and organic compounds (glycine, corn starch, chitin, or iota-carrageenan etc.) are used as the C source [253]. The evaporation of salt and water gives WO_3. Subsequently, the C from the organic reduces WO_3 to WC [253].

Yang et al. [254] synthesized WC (with a particle size of 300–500nm) by mechano-chemical method. Firstly, W and activated-carbon (AC) powders were mechanically activated under an argon atmosphere using a high-energy planetary mill (10 mm hardened steel ball, ball-to-powder ratio: 5:1, and rotational speed 1200 rpm). After milling, the mechanically activated powder was mixed with a KCl and NaCl ($\text{molar ratio} = 1:1$) mixture (60wt%) and heated at 1000^0C for 1h. The reaction product was then allowed to be cold down to room temperature in the air. To obtain the final product (free of salt impurities) the product was boiled several times in distilled water.

Zhang et al. [255] combined a pre-dried salt mixture (NaCl and KCl salts mixed in a 1:1 molar ratio) with mixtures containing WO_3 and graphite in different molar ratios. Salt mixture to WO_3- graphite mixture weight ratio was kept at 1:30. The resulting powder mixtures were then heated at 950^0C-1150^0C for different durations under the flowing Ar atmosphere. After heat treatment, all the products were boiled repeatedly in distilled water to remove the salt impurities. The optimum conditions to produce submicron continuous WC coatings by this method were found heat treatment at 1100^0C for 60min, and WO_3/graphite molar ratio ranging from 1:15 to 1:5.

Qiu et al. [256] introduced a method to synthesize WC using WO_3, C black, and NaCl as starting materials. The process involved ball milling WO_3 and C black in a 1:4 molar ratio for 12h, adding NaCl (with salt to milled WO_3-C mixture weight of 1:1) and ethyl alcohol, followed by further milling for 12h and drying at 50^0C. The resulting powder was calcined at various temperatures for 2h, cold down to room temperature, washed several times in distilled water to remove salt, and treated to remove residual carbon. This method successfully produced WC plate particles at temperature higher than 1200°C.

Effect of Reaction Conditions

The conversion of DRM substrates over WC catalyst increases with increasing both temperature and pressure [114, 115, 159, 245]. Additionally, the operating pressure is one of the factors that

decide the lifetime of the WC catalyst in DRM reaction [114, 115]. At low pressure (1 bar), with unswerving activity/stability only for the first 8h on the stream, the catalytic action of α-WC catalyst for DRM reaction disappeared completely in almost the next 20h, in the results of the experimental study done by Claridge et al. [115]. But the stability of the carbide phase (α-WC) at high pressure (8.3 bar) led to a consistent catalytic behavior for DRM reaction, for the total testing time (72h) on stream. In investigating the effect of using a stoichiometric amount of the reactants (CH_4/CO_2) on the catalytic behavior of WC and Mo_2C for DRM, York et al. [114] got experimental results at 1bar, which are also in agreement with the results of the work done by Claridge et al. [115]. DRM reaction at low or atmospheric pressure over the WC catalyst results in the conversion of WC to WO_2 [114, 115]. This bulk oxidation of the WC catalyst at ambient pressure is irreversible and causes permanent deactivation of the WC catalyst. At reduced pressure, there is no other explanation for the deactivation of WC catalyst in the DRM reaction. Because analysis of the used WC catalyst sample shows only the presence of WO_2 molecules and there are no signs of coke formation or metal sintering [114, 115]. Overall, flowing H_2 or H_2/C_2H_6 mixture over spent WC is not helpful in restoring its catalytic activity [159]. However, reducing the used WC catalyst under H_2 atmosphere at 773K for 3h, helps in removing the accumulated $C_{(s)}$, but reusing this WC catalyst for DRM reaction is not good for getting higher substrates' conversion for a very long time [126]. Increasing GHSV in DRM over WC catalyst, decreases CH_4/CO_2 conversion and H_2/CO yield [241]. At very high GHSV CH_4 activation/dissociation rate cannot reach equilibrium with CO_2 activation/dissociation because CH_4 decomposition is a slow process in comparison with CO_2 dissociative adsorption, and at high GHSV CH_4 molecules get very little opportunity to come in contact with the active sites of the catalyst [241].

WC as Support for Metal catalysts in Catalyzing DRM reaction

WC as support is good for the generation of oxygen vacancies on the surface of the metal catalysts, which in turn enhances the metal catalysts' stability, coking resistance, ability for CH_4/CO_2 conversion and H_2/CO yield, in DRM reaction [257, 258]. Therefore, WC as support, either in pure form or as a component of composite support, has been used widely for metal-based catalysts, to improve their functionality for DRM reaction. A summary of the performance of the TMCs as support for improving the functionality of metal catalysts for CH_4 reforming reactions is provided in Table 6. Bolatava et al. [259] synthesized WC (technically a mixture of α-WC and β-W_2C) by the vacuum-free electric arc, and used it as a support for Ni, Co, and Ni-Co (with different Ni and Co

wt.%) catalysts to enhance their activity/stability for DRM reaction. M/WC (M=Ni or Co or Ni-Co) catalysts were synthesized by deposition precipitation (DP) or incipient wetness impregnation (IWI). M/WC catalysts especially with high Ni content, synthesized by DP were found to be very active/stable for DRM reaction. CH_4/CO_2 conversion and H_2/CO yield in DRM over Ni-Co/WC catalyst increase by increasing temperature and Ni wt.% in Ni-Co/WC catalyst, but decreases with increasing WHSV [259].

Table 6: Summary of the performance of the TMCs as support in improving the functionality of metal catalysts for CH4 reforming reactions.

Active Site	Support	SM, RT	App	Synthesis Conditions	Reaction Conditions	Feed Comp.	Max Con [%]	Selectivity [%]	Comment	Refs
Ce-Co	WC-AC	SM: TPR RT: FBR	DRM 2021	P: 1atm / T: 650-950^{0}C TR: 1.7^{0}C/min H_2: 100% H_2 flow: – TC: 2h	P: 1atm /T: 800^{0}C GHSV: – Flow: 120ml/min TOS: 10h	CH_4: 1 CO_2: 1	CH_4: 91.0 CO_2: 93.0	H_2: – CO: – H_2/CO: 92.0	TPR of W/AC under H_2 helps in synthesizing a very active/stable WC-AC composite support. WC content in WC-AC must be highly optimized for a better catalytic performance. Ce heightens the activity of Co/WC-AC for DRM.	[257]
Y-Co	WC-AC	SM: TPR RT: –	DRM 2022	P: 1atm / T: 650-950^{0}C TR: 3.5^{0}C/min H_2: 100% H_2 flow: 150ml/min TC: 2h	P: 1atm / T: 800^{0}C GHSV: 4800ml$g^{-1}h^{-1}$ Flow: 120ml/min TOS: 10h	CH_4: 1 CO_2: 1	CH_4: 92.0 CO_2: 94.0	H_2: – CO: – H_2/CO: 85.0	Y is the best promoter amongst Y, Mn and Gd for Co/WC-AC catalyst to enhance the activity/stability for DRM reaction.	[258]
Ni	WC	SM: VEA RT: FBR	DRM 2022	Anode: Graphite rod Cathode: Graphite crucible I: 220A V: 63V TC: 45s	P: 1atm / T: 800^{0}C GHSV: – WHSV: 12000ml$g^{-1}h^{-1}$ Flow: – TOS: 80h	CH_4: 1 CO_2: 1	CH_4: 80.0 CO_2: 88.0	H_2: – CO: – H_2/CO: 80.0	WC synthesized by the VEA method can be used as a support to boost the catalytic function of Ni-Co for DRM reaction. Ni-Co/WC with minimum or zero Co content is a highly active and stable catalyst for DRM reaction.	[259]
Co Ni-Co	WC-AC	SM: TPR RT: –	DRM 2023	P: – / T: 650-950^{0}C TR: – N_2/H_2: 1 N_2/H_2 flow: 310ml/min TC: 2.5h	P: – / T: 800^{0}C GHSV: – Flow: 1120ml/min TOS: 24h	CH_4: 1 CO_2: 1	CH_4: 86.4 CO_2: 86.5 CH_4: 91.9 CO_2: 90.9	H_2: – CO: – H_2/CO: 90.0 H_2: – CO: – H_2/CO: 98.0	Ni-Co/WC-AC catalyst with a specific Ni/Co ratio is way better than Co/WC-AC for DRM reaction, in terms of activity and C deposition resistance.	[260]
Ni	SiC	SM: – RT: –	TRM 2012	–	P: 1atm / T: 1073K GHSV: 60000ml$h^{-1}g^{-1}$ Flow: 100ml/min TOS: 250min	CH_4: 1 O_2: 0.5 CO_2: 0.5 $H_2O_{(s)}$: 0.1	CH_4: – CO_2: –	H_2: – CO: – H_2/CO: 890.0	SiC as support for Ni catalyst promotes H_2O conversion more than CO_2 conversion in the TRM process and enhances the H_2/CO ratio.	[93]
Ni	β-SiC	SM: – RT: –	TRM 2013	–	P: 1atm / T: 1073K GHSV: 60000h^{-1} Flow: 100Nml/min TOS: 500min	CH_4: – O_2: – CO_2: – $H_2O_{(s)}$: –	CH_4: – CO_2: –	H_2: – CO: – H_2/CO: 210.0	Increasing the flow rate of H_2O and O_2 in the reactant stream of TRM reaction over Ni/β-SiC increases the H_2/CO yield and helps in using the optimum pressure/temperature conditions.	[238]
Mg-Ni	β-SiC	SM: – RT: –	TRM 2013	–	P: 1atm / T: 1073K GHSV: – WHSV:60000Nml$h^{-1}g^{-1}$ Flow: 100Nml/min TOS: 24h	CH_4: 1 O_2: 0.1 CO_2: 0.5 $H_2O_{(s)}$: 0.5	CH_4: 97.9 CO_2: 43.2	H_2: – CO: – H_2/CO: 276.0	Mg as a promoter amongst alkaline and alkaline-earth cocations is the best promoter to enhance the activity/stability of Ni/β-SiC catalyst for TRM reaction.	[239]
Mg-Ni	β-SiC	SM: – RT: –	TRM 2013	–	P: 1atm / T: 1073K WHSV:60000ml$h^{-1}g^{-1}$ Flow: 100ml/min TOS: 24h	CH_4: 1 O_2: 0.1 CO_2: 0.5 $H_2O_{(s)}$: 0.5	CH_4: – CO_2: –	H_2: – CO: – H_2/CO: 336.0	Mg-Ni/β-SiC catalyst, with Ni/Mg molar ratio 1/1 and synthesized by impregnating β-SiC support with Mg first and then Ni, shows the highest activity/stability for TRM reaction.	[240]

In terms of composite support, WC—AC composite support has been widely used for DRM reaction. In synthesizing WC—AC composite support by TPR method, the composition of the gas used for the carburization of the precursor, has a big influence on the role that WC—AC composite support plays in promoting the catalytic role of an active metal for DRM reaction [243]. The WC—AC composite support synthesized by carburizing the precursor under H_2 gas than under CH_4/H_2 mixture in the TPR method, has more CO_2 adsorption/activation ability and oxygen vacancies, and therefore is a better support for the Co catalyst in DRM reaction [243, 257]. The WC—AC composite support synthesized by using H_2 as carburizing gas has W_2C as a dominant phase and has a better interaction with Co metal, while the WC—AC composite support synthesized by using CH_4/H_2 as carburizing gas has WC as a dominant phase [243, 257]. The particle size of W_2C is smaller than that of WC, but WC has a better dispersion [243, 257]. In DRM reaction over Co/WC—AC no metal sintering or oxidation takes place [243]. However, amorphous, filamentous, and graphitic C forms, but the major reason for the catalyst deactivation is graphitic C [243]. Another reason for the deactivation of the Co/WC—AC catalyst in DRM reaction is the interaction b/w WC and Ca species of AC [243]. This interaction results in the formation of inactive $CaWO_4$ species [243]. The spent Co/WC—AC catalyst has C-α (amorphous C), C-β (filamentous C), and C-γ (graphitic C) species, depending upon the temperature used for the DRM reaction [243, 257]. C-β and C-γ species are very stable and deposition of these species makes the catalyst inactive, while C-α species are active species and can easily be gasified [243, 257]. W—C is a very strong covalent bond, therefore WC prevents the loss of C from AC [243].

Zhang et al. [260] synthesized WC—AC composite support and examined its effect on the catalytic performance of Co-based catalysts for DRM reaction. Regarding WC—AC a few points need to be highlighted. First, WC—AC composite support itself is very poor in catalyzing DRM reaction, but it helps in the removal of the $C_{(s)}$, deposited on the surface of the metal catalysts in DRM reaction, by gasification [243]. Second, WC—AC composite support has a very large surface area, which facilitates the loading of more amount of the active species for the reaction, but adding a promoter for a metal catalyst already loaded on WC—AC composite support, negatively impacts the surface area of the WC—AC composite support [243, 258]. Third, WC improves the interaction between Co and AC in Co/WC—AC catalyst, this interaction makes Co thermally more stable [257, 258]. Fourth, WC—AC composite supported metal catalysts always give a H_2/CO yield ratio greater than 1 in DRM reaction because WC—AC composite support facilitates CH_4 decomposition/conversion

[243]. DRM feed conversion, when using Co/WC—AC catalyst, is initially good, but $C_{(s)}$ deposition and oxidation of Co with time stops the catalysis. The wt.% of WC in Co/WC-AC must be highly optimized for a better catalytic action [257]. A bi-metal active site (e.g., Ni-Co) is better than a single metal, in catalytic function. Ni-Co/WC-AC catalyst is way better in activity/stability, and oxidation/coking resistance than Co/WC—AC, for DRM reaction. Increasing Ni loading wt.% to a specific value improves the DRM feed conversion. CH_4/CO_2 conversion and H_2/CO yield were found maximum when the wt.% loading of both the metals (Ni and Co) was 10 in the Ni-Co/WC-AC catalyst. DRM reaction proceeds on the surface of the catalyst in the steps given in Equations 95-100 [260]. The adsorbed CH_x^* species react with O^* to form CHO intermediate species. So, the production of CHO species is directly affected by the rate of formation of CH_x^* and O^* species which in turn affects the rate of conversion of DRM substrates.

$$CH_4 \rightarrow CH_3^* + H^* \quad (95)$$

$$CH_3^* \rightarrow CH_2^* + H^* \quad (96)$$

$$CH_2^* \rightarrow CH^* + H^* \quad (97)$$

$$CH^* \rightarrow C^* + H^* \quad (98)$$

$$CO_2 \rightarrow CO^* + O^* \quad (99)$$

$$CH_x^* + O^* \rightarrow CH_xO^* \quad (100)$$

Ni, in Ni-Co/WC-AC catalyst, improves the percentage of WC content, forms Ni-Co alloy, enhances the active metal-support interaction and electron (e^-) migration between them, and increases the number of oxygen vacancies. Due to all these functions performed by Ni, not only CH_4/CO_2 activation/dissociation increase but the C—C bonding state is also affected. Therefore, only amorphous C deposits on the surface of the catalyst and can be oxidized easily. In this way, Ni-Co/WC-AC catalyst shows better $C_{(s)}$ deposition resistance than Co/WC-AC, in DRM reaction. Zhang et al. [258] used Y, Gd, and Mn as promoters to enhance the activity/stability of the Co/WC-AC catalyst for DRM reaction. Y as a promoter causes the maximum reduction in surface area of WC-AC, but WC species were found maximum in Y-promoted Co/WC-AC catalyst. The Y-promoted Co/WC-AC catalyst displayed the maximum activity and coking resistance in the DRM reaction. Ce is also a good promoter to boost the catalytic function of Co/WC-AC [257].

Being a H rich compound, CH_4 is one of the best sources to be considered for getting H_2, and thermal/plasma-assisted CH_4 reforming is one of the best processes to be considered for producing H_2 from CH_4. As reviewed above, MCs show enormous potential as catalysts for CH_4-reforming based H_2 production reactions. The redox cycle of MCs in CH_4 reforming reactions is very important for the catalysis to keep going and produce the desired yield, and MC and MC—O species are very important for the establishment of this redox cycle.

A schematic of the common problems in DRM over a MC catalyst is presented in Figure 17. In all cases (when using a MC as a catalyst for CH_4-reforming-based H_2 production reaction), higher oxide ($H_2O_{(s)}$, CO_2 and O_2) conversion than CH_4 reveals the fact that a MC is more reactive towards oxides than CH_4. A greater oxides' activation/dissociation/consumption rate than CH_4, leads to the conversion of a MC to a MO_2 that eventually stops catalysis. So, to create a balance between oxides' and CH_4 conversion, the introduction of a second metal (that can promote CH_4 conversion) in the MC lattice, in correct proportion, becomes mandatory. The proportion of the promoter (or second metal) in MC's lattice, must be monitored strictly because in a scenario where CH_4 conversion is higher than oxides, deposition of the excess $C_{(s)}$ (produced due to CH_4 decomposition) on the catalyst surface will cause the deactivation of catalyst. The reaction of the C atoms of a MC with O^* species (generated by the dissociation of adsorbed oxide molecules) results in the absence of C atoms from the MC lattice. This puts MC at high risk of oxidation and ultimately deactivation. Similarly, the generation of excess C^* species (generated by the dissociation of adsorbed CH_4 molecules) puts the catalyst at high risk of deactivation by $C_{(s)}$ deposition.

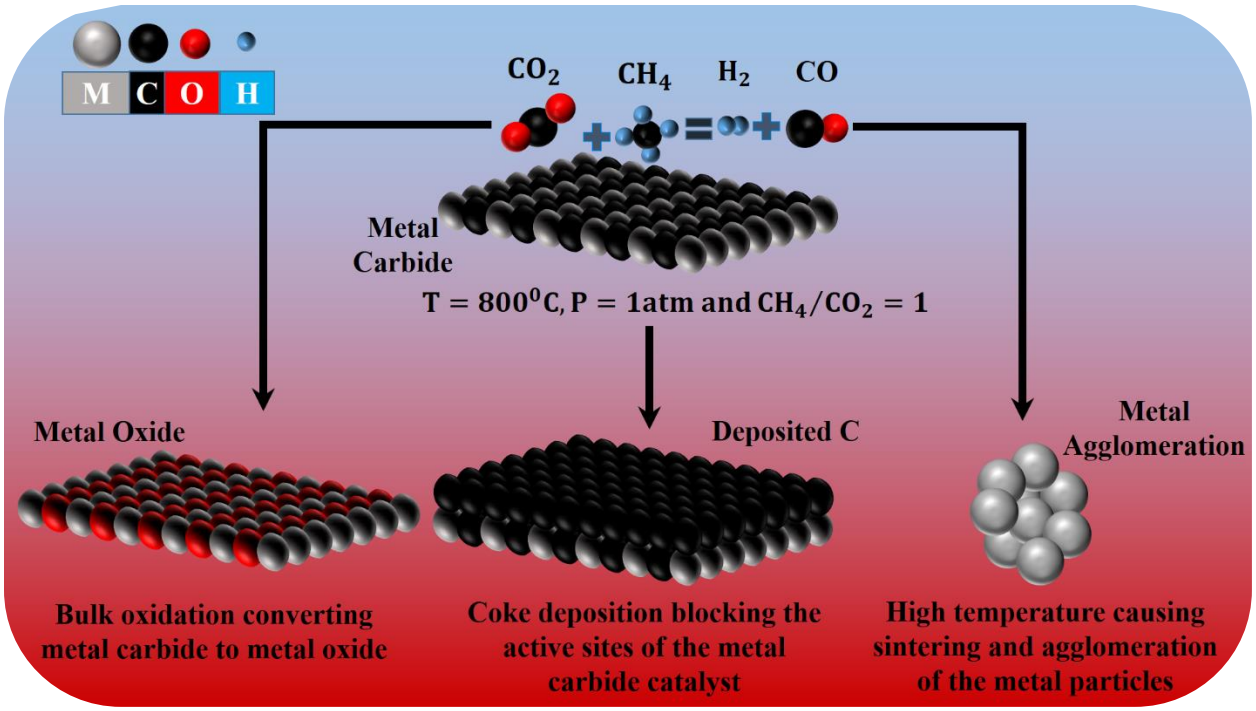

Figure 17. Schematic of the common problems in metal-carbide catalytic DRM reaction.

Summary of the strategies that help in improving the catalytic function of MCs in DRM reaction are summarized in Figure 18. For a MC catalyst to last longer in CH_4-reforming-based H_2 production reaction, O^* and C^* species must be produced in evenness so that they are available to react with each other rather than interacting with the catalyst and ceasing its functionality. A high surface-to-bulk ratio and a high dispersion on support can also enhance the catalytic performance of MCs. The catalytic properties of MCs are related to their phases, crystal structures, and electronic structures, and can be adjusted by using different types of catalyst precursors, catalyst-precursor-synthesizing-methods/conditions, pre-treatment-methods/conditions, C sources, MC synthesizing methods/conditions, promoters, and support. Reaction conditions, like temperature, pressure, and feed composition also affect the catalytic properties of MCs, and must be monitored/regulated strictly and constantly.

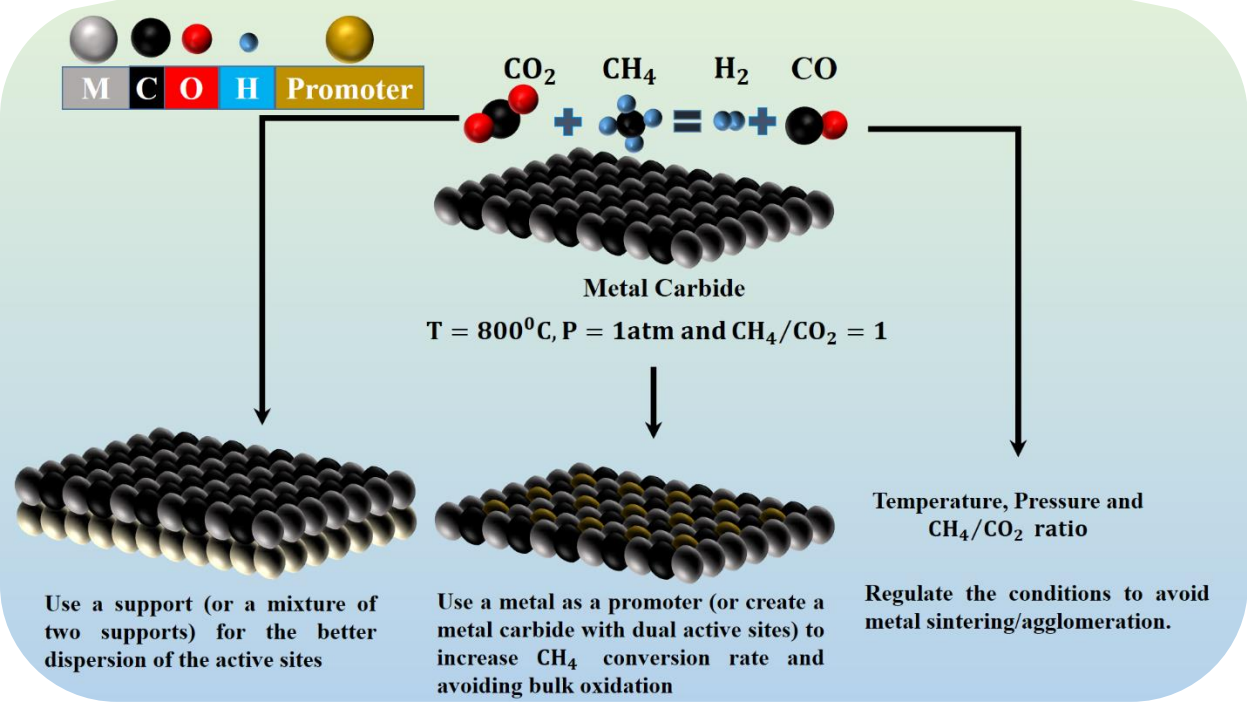

Figure 18. Schematic of the strategies that help to overcome the problems in metal-carbide catalytic DRM reaction.

CHAPTER 3: METHODOLOGY

Synthesis of TMC catalysts

To synthesize Mo_2C and WC catalysts, the combination of mechanical activation followed by molten salt synthesis was employed. The process began with preparing mixtures of metal and carbon powders, using Mo in both nanopowder and micro powder forms, and W only in nanopowder form, combined with either nano-sized super activated carbon or nano-sized black carbon at various molar ratios (0.2/1, 0.5/1, 1/1, and 2/1 for Mo_2C, and 1/1 for WC). These mixtures were then mechanically activated in a high-energy planetary ball mill at 550 RPM for 24 hours with a ball to metal+carbon weight ratio of 10/1. The milled powders were subsequently mixed with a NaCl and KCl salt mixture, which constituted 60% of the total weight, and heated at 1000^0C for 3 hours under a flowing Ar atmosphere. After cooling, the samples were boiled in de-ionized water to dissolve the salt, leaving only the metal carbide, and then dried in an oven at 100^0C for 24 hours. This method ensured thorough mixing and uniform distribution of reactants, facilitating the carburization reaction. As a result, eight different Mo_2C catalysts were produced, considering the variations in Mo sources and carbon types, while only two WC catalysts were synthesized due to the single source of W. Figure 19 illustrates the schematic representation of the synthesis steps followed for the preparation of the catalysts, including the final product. The crystallographic phases of the synthesized catalysts were characterized using X-ray diffraction (XRD). Scanning electron microscopy (SEM) was employed for morphological analysis, while energy dispersive X-ray spectroscopy (EDS) was used to determine the elemental composition of the catalysts.

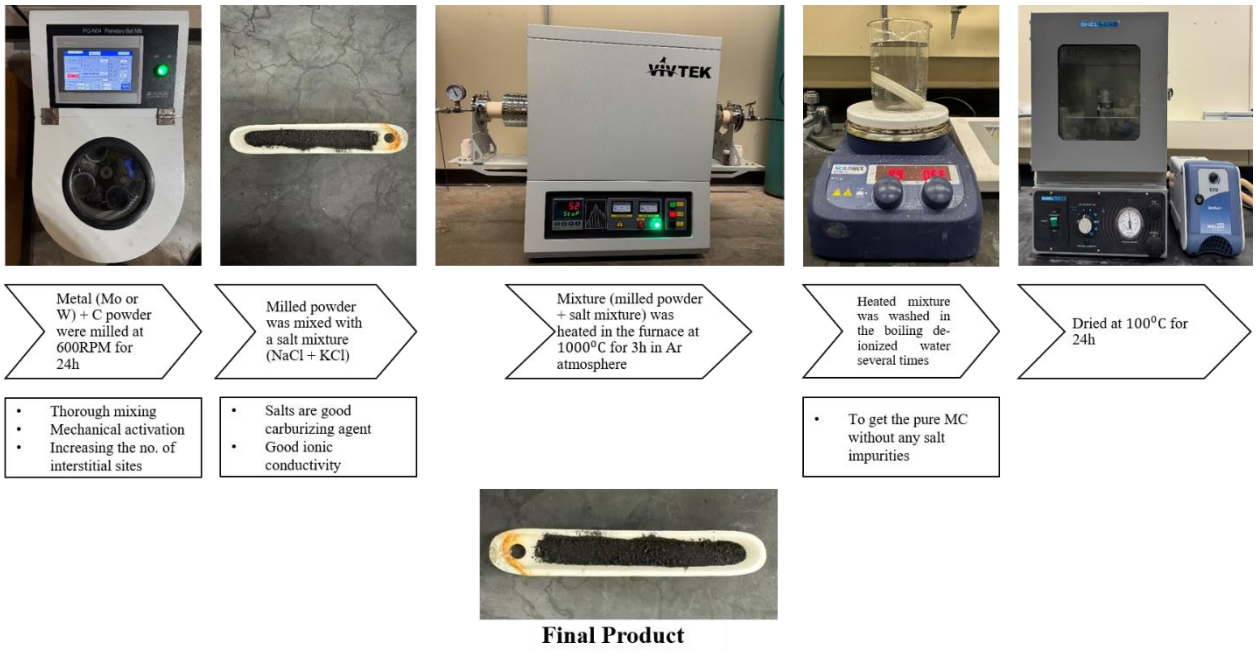

Figure 19. Schematic representation of the synthesis steps followed for the preparation of the catalysts.

Experimental set-up and procedure

In the experiments, a dielectric barrier discharge (DBD) fixed-bed reactor was utilized, featuring two glass tubes as the dielectric barriers. One glass tube had an outer diameter (OD) of 12mm and an inner diameter (ID) of 8mm, while the other had an OD of 5mm and an ID of 3mm. These glass tubes served as the dielectric layers. The clearance between the two dielectric materials was found 1.5mm. The gap between the dielectric barriers was filled with glass beads of 1mm in size, and the catalyst was coated on these glass beads. A stainless-steel wire was used as the high voltage electrode, connected to a DC power source. The outer electrode, which served as the ground electrode, was a stainless-steel mesh wrapped around the external surface of the larger glass tube. The discharge length of this system was 10cm, and the discharge gap between the two electrodes was maintained at 4.5mm (clearance/gap between the dielectric barriers + thickness of the dielectric barriers) (Figure 20). A high voltage probe connected to the inner electrode measured the applied voltage during the discharge process. Electrical signals produced on the electrodes were recorded using a digital oscilloscope. The applied power was calculated by using the formula given in Equation 101. The applied voltage and current can be determined from the display of the DC supply. A schematic of the reaction set-up is shown in Figure 21(a), while the actual set-up in the lab is shown in Figure 21(b). In all the experiments, a DC voltage of 800V was applied, with a current of

0.173A, resulting in a power output of 140W. The operating frequency was 5kHz, and a delay of 1 microsecond was applied. The feed gas consisted of a methane (CH_4) and carbon dioxide (CO_2) mixture in 1:1 ratio, with a total flow rate of 30 ml/min. For all the experiments involving catalysts, 0.1g of catalyst was used, which was coated onto glass beads placed in the discharge gap. A digital thermal camera was employed to measure the temperature of the discharge zone in the reactor, providing accurate temperature readings during the process.

$$P = VI \tag{101}$$

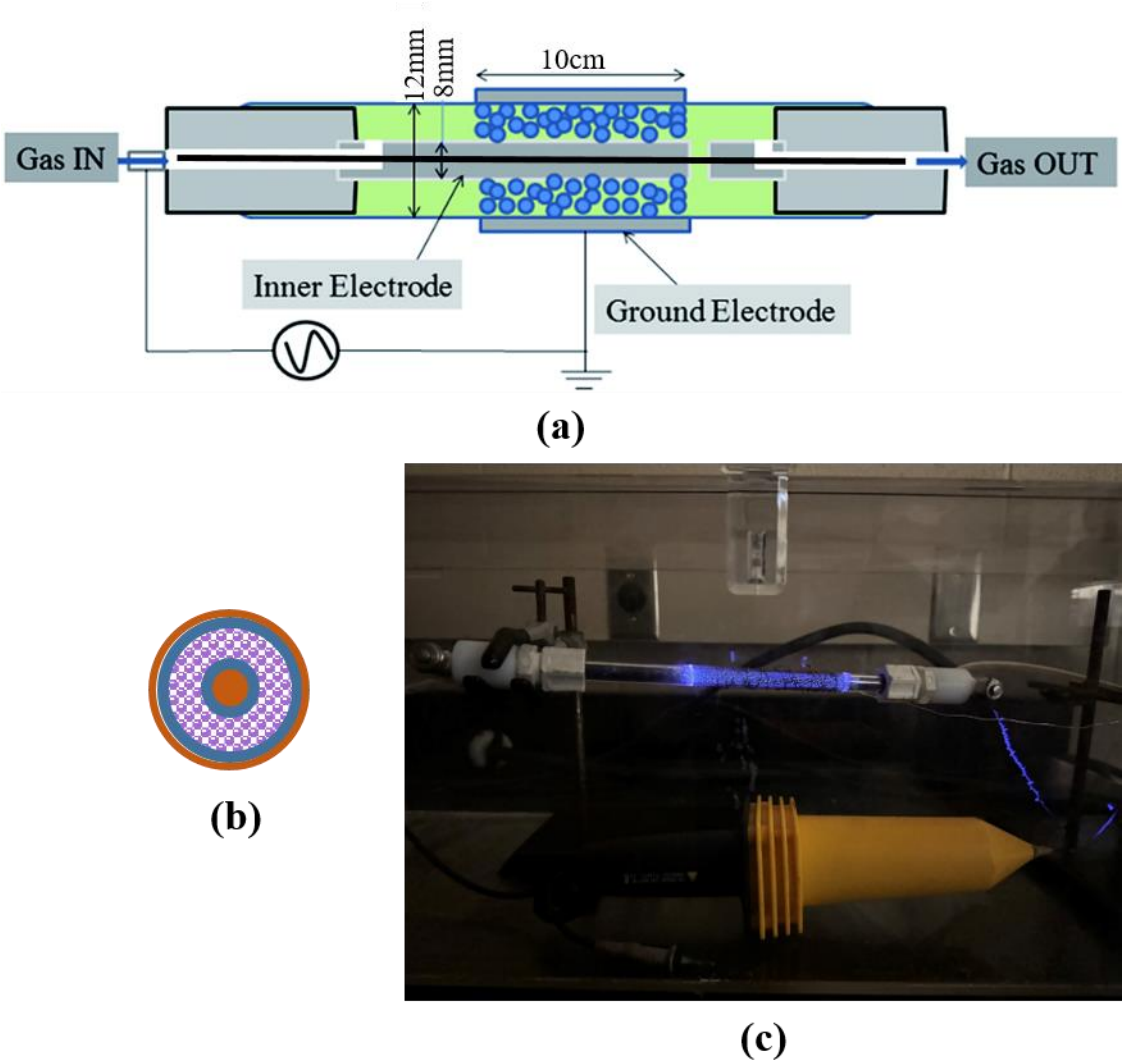

Figure 20. (a) Schematic of the DBD plasma fixed-bed reactor [1]. (b) Cross-section of the DBD plasma fixed-bed reactor. (c) In-operation DBD plasma fixed-bed reactor.

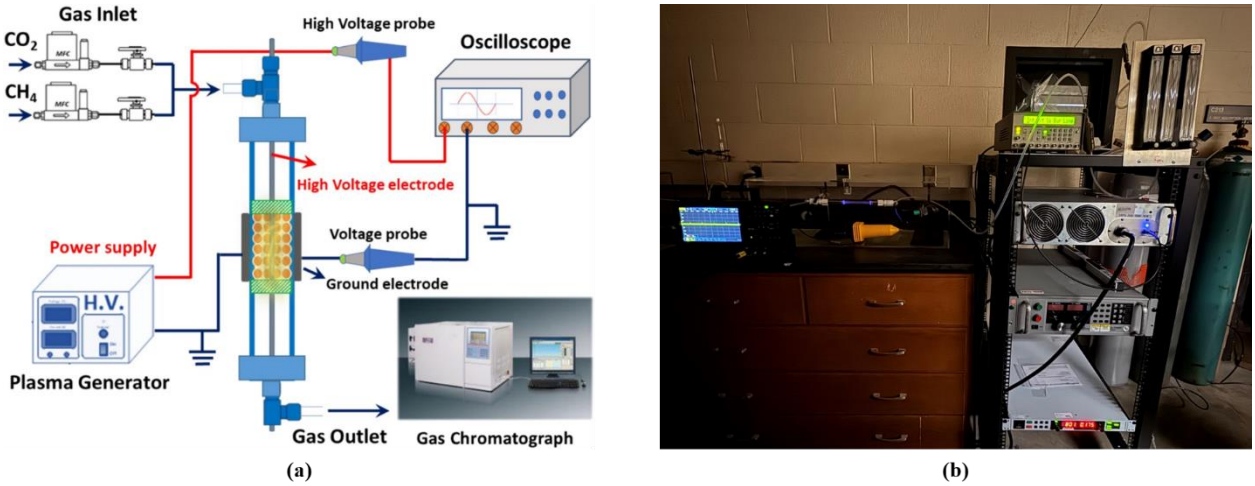

Figure 21. (a) Schematic of the experimental set-up [2]. (b) Actual experimental set-up in-operation.

A Shimadzu GC-2014 (Figure 22) equipped with a ShinCarbon column (2.0m length, 0.53mm ID, 212µm film thickness) was employed for the analysis of the collected gas samples. Ar served as the carrier gas. To ensure accuracy in the gas concentration measurements, gas chromatograph (GC) was calibrated using known standard samples. Five calibration standards were prepared with varying concentrations of target gas components as shown in Table 7. However, the calibration results indicated a consistent underestimation of gas concentrations by approximately 5%, with the GC readings being 5% lower than the actual concentrations of the known samples. As a result, for all subsequent analyses of the gas samples collected during the experiments, the GC system consistently underestimated the concentration of each gas present in the product samples by this same 5%. This systematic error was accounted for in the interpretation of the experimental results.

Table 7: Composition of the standards used for calibrating GC

Standard	CO_2 (mol %)	CO (mol %)	H_2 (mol %)	CH_4 (mol %)
1	1 %	1 %	1%	1%
2	15 %	7 %	-	4.5 %
3	-	-	99.99 %	-
4	-	-	-	99.99 %
5	99.8 %	-	-	-

Figure 22. Shimadzu GC-2014.

The GC was operated under the following conditions:

- Column temperature: 40 °C (isothermal)
- Injector temperature: 250^0C
- Injection mode: Split
- Sampling time: 1min
- Pressure: 278.5kPa
- Total flow: 10.5mL/min
- Linear velocity: 187.9cm/s
- Purge flow: 3.0mL/min.
- Split ratio: 2
- End time = 9.75min

The detector (DTCD) was operated at a temperature of 100^0C with a filament current of 70 mA. Byproducts produced during the experiments were not analyzed.

Data analysis

Feed conversions, syngas yield, H_2 selectivity, and CO selectivity were calculated as follows:

$$CH_{4_{converted}} = \frac{CH_{4_{in}} - CH_{4_{out}}}{CH_{4_{in}}} \times 100 \quad (102)$$

$$CO_{2_{converted}} = \frac{CO_{2_{in}} - CO_{2_{out}}}{CO_{2_{in}}} \times 100 \quad (103)$$

$$H_{2_{yield}}(\%) = \frac{H_{2_{out}}}{2CH_{4_{in}}} \times 100 \quad (104)$$

$$CO_{yield}(\%) = \frac{CO_{out}}{CH_{4_{in}} + CO_{2_{in}}} \times 100 \quad (105)$$

$$H_{2_{selectivity}} = \frac{H_{2_{out}}}{H_{2_{out}} + CO_{out}} \times 100 \quad (106)$$

$$CO_{selectivity} = \frac{CO_{out}}{CO_{out} + H_{2_{out}}} \times 100 \quad (107)$$

CHAPTER 4: RESULTS AND DISCUSSIONS

This study on the use of TMC catalysts, specifically Mo_2C and WC, in conjunction with DBD plasma for the DRM process, has yielded significant insights and improvements in several key areas.

Baseline comparison: Plasma-only system

To establish a baseline for evaluating the improvements made by TMC catalysts, experiments were first conducted using only the DBD plasma system without any catalyst. In this setup, the DC voltage applied was 800V, the current was 0.173A, resulting in a power output of 140W, with a frequency of 5kHz and a delay of 1 microsecond. The results (**Figure 23**) showed a H_2 yield of 10%, CO yield of 10%, H_2 selectivity of 49%, CO selectivity of 51%, CH_4 conversion of 9%, and CO_2 conversion of 13%. These values serve as a reference point to assess the enhancements achieved by incorporating TMC catalysts into the system.

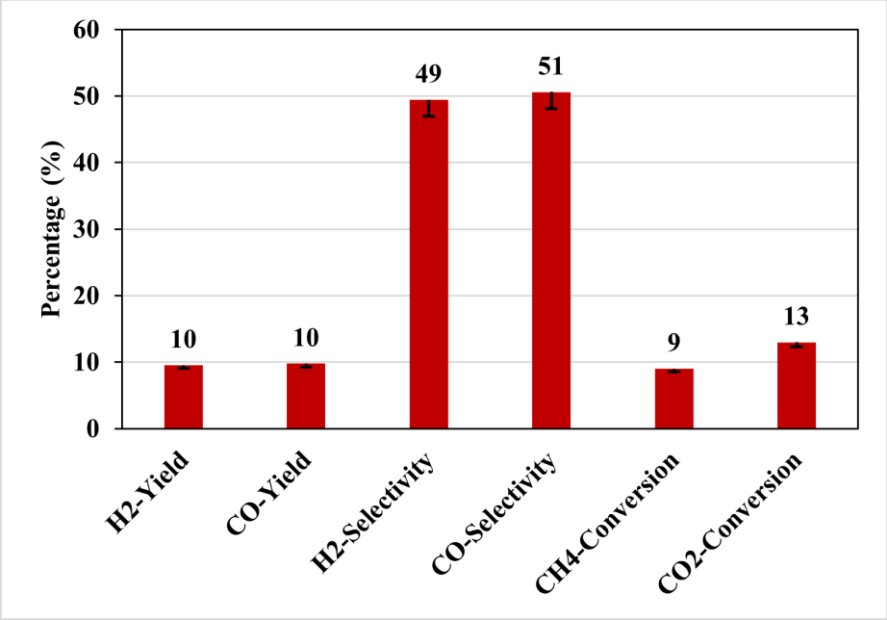

Figure 23. DRM over DBD-plasma only system. Reaction conditions: CH_4 : CO_2 = 1 : 1, flowrate = 30ml/min, f = 5kHz, V = 800V, I = 0.173A, and P = 140W.

Mo_2C Catalysts

Characterization

XRD

To confirm the successful synthesis of Mo_2C catalysts and evaluate their phase purity, synthesized Mo_2C catalysts were analyzed using X-ray diffraction (XRD). The XRD analysis revealed a significant influence of the precursor composition on the final product's phase purity. Lower Mo/C ratios (0.2/1 and 0.5/1) resulted in impure products, with the presence of unreacted C, MoC_{1-x}, MoO_2, and MoO_3 detected (Figure 24 (a & b)). Specifically, the 0.2/1 ratio yielded a mixture of phases (Figure 24 (a)), while the 0.5/1 ratio showed traces of MoO_2 alongside Mo_2C (Figure 24 (b)). In contrast, higher Mo/C ratios (1/1 and 2/1) produced pure or nearly pure Mo_2C with minimal traces of unreacted carbon (Figure 24 (c & d)). The observed phase purity at higher Mo/C ratios suggests an optimal stoichiometric balance for Mo_2C formation, potentially leading to enhanced catalytic performance due to a more uniform surface composition and increased availability of active sites.

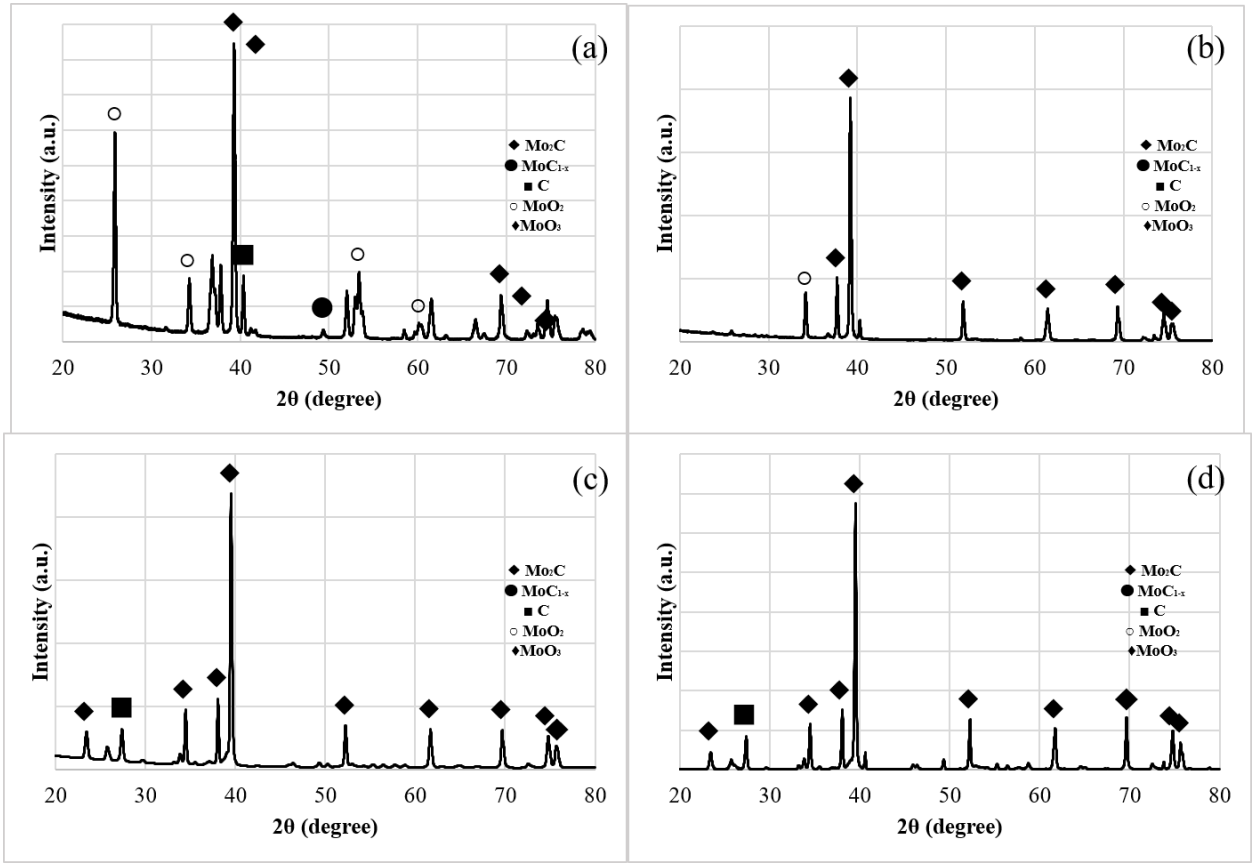

Figure 24. XRD patterns of Mo_2C catalysts synthesized by using different Mo/C ratios. (a) Mo/C = 0.2/1, (b) Mo/C = 0.5/1, (c) Mo/C = 1/1, and (d) Mo/C = 2/1.

Impact of Mo powder size, carbon type and Mo/C

Impact on syngas yield, H_2 and CO selectivity, and feed conversion

The use of different sizes of Mo powder (nanopowder vs. micropowder) significantly impacted the catalytic performance. For instance, Mo_2C catalysts synthesized with micropowder Mo and nanopowder carbon black showed higher CH_4 conversion (up to 73%) **(Figure 25)** and CO_2 conversion (up to 49%) **(Figure 25)** compared to those synthesized with nanopowder Mo (Figure 26). This can be attributed to the larger surface area and better dispersion of micropowder Mo, which enhances the interaction between Mo and carbon, leading to a more efficient carburization process and higher catalytic activity. The larger particles may also reduce the sintering effect, maintaining the catalyst's surface area and activity over time [73, 261].

The type of carbon used (superactivated carbon vs. carbon black) also influenced the catalytic performance. Catalysts synthesized with superactivated carbon generally showed slightly lower conversions compared to those with carbon black (Figure 26 and 25). This difference can be explained by the varying surface properties and reactivity of the carbon sources. Superactivated carbon, with its high surface area and porosity, may lead to a more uniform distribution of Mo, but it might also result in a slightly lower carburization efficiency compared to carbon black, which has a more graphitic structure that can facilitate better Mo-C bonding [261].

The Mo/C molar ratio played a crucial role in determining the catalytic activity. For Mo_2C catalysts, a Mo/C ratio of 1/1 often resulted in the highest conversions. For example, with micropowder Mo and carbon black, a Mo/C ratio of 1/1 yielded the highest CH_4 conversion (73%) and CO_2 conversion (49%) (Figure 25). This optimal ratio ensures the formation of the desired β-Mo_2C phase, which is known for its high catalytic activity in DRM reactions. Deviations from this ratio can lead to the formation of other phases (e.g., α-MoC_{1-x}) or incomplete carburization (as also confirmed by the XRD patterns (Figure 24) of Mo_2C catalysts synthesized with different Metal/Carbon ratio), resulting in lower catalytic performance [261].

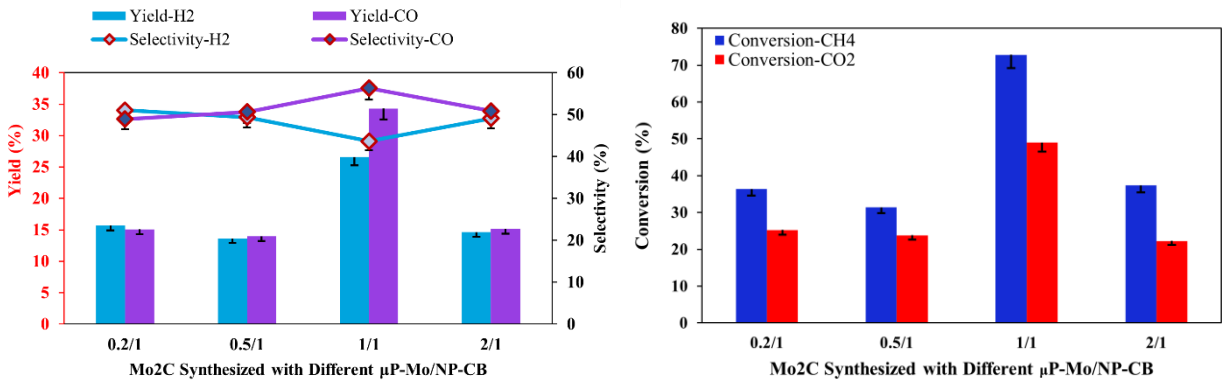

Figure 25. DBD-plasma assisted DRM over Mo_2C catalysts, synthesized by using µP-Mo and NP-CB. Reaction conditions: CH_4 : CO_2 = 1 : 1, flowrate = 30ml/min, f = 5kHz, V = 800V, I = 0.173A, and P = 140W.

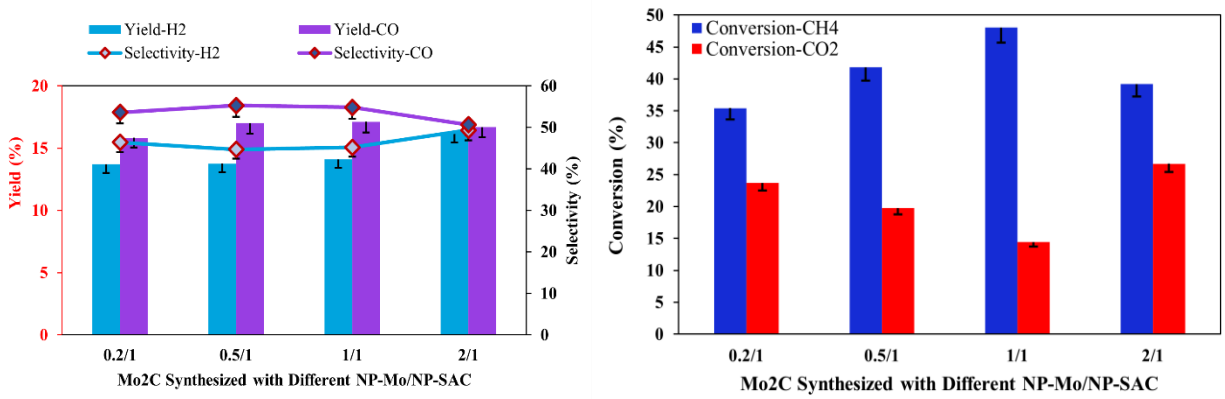

Figure 26. DBD-plasma assisted DRM over Mo_2C catalysts, synthesized by using NP-Mo and NP-SAC. Reaction conditions: CH_4 : CO_2 = 1 : 1, flowrate = 30ml/min, f = 5kHz, V = 800V, I = 0.173A, and P = 140W.

Impact on DBD discharge and reaction efficiency

Enhancing Utilization of Short-lived Reactive Species with Mo_2C Catalysts

The short-lived nature of reactive species in DBD-plasma system can be effectively addressed with the use of TMC catalysts. The increased surface area and better dispersion of micropowder Mo, along with the graphitic structure of carbon black, facilitated more efficient interactions between the plasma-generated reactive species and the catalyst surface. This interaction enhanced the utilization of short-lived reactive species, resulting in improved performance, including a H_2 yield of up to 27%, CH_4 conversion of up to 73%, and CO_2 conversion of up to 49% (Figure 25).

The optimal Mo/C ratio of 1/1 ensured the formation of the β-Mo2C phase (Figure 24 (c)), which has a high affinity for CO2 and CH4. This phase enhanced the adsorption and activation of these reactants, aligning with the plasma-generated reactive species to sustain a longer and more efficient reaction cycle. This synergy improved the overall conversion rates and product yields, overcoming the limitations posed by the short-lived nature of DBD reactive species.

1.5 WC catalysts

Characterization

XRD

To confirm the successful synthesis of WC catalyst and evaluate its phase composition, the synthesized WC was analyzed using X-ray diffraction (XRD). The XRD analysis revealed the presence of multiple tungsten carbide phases in the synthesized material (Figure 27). Predominantly, the diffraction patterns confirmed the formation of WC as the primary phase (Figure 27). However, the analysis also indicated the presence of W_2C as a secondary phase (Figure 27). Additionally, trace amounts of unknown impurities were detected in the XRD patterns (Figure 27). The presence of both WC and W_2C phases suggests that the chosen W/C ratio of 1/1 may not be optimal for producing single-phase WC. This mixed-phase composition could potentially influence the catalyst's performance in various applications, as different tungsten carbide phases are known to exhibit distinct catalytic properties.

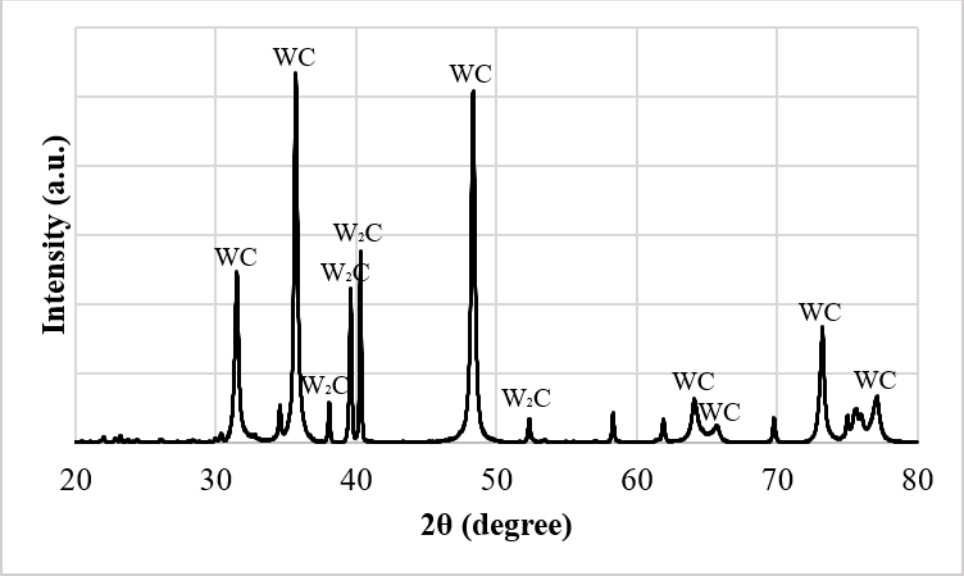

Figure 27. XRD pattern of the synthesized WC catalyst.

1.5.1 WC catalyzing DBD-plasma-assisted DRM reaction

For WC catalysts, the use of nanopowder W and different carbon sources (superactivated carbon vs. carbon black) also showed improvements. The WC catalysts synthesized with nanopowder W and carbon black, particularly at a W/C ratio of 1/1, demonstrated higher CH_4 conversion (up to 41%) and CO_2 conversion (up to 17%) compared to those with superactivated carbon (Figure 28). The graphitic structure of carbon black facilitated better W-C bonding, enhancing the catalyst's stability and activity under DBD plasma conditions. This resulted in a more sustained and efficient reaction.

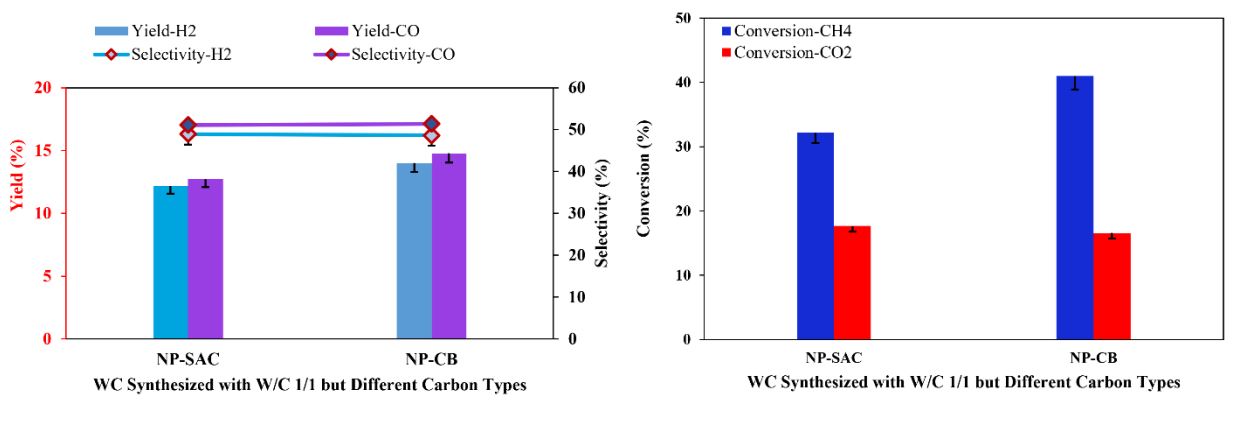

Figure 28. DBD-plasma assisted DRM over WC catalysts, synthesized by using NP-W and different types of C. Reaction conditions: CH_4 : CO_2 = 1 : 1, flowrate = 30ml/min, f = 5kHz, V = 800V, I = 0.173A, and P = 140W.

Synergistic effects of TMC catalysts and DBD plasma on DRM process

The combination of TMC catalysts with DBD plasma is crucial for enhancing both CH_4 and CO_2 activation. The plasma activates the CH_4 and CO_2 molecules before they adsorb onto the catalyst surface, lowering the energy barrier for their conversion into intermediates. This synergistic effect significantly enhances catalytic activity, as observed in studies where the addition of catalysts to the DBD plasma increased the reaction rate and reduced coking compared to uncatalyzed DRM [73, 262].

Influence of Electrical conductivity of TMCs on DBD-plasma assisted DRM process

The electrical conductivity of TMCs played a crucial role in the performance of the DBD plasma system. The unique electronic structure of TMCs, particularly Mo_2C, which exhibits a strong

hybridization between C p and Mo d orbitals, enhanced the conductivity and electron transfer during the reaction. The presence of a graphitized carbon layer around Mo_2C nanoparticles further improved the electrical conductivity, acting as an electronic bridge and minimizing the distance to the surface, thus enhancing the overall electrocatalytic activity [73].

Role of TMC catalysts in CO_2 activation in DBD-plasma assisted DRM process

One of the primary objectives of this study was to improve CO_2 dissociation rate and catalyst stability. The results indicate that certain Mo_2C catalyst configurations, particularly those with micropowder Mo and carbon black, significantly enhanced CO_2 conversion rate. This improvement can be attributed to the high basicity of the catalysts, which helps in capturing CO_2 and accelerating the overall reaction, similar to the role of MgO in traditional DRM catalysts. The oxygen binding energy (OBE) on the TMC surface also plays a critical role; catalysts with optimal OBE facilitate the removal of oxygen from the surface, completing the catalytic cycle for CO_2 conversion [262, 263].

Temperature Monitored During the Dry Reforming of Methane (DRM) Process

One of the primary objectives of this study was to process the dry reforming of methane (DRM) at the lowest possible temperature compared to conventional thermal DRM reactions. Notably, experiments revealed that the temperature within the plasma discharge region was approximately 160°C (Figure 29), which is substantially lower than the temperatures (700^0C to 1000^0C) conventionally used for DRM reactions. This observation suggests that DBD plasma can effectively enhance the catalytic efficiency of TMC catalysts at much milder conditions, offering a promising approach for more energy-efficient and sustainable DRM processes.

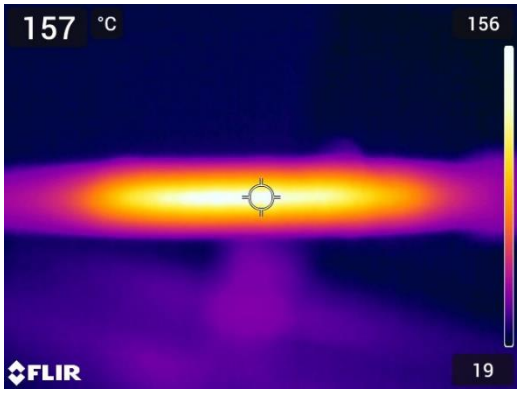

Figure 29. Thermal image of the plasma-discharge

Mitigation of Catalyst Coking in DBD-Plasma Assisted DRM over TMC Catalysts

One of the objectives of this study was to prevent coking or carbon deposition on the surface of TMC catalysts, a pervasive issue in conventional thermal DRM reactions. Specifically, the Mo_2C catalyst with the minimum Mo/C ratio of 0.2/1 (but with maximum C content) was selected for detailed analysis to assess carbon deposition. Elemental composition obtained by Energy-Dispersive Spectroscopy (EDS) of the catalyst revealed minimal or no carbon deposition on the surface of the used Mo_2C catalyst, when compared with the freshly synthesized sample (Figure 30). Additionally, individual carbon (C) mapping of both the fresh and used catalyst (Figure 32) further supported this observation, showing no significant carbon deposition on the surface of the catalyst after use. This was further corroborated by the absence of dark spots in the compositional analysis of the post-reaction catalyst (Figure 31), indicating no significant carbon buildup. Additionally, the catalyst's performance was evaluated over a 1-hour period, with product gas samples collected at 15-minute intervals, showing consistent reaction yields and reactant conversions (Figure 33). This stability in catalytic activity confirmed that the active sites were not blocked by carbon deposits. The morphology of the fresh and used catalysts, analyzed using SEM, also showed no significant differences (Figure 34), with the used catalyst displaying more dispersed particles due to the use of glass beads coated with the catalyst. These findings demonstrate DBD-plasma assisted approach effectively mitigated the coking issue commonly associated with catalysts in conventional thermal DRM reactions, enhancing the catalyst's stability and efficiency.

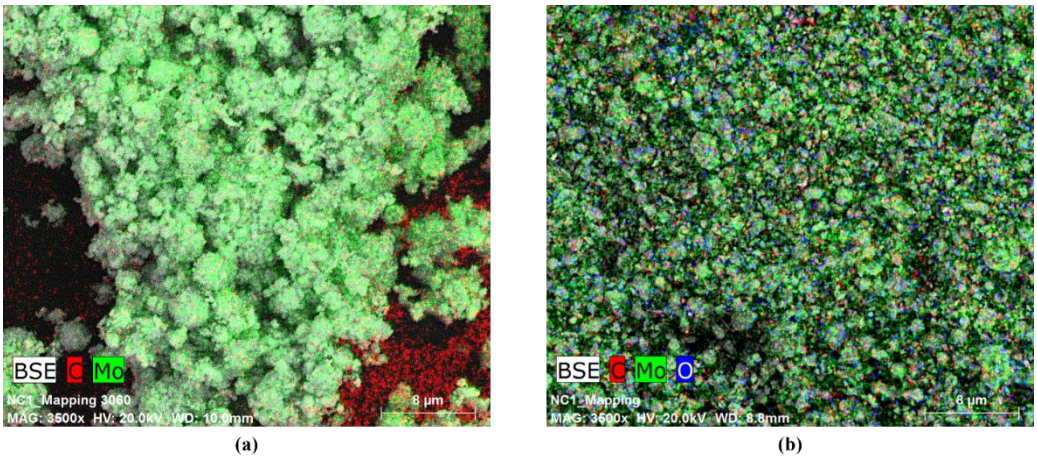

Figure 30. Elemental composition of Mo_2C (synthesized with Mo/C = 0.2/1) obtained by EDS. (a) Freshly synthesized catalyst. (b) Post-reaction catalyst.

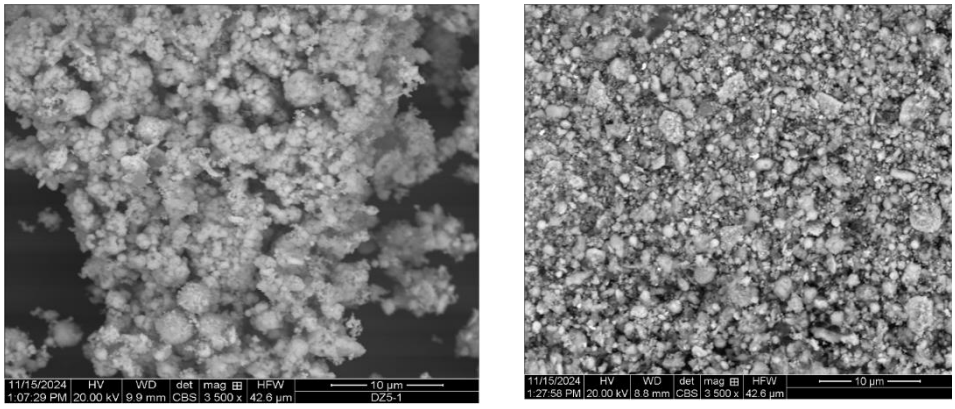

Figure 32. Compositional analysis of Mo2C (synthesized with Mo/C = 0.2/1) obtained by SEM. (a) Freshly synthesized catalyst. (b) Post-reaction.

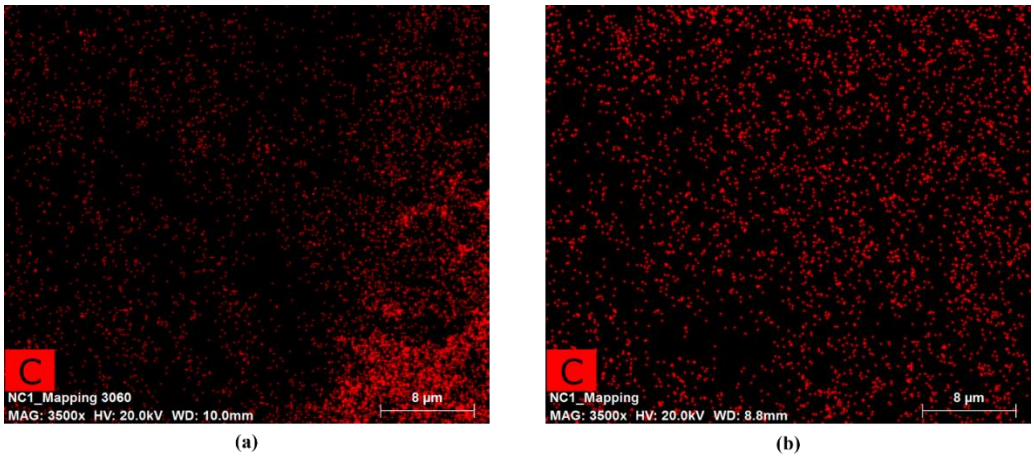

Figure 31. C mapping of Mo2C (synthesized with Mo/C = 0.2/1), obtained by EDS. (a) Freshly synthesized catalyst. (b) Post-reaction catalyst.

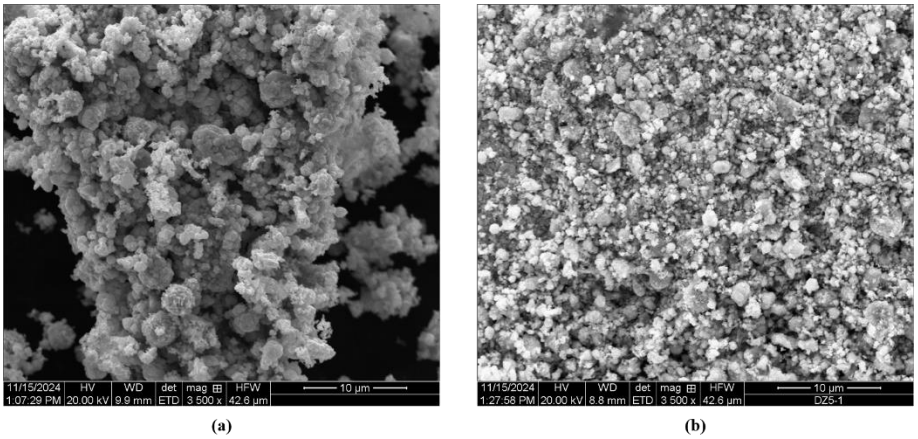

Figure 34. Structural morphology of Mo2C (synthesized with Mo/C = 0.2/1). (a) Freshly synthesized catalyst. (b) Post-reaction catalyst.

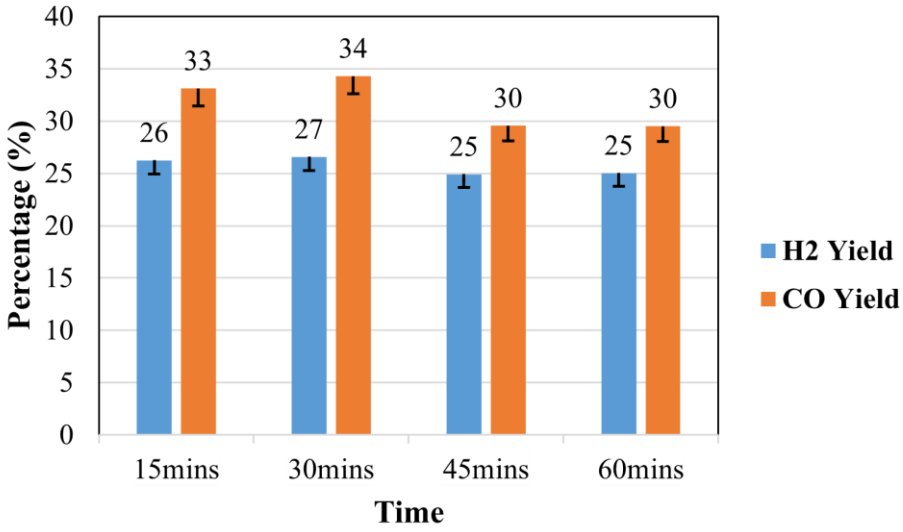

Figure 33. Catalytic activity of Mo_2C (synthesized with Mo/C = 0.2/1). Reaction conditions: CH_4 : CO_2 = 1 : 1, flowrate = 30ml/min, f = 5kHz, V = 800V, I = 0.173A, and P = 140W.

Energy Density Comparison for the Conversion of CH_4 to H_2

The conversion of CH_4 to H_2 is a highly worthwhile process, particularly when considering the energetic and environmental benefits. In the context of DRM, this process converts two major greenhouse gases, CH_4 and CO_2, into syngas (CO and H_2), which can be further transformed into fuels or higher-value chemicals [165]. From an energy density perspective, CH_4 has a higher volume energy density compared to hydrogen. CH_4 contains approximately 55.5MJ/m³ at standard temperature and pressure (STP), while H_2 contains about 13.4MJ/m³ at STP. However, H_2 has a significantly higher energy-mass density, with approximately 120MJ/kg, compared to CH_4 55.5MJ/kg [264].

The use of advanced technologies such as DBD plasma can enhance the efficiency and stability of the DRM reaction. Overall, the conversion of CH4 to H2 is not only environmentally beneficial by reducing greenhouse gas emissions but also offers a promising route for producing a high-energy-density fuel with significant potential for industrial and energy applications.

Limitations of Upscaling DBD Plasma Assisted DRM Reaction

Despite the promising advancements in DBD plasma assisted DRM, several limitations hinder the upscaling of this technology. One of the primary challenges is the stability and longevity of the catalysts used in the process. Traditional Ni-based catalysts, for instance, are prone to deactivation due to high temperatures, sintering of active metal particles, and coke deposition on the catalyst surface. The energy consumption and efficiency of the DBD plasma system also pose significant challenges. While DBD plasma can activate thermodynamically restricted reactions at lower temperatures, it still requires considerable energy input, and the conversion rates can be affected by various parameters such as discharge power, flow rates, and catalyst properties [262, 265]. Additionally, the scalability of the reactor design is a critical issue. DBD plasma generates microdischarges that are highly dependent on the geometric characteristics of the reactor, operating temperature, and pressure. Maintaining uniform plasma distribution and controlling the electron energy distribution function (EEDF) across larger reactor volumes is complex and can lead to variations in reaction pathways and product distribution. Furthermore, the use of diluent gases like argon, helium, or nitrogen, which are often necessary to control the discharge characteristics and reduce coke formation, adds to the operational complexity and cost. These gases can alter the reaction mechanisms and H_2/CO ratios, requiring careful optimization to achieve desired outcomes

Lastly, the deactivation mechanisms of TMC catalysts need to be thoroughly understood to ensure long-term stability. Bulk oxidation of the TMCs and changes in the catalyst's surface chemistry can lead to rapid deactivation, highlighting the need for robust catalyst design and optimization strategies [128]. Addressing these challenges is crucial for the successful upscaling and industrial implementation of DBD plasma assisted DRM reactions.

CHAPTER 5: Conclusion

In conclusion, this study underscores the significant potential of Transition Metal Carbide (TMC) catalysts, particularly Mo_2C, in enhancing CO_2 conversion and overall efficiency in the DRM process when combined with cold plasma. The optimization of Mo powder size, carbon type, and metal/carbon ratio was critical in achieving the best catalytic performance, with micropowder Mo and carbon black yielding the highest CH_4 and CO_2 conversions. The electrical conductivity of TMCs, especially Mo_2C, facilitating better transfer of plasma-generated reactive species to reactants, playing a pivotal role in effectively utilizing short-lived DBD discharge species and improving reaction efficiency. This synergy lead to improved H_2 yield, higher CH_4 conversion, and enhanced CO_2 conversion. The high basicity of Mo_2C and its optimal oxygen binding energy further accelerated the reaction, aligning with existing research on plasma-catalyst systems in DRM reaction. Overall, this study highlights the importance of TMC catalysts in achieving sustainable and efficient CO_2 conversion and H_2 production.

References

1. Ray, D. and C. Subrahmanyam, *CO2 decomposition in a packed DBD plasma reactor: influence of packing materials.* RSC Advances, 2016. **6**(45): p. 39492-39499.
2. Diao, Y., et al., *Plasma-assisted dry reforming of methane over Mo2C-Ni/Al2O3 catalysts: Effects of β-Mo2C promoter.* Applied Catalysis B: Environmental, 2022. **301**: p. 120779.
3. Viswanathan, B., *Chapter 3 - Natural Gas*, in *Energy Sources*, B. Viswanathan, Editor. 2017, Elsevier: Amsterdam. p. 59-79.
4. Mar, K.A., et al., *Beyond CO2 equivalence: The impacts of methane on climate, ecosystems, and health.* Environmental Science & Policy, 2022. **134**: p. 127-136.
5. Shindell, D., J. Fuglestvedt, and W. Collins, *The social cost of methane: theory and applications.* Faraday Discussions, 2017. **200**: p. 429-451.
6. Arora, S. and R. Prasad, *An overview on dry reforming of methane: strategies to reduce carbonaceous deactivation of catalysts.* RSC Advances, 2016. **6**(110): p. 108668-108688.
7. Byrom, R.E. and K.P. Shine, *Methane's Solar Radiative Forcing.* Geophysical Research Letters, 2022. **49**(15): p. e2022GL098270.
8. Forster, P., et al., *The Earth's energy budget, climate feedbacks, and climate sensitivity.* 2021.
9. Cain, M., et al., *Improved calculation of warming-equivalent emissions for short-lived climate pollutants.* npj Climate and Atmospheric Science, 2019. **2**(1): p. 29.
10. Heald, C.L. and J.H. Kroll, *The fuel of atmospheric chemistry: Toward a complete description of reactive organic carbon.* Science Advances, 2020. **6**(6): p. eaay8967.
11. Butler, T., A. Lupascu, and A. Nalam, *Attribution of ground-level ozone to anthropogenic and natural sources of nitrogen oxides and reactive carbon in a global chemical transport model.* Atmos. Chem. Phys., 2020. **20**(17): p. 10707-10731.
12. Emberson, L., *Effects of ozone on agriculture, forests and grasslands.* Philosophical Transactions of the Royal Society A: Mathematical, Physical and Engineering Sciences, 2020. **378**(2183): p. 20190327.
13. Watanabe, M., et al., *Nitrogen Use Efficiency for Growth of Fagus crenata Seedlings Under Elevated Ozone and Different Soil Nutrient Conditions.* Forests, 2020. **11**(4): p. 371.
14. Fuhrer, J., et al., *Current and future ozone risks to global terrestrial biodiversity and ecosystem processes.* Ecology and Evolution, 2016. **6**(24): p. 8785-8799.
15. Zhang, J.J., Y. Wei, and Z. Fang, *Ozone Pollution: A Major Health Hazard Worldwide.* Front Immunol, 2019. **10**: p. 2518.
16. Agency, I.E., *World Energy Outlook 2022*. 2022.
17. Jackson, R.B., et al., *Increasing anthropogenic methane emissions arise equally from agricultural and fossil fuel sources.* Environmental Research Letters, 2020. **15**(7): p. 071002.
18. Saunois, M., et al., *The global methane budget 2000–2012.* Earth Syst. Sci. Data, 2016. **8**(2): p. 697-751.
19. Saunois, M., et al., *The Global Methane Budget 2000–2017.* Earth Syst. Sci. Data, 2020. **12**(3): p. 1561-1623.
20. Bolt, H.M., *Methane*, in *Reference Module in Biomedical Sciences*. 2022, Elsevier.
21. Liang, F.-Y., et al., *The role of natural gas as a primary fuel in the near future, including comparisons of acquisition, transmission and waste handling costs of as with competitive alternatives.* Chemistry Central Journal, 2012. **6**(1): p. S4.

22. Hanif, M.A., et al., *Chapter 1 - Energy resources and utilization*, in *Renewable and Alternative Energy Resources*, M.A. Hanif, et al., Editors. 2022, Academic Press. p. 1-30.
23. Yıldız, İ., *1.12 Fossil Fuels*, in *Comprehensive Energy Systems*, I. Dincer, Editor. 2018, Elsevier: Oxford. p. 521-567.
24. Ahmad, M., et al., *Financial Risk, Renewable Energy Technology Budgets, and Environmental Sustainability: Is Going Green Possible?* Frontiers in Environmental Science, 2022. **10**.
25. Yue, M., et al., *Hydrogen energy systems: A critical review of technologies, applications, trends and challenges.* Renewable and Sustainable Energy Reviews, 2021. **146**: p. 111180.
26. Arutyunov, V.S. and G.V. Lisichkin, *Energy resources of the 21st century: problems and forecasts. Can renewable energy sources replace fossil fuels†.* Russian Chemical Reviews, 2017. **86**(8): p. 777.
27. Abe, J.O., et al., *Hydrogen energy, economy and storage: Review and recommendation.* International Journal of Hydrogen Energy, 2019. **44**(29): p. 15072-15086.
28. Dincer, I. and C. Acar, *Review and evaluation of hydrogen production methods for better sustainability.* International Journal of Hydrogen Energy, 2015. **40**(34): p. 11094-11111.
29. Ishaq, H., I. Dincer, and C. Crawford, *A review on hydrogen production and utilization: Challenges and opportunities.* International Journal of Hydrogen Energy, 2022. **47**(62): p. 26238-26264.
30. Momirlan, M. and T.N. Veziroglu, *The properties of hydrogen as fuel tomorrow in sustainable energy system for a cleaner planet.* International Journal of Hydrogen Energy, 2005. **30**(7): p. 795-802.
31. Osman, A.I., et al., *Hydrogen production, storage, utilisation and environmental impacts: a review.* Environmental Chemistry Letters, 2022. **20**(1): p. 153-188.
32. Viswanathan, B., *Chapter 9 - Hydrogen as an Energy Carrier*, in *Energy Sources*, B. Viswanathan, Editor. 2017, Elsevier: Amsterdam. p. 161-183.
33. Revankar, S.T., *Chapter Four - Nuclear Hydrogen Production*, in *Storage and Hybridization of Nuclear Energy*, H. Bindra and S. Revankar, Editors. 2019, Academic Press. p. 49-117.
34. Parra, D., et al., *A review on the role, cost and value of hydrogen energy systems for deep decarbonisation.* Renewable and Sustainable Energy Reviews, 2019. **101**: p. 279-294.
35. Nikolaidis, P. and A. Poullikkas, *A comparative overview of hydrogen production processes.* Renewable and Sustainable Energy Reviews, 2017. **67**: p. 597-611.
36. Kim, J. and M. Yang, *Chapter 18 - Hydrogen production methods: Benefits, opportunities, costs, and risks*, in *Hydrogen Economy (Second Edition)*, A. Scipioni, A. Manzardo, and J. Ren, Editors. 2023, Academic Press. p. 573-594.
37. Lamb, J.J. and B. Austbø, *Chapter | two - Current Use of Bioenergy and Hydrogen*, in *Hydrogen, Biomass and Bioenergy*, J.J. Lamb and B.G. Pollet, Editors. 2020, Academic Press. p. 9-20.
38. Nnabuife, S.G., et al., *Present and Projected Developments in Hydrogen Production: A Technological Review∗.* Carbon Capture Science & Technology, 2022. **3**: p. 100042.
39. Ji, M. and J. Wang, *Review and comparison of various hydrogen production methods based on costs and life cycle impact assessment indicators.* International Journal of Hydrogen Energy, 2021. **46**(78): p. 38612-38635.

40. Olabi, A.G., et al., *Large-vscale hydrogen production and storage technologies: Current status and future directions.* International Journal of Hydrogen Energy, 2021. **46**(45): p. 23498-23528.
41. Proost, J., *Critical assessment of the production scale required for fossil parity of green electrolytic hydrogen.* International Journal of Hydrogen Energy, 2020. **45**(35): p. 17067-17075.
42. IEA, I. *Global Hydrogen Review 2021*. 2021. IEA Paris, France.
43. Spath, P.L. and M.K. Mann, *Life cycle assessment of hydrogen production via natural gas steam reforming*. 2000, National Renewable Energy Lab.(NREL), Golden, CO (United States).
44. Zhang, H., Z. Sun, and Y.H. Hu, *Steam reforming of methane: Current states of catalyst design and process upgrading.* Renewable and Sustainable Energy Reviews, 2021. **149**: p. 111330.
45. Pakhare, D. and J. Spivey, *A review of dry (CO2) reforming of methane over noble metal catalysts.* Chemical Society Reviews, 2014. **43**(22): p. 7813-7837.
46. Torrez-Herrera, J.J., S.A. Korili, and A. Gil, *Recent progress in the application of Ni-based catalysts for the dry reforming of methane.* Catalysis Reviews, 2023. **65**(4): p. 1300-1357.
47. Alli, R.D., et al., *Tri-reforming of methane for syngas production using Ni catalysts: Current status and future outlook.* Catalysis Today, 2023. **407**: p. 107-124.
48. Chen, L., et al., *Catalytic Hydrogen Production from Methane: A Review on Recent Progress and Prospect.* Catalysts, 2020. **10**(8): p. 858.
49. Farooqi, A.S., et al., *A comprehensive review on improving the production of rich-hydrogen via combined steam and CO2 reforming of methane over Ni-based catalysts.* International Journal of Hydrogen Energy, 2021. **46**(60): p. 31024-31040.
50. Naikoo, G.A., et al., *Thermocatalytic Hydrogen Production Through Decomposition of Methane-A Review.* Frontiers in Chemistry, 2021. **9**.
51. Siang, T.J., et al., *A review on state-of-the-art catalysts for methane partial oxidation to syngas production.* Catalysis Reviews: p. 1-57.
52. Hasnan, N.S.N., et al., *Recent developments in methane decomposition over heterogeneous catalysts: an overview.* Materials for Renewable and Sustainable Energy, 2020. **9**(2): p. 8.
53. Muraza, O. and A. Galadima, *A review on coke management during dry reforming of methane.* International Journal of Energy Research, 2015. **39**(9): p. 1196-1216.
54. Ma, Y., et al., *Molybdenum carbide as alternative catalyst for hydrogen production – A review.* Renewable and Sustainable Energy Reviews, 2017. **75**: p. 1101-1129.
55. Chen, J.G., *Carbide and Nitride Overlayers on Early Transition Metal Surfaces: Preparation, Characterization, and Reactivities.* Chemical Reviews, 1996. **96**(4): p. 1477-1498.
56. Hwu, H.H. and J.G. Chen, *Surface Chemistry of Transition Metal Carbides.* Chemical Reviews, 2005. **105**(1): p. 185-212.
57. Levy, R.B. and M. Boudart, *Platinum-Like Behavior of Tungsten Carbide in Surface Catalysis.* Science, 1973. **181**(4099): p. 547-549.
58. Ahmad, S., et al., *An Overview of Recent Advances in the Synthesis and Applications of the Transition Metal Carbide Nanomaterials.* Nanomaterials (Basel), 2021. **11**(3).
59. Lin, Z., S.R. Denny, and J.G. Chen, *Transition metal carbides and nitrides as catalysts for thermochemical reactions.* Journal of Catalysis, 2021. **404**: p. 929-942.

60. Michalsky, R., Y. Zhang, and A.A. Peterson, *Trends in the Hydrogen Evolution Activity of Metal Carbide Catalysts.* ACS Catalysis, 2014. **4**: p. 1274-1278.
61. Zhang, X., et al., *Progress in hydrogen production over transition metal carbide catalysts: challenges and opportunities.* Current Opinion in Chemical Engineering, 2018. **20**: p. 68-77.
62. Liu, Y., et al., *Metal Carbides as Alternative Electrocatalyst Supports.* ACS Catalysis, 2013. **3**(6): p. 1184-1194.
63. Pang, J., et al., *Transition metal carbide catalysts for biomass conversion: A review.* Applied Catalysis B: Environmental, 2019. **254**: p. 510-522.
64. Zhang, H., et al., *Transition-Metal Carbides as Hydrogen Evolution Reduction Electrocatalysts: Synthetic Methods and Optimization Strategies.* Chemistry – A European Journal, 2021. **27**(16): p. 5074-5090.
65. Zhang, Q., et al., *Transition Metal Carbides (TMCs) Catalysts for Gas Phase CO2 Upgrading Reactions: A Comprehensive Overview.* Catalysts, 2020. **10**(9): p. 955.
66. Zhang, S.B.X.Y., et al., *Role and dynamics of transition metal carbides in methane coupling.* Chemical Science, 2023. **14**(22): p. 5899-5905.
67. Cai, Y., et al., *Recent Advances in Ni-Based Catalysts for CH4-CO2 Reforming (2013–2023).* Atmosphere, 2023. **14**(9): p. 1323.
68. Álvarez Moreno, A., et al., *Bimetallic Ni–Ru and Ni–Re Catalysts for Dry Reforming of Methane: Understanding the Synergies of the Selected Promoters.* Frontiers in Chemistry, 2021. **9**.
69. Wang, G., et al., *Study on High Activity and Outstanding Stability of Hollow-NiPt@SiO2 Core–Shell Structure Catalyst for DRM Reaction.* Frontiers in Chemistry, 2020. **8**.
70. Palma, V., et al., *A Review about the Recent Advances in Selected NonThermal Plasma Assisted Solid-Gas Phase Chemical Processes.* Nanomaterials (Basel), 2020. **10**(8).
71. Vaiano, V. and G. Iervolino, *Non-Thermal Plasma-Assisted Catalytic Reactions for Environmental Protection.* Catalysts, 2021. **11**(4): p. 509.
72. Adesina, K., et al., *A Review of Dielectric Barrier Discharge Cold Atmospheric Plasma for Surface Sterilization and Decontamination.* IEEE Transactions on Radiation and Plasma Medical Sciences, 2024. **8**(3): p. 295-306.
73. Li, J., et al., *A Review of Recent Advances of Dielectric Barrier Discharge Plasma in Catalysis.* Nanomaterials (Basel), 2019. **9**(10).
74. Agyekum, E.B., et al., *A Critical Review of Renewable Hydrogen Production Methods: Factors Affecting Their Scale-Up and Its Role in Future Energy Generation.* Membranes (Basel), 2022. **12**(2).
75. Fan, Z., et al., *Catalytic decomposition of methane to produce hydrogen: A review.* Journal of Energy Chemistry, 2021. **58**: p. 415-430.
76. Hussien, A.G.S. and K. Polychronopoulou, *A Review on the Different Aspects and Challenges of the Dry Reforming of Methane (DRM) Reaction.* Nanomaterials, 2022. **12**(19): p. 3400.
77. Aniruddha, R., et al., *Sorption enhanced reforming: A potential route to produce pure H2 with in-situ carbon capture.* Fuel, 2023. **351**: p. 128925.
78. Dan, M., et al., *Combined steam and dry reforming of methane for syngas production from biogas using bimodal pore catalysts.* Catalysis Today, 2021. **366**: p. 87-96.
79. Patlolla, S.R., et al., *A review of methane pyrolysis technologies for hydrogen production.* Renewable and Sustainable Energy Reviews, 2023. **181**: p. 113323.

80. Dawa, T. and B. Sajjadi, *Exploring the potential of perovskite structures for chemical looping technology: A state-of-the-art review.* Fuel Processing Technology, 2024. **253**: p. 108022.
81. Barelli, L., et al., *Hydrogen production through sorption-enhanced steam methane reforming and membrane technology: A review.* Energy, 2008. **33**(4): p. 554-570.
82. Al-Qahtani, A., et al., *Uncovering the true cost of hydrogen production routes using life cycle monetisation.* Applied Energy, 2021. **281**: p. 115958.
83. Smirniotis, P. and K. Gunugunuri, *Water gas shift reaction: research developments and applications*. 2015: Elsevier.
84. Bartels, J.R., M.B. Pate, and N.K. Olson, *An economic survey of hydrogen production from conventional and alternative energy sources.* International Journal of Hydrogen Energy, 2010. **35**(16): p. 8371-8384.
85. Ayodele, F.O., et al., *An Overview of Economic Analysis and Environmental Impacts of Natural Gas Conversion Technologies.* Sustainability, 2020. **12**(23): p. 10148.
86. Lumbers, B., et al., *Mathematical modelling and simulation of the thermo-catalytic decomposition of methane for economically improved hydrogen production.* International Journal of Hydrogen Energy, 2022. **47**(7): p. 4265-4283.
87. Korányi, T.I., et al., *Recent Advances in Methane Pyrolysis: Turquoise Hydrogen with Solid Carbon Production.* Energies, 2022. **15**(17): p. 6342.
88. Mahmoudi, M., et al., *Hydrogen production by methane decomposition over Ni-doped activated carbons: effect of the activation method.* Comptes Rendus. Chimie, 2022. **25**: p. 225-236.
89. Raza, J., et al., *Methane decomposition for hydrogen production: A comprehensive review on catalyst selection and reactor systems.* Renewable and Sustainable Energy Reviews, 2022. **168**: p. 112774.
90. Li, W., et al., *Effect of molybdenum carbide concentration on the Ni/ZrO2 catalysts for steam-CO2 bi-reforming of methane.* RSC Advances, 2015. **5**(122): p. 100865-100872.
91. York, A., T. Xiao, and M. Green, *Brief Overview of the Partial Oxidation of Methane to Synthesis Gas.* Topics in Catalysis, 2003. **22**: p. 345-358.
92. Song, C. and W. Pan, *Tri-reforming of methane: a novel concept for catalytic production of industrially useful synthesis gas with desired H2/CO ratios.* Catalysis Today, 2004. **98**(4): p. 463-484.
93. García-Vargas, J.M., et al., *Precursor influence and catalytic behaviour of Ni/CeO2 and Ni/SiC catalysts for the tri-reforming process.* Applied Catalysis A: General, 2012. **431-432**: p. 49-56.
94. Wang, S., G.Q. Lu, and G.J. Millar, *Carbon Dioxide Reforming of Methane To Produce Synthesis Gas over Metal-Supported Catalysts: State of the Art.* Energy & Fuels, 1996. **10**(4): p. 896-904.
95. Raghda Ahmed, E.-N. and G. Alaa Ali, *Syngas Production, Properties, and Its Importance*, in *Sustainable Alternative Syngas Fuel*, G. Chaouki and I. Abrar, Editors. 2019, IntechOpen: Rijeka. p. Ch. 2.
96. Xie, S., et al., *Photocatalytic and photoelectrocatalytic reduction of CO2 using heterogeneous catalysts with controlled nanostructures.* Chemical Communications, 2016. **52**(1): p. 35-59.

97. Zhang, K., et al., *A Study on CO2 Decomposition to CO and O2 by the Combination of Catalysis and Dielectric-Barrier Discharges at Low Temperatures and Ambient Pressure.* Industrial & Engineering Chemistry Research, 2017. **56**(12): p. 3204-3216.
98. Alipour, Z., et al., *Syngas production through dry reforming: A review on catalysts and their materials, preparation methods and reactor type.* Chemical Engineering Journal, 2023. **452**: p. 139416.
99. González-Castaño, M., B. Dorneanu, and H. Arellano-García, *The reverse water gas shift reaction: a process systems engineering perspective.* Reaction Chemistry & Engineering, 2021. **6**(6): p. 954-976.
100. Sandoval-Diaz, L.E., R. Schlögl, and T. Lunkenbein, *Quo Vadis Dry Reforming of Methane?—A Review on Its Chemical, Environmental, and Industrial Prospects.* Catalysts, 2022. **12**(5): p. 465.
101. Nikoo, M.K. and N.A.S. Amin, *Thermodynamic analysis of carbon dioxide reforming of methane in view of solid carbon formation.* Fuel Processing Technology, 2011. **92**(3): p. 678-691.
102. Edwards, J.H. and A.M. Maitra, *The chemistry of methane reforming with carbon dioxide and its current and potential applications.* Fuel Processing Technology, 1995. **42**(2): p. 269-289.
103. Tsang, S.C., J.B. Claridge, and M.L.H. Green, *Recent advances in the conversion of methane to synthesis gas.* Catalysis Today, 1995. **23**(1): p. 3-15.
104. Yang, L. and X. Ge, *Chapter Three - Biogas and Syngas Upgrading*, in *Advances in Bioenergy*, Y. Li and X. Ge, Editors. 2016, Elsevier. p. 125-188.
105. Zhang, J., H. Wang, and A.K. Dalai, *Development of stable bimetallic catalysts for carbon dioxide reforming of methane.* Journal of Catalysis, 2007. **249**(2): p. 300-310.
106. Wang, X., et al., *Thermodynamic analysis of glycerol dry reforming for hydrogen and synthesis gas production.* Fuel, 2009. **88**(11): p. 2148-2153.
107. Oemar, U., K. Hidajat, and S. Kawi, *Pd–Ni catalyst over spherical nanostructured Y2O3 support for oxy-CO2 reforming of methane: Role of surface oxygen mobility.* International Journal of Hydrogen Energy, 2015. **40**(36): p. 12227-12238.
108. Sobieraj, K., et al., *Carbon Monoxide Fate in the Environment as an Inspiration For Biorefinery Industry: A Review.* Frontiers in Environmental Science, 2022. **10**.
109. Zhang, T. and M.D. Amiridis, *Hydrogen production via the direct cracking of methane over silica-supported nickel catalysts.* Applied Catalysis A: General, 1998. **167**(2): p. 161-172.
110. Otsuka, K., S. Takenaka, and H. Ohtsuki, *Production of pure hydrogen by cyclic decomposition of methane and oxidative elimination of carbon nanofibers on supported-Ni-based catalysts.* Applied Catalysis A: General, 2004. **273**(1): p. 113-124.
111. Satyanarayana, C.V., D. Srikant, and H.R. Gurav, *Chapter 5 - Catalyst Deactivation and Regeneration*, in *Industrial Catalytic Processes for Fine and Specialty Chemicals*, S.S. Joshi and V.V. Ranade, Editors. 2016, Elsevier: Amsterdam. p. 187-219.
112. Schuurman, Y., et al., *Use of transient kinetics techniques for studying the methane reforming by carbon dioxide.* Catalysis Today, 1997. **38**(1): p. 129-135.
113. Cui, Y., et al., *Kinetic study of the catalytic reforming of CH4 with CO2 to syngas over Ni/α-Al2O3 catalyst: The effect of temperature on the reforming mechanism.* Applied Catalysis A: General, 2007. **318**: p. 79-88.

114. P. E. York, A., et al., *Molybdenum and tungsten carbides as catalysts for the conversion of methane to synthesis gas using stoichiometric feedstocks.* Chemical Communications, 1997(1): p. 39-40.
115. Claridge, J.B., et al., *New Catalysts for the Conversion of Methane to Synthesis Gas: Molybdenum and Tungsten Carbide.* Journal of Catalysis, 1998. **180**(1): p. 85-100.
116. Bian, Z., et al., *A Review on Bimetallic Nickel-Based Catalysts for CO2 Reforming of Methane.* ChemPhysChem, 2017. **18**(22): p. 3117-3134.
117. Yentekakis, I.V., P. Panagiotopoulou, and G. Artemakis, *A review of recent efforts to promote dry reforming of methane (DRM) to syngas production via bimetallic catalyst formulations.* Applied Catalysis B: Environmental, 2021. **296**: p. 120210.
118. Bhattar, S., et al., *A review on dry reforming of methane over perovskite derived catalysts.* Catalysis Today, 2021. **365**: p. 2-23.
119. Fan, M.-S., A.Z. Abdullah, and S. Bhatia, *Catalytic Technology for Carbon Dioxide Reforming of Methane to Synthesis Gas.* ChemCatChem, 2009. **1**(2): p. 192-208.
120. Seo, H.O., *Recent Scientific Progress on Developing Supported Ni Catalysts for Dry (CO2) Reforming of Methane.* Catalysts, 2018. **8**(3): p. 110.
121. Wang, L. and F. Wang, *Design Strategy, Synthesis, and Mechanism of Ni Catalysts for Methane Dry Reforming Reaction: Recent Advances and Future Perspectives.* Energy & Fuels, 2022. **36**(11): p. 5594-5621.
122. Ferreira-Aparicio, P., et al., *Alumina supported molybdenum-nickel carbides as catalysts for the dry reforming of methane.* Studies in Surface Science and Catalysis, 2001. **138**.
123. Oyama, S.T., *Preparation and catalytic properties of transition metal carbides and nitrides.* Catalysis Today, 1992. **15**(2): p. 179-200.
124. Silva, C.G., F.B. Passos, and V.T. da Silva, *Influence of the support on the activity of a supported nickel-promoted molybdenum carbide catalyst for dry reforming of methane.* Journal of Catalysis, 2019. **375**: p. 507-518.
125. Guo, J., et al., *A Carbide Catalyst Effective for the Dry Reforming of Methane at Atmospheric Pressure*, in *Advances in CO₂ Conversion and Utilization*. 2010, American Chemical Society. p. 181-196.
126. Naito, S., et al., *Marked difference of catalytic behavior by preparation methods in CH4 reforming with CO2 over Mo2C and WC catalysts.* Studies in Surface Science and Catalysis, 2000. **143**.
127. Shi, C., et al., *Ni-modified Mo2C catalysts for methane dry reforming.* Applied Catalysis A: General, 2012. **431-432**: p. 164-170.
128. Yao, Z., et al., *Insights into the deactivation mechanism of metal carbide catalysts for dry reforming of methane via comparison of nickel-modified molybdenum and tungsten carbides.* RSC Advances, 2016. **6**(24): p. 19944-19951.
129. Zhang, A., et al., *In-situ synthesis of nickel modified molybdenum carbide catalyst for dry reforming of methane.* Catalysis Communications, 2011. **12**(9): p. 803-807.
130. Zhang, L., et al., *Finding of a new cycle route in Ni/Mo2C catalyzed CH4–CO2 reforming.* Catalysis Science & Technology, 2021. **11**(2): p. 479-483.
131. Bitter, J.H., K. Seshan, and J.A. Lercher, *Mono and Bifunctional Pathways of CO2/CH4Reforming over Pt and Rh Based Catalysts.* Journal of Catalysis, 1998. **176**(1): p. 93-101.
132. Prins, R., *Eley–Rideal, the Other Mechanism.* Topics in Catalysis, 2018. **61**(9): p. 714-721.

133. Ferreira-Aparicio, P., et al., *Mechanistic aspects of the dry reforming of methane over ruthenium catalysts.* Applied Catalysis A: General, 2000. **202**(2): p. 183-196.
134. Bradford, M.C.J. and M. Albert Vannice, *The role of metal–support interactions in CO2 reforming of CH4.* Catalysis Today, 1999. **50**(1): p. 87-96.
135. Naito, S., M. Tsuji, and T. Miyao, *Mechanistic difference of the CO2 reforming of CH4 over unsupported and zirconia supported molybdenum carbide catalysts.* Catalysis Today, 2002. **77**(3): p. 161-165.
136. Erdöhelyi, A., et al., *Catalytic reaction of methane with carbon dioxide over supported palladium.* Applied Catalysis A: General, 1994. **108**(2): p. 205-219.
137. Mark, M.F. and W.F. Maier, *CO2-reforming of methane on supported Rh and Ir catalysts.* Journal of Catalysis, 1996. **164**(1): p. 122-130.
138. Slagtern, A., et al., *Specific Features Concerning the Mechanism of Methane Reforming by Carbon Dioxide over Ni/La2O3Catalyst.* Journal of Catalysis, 1997. **172**(1): p. 118-126.
139. Niu, J., et al., *Dry (CO2) reforming of methane over Pt catalysts studied by DFT and kinetic modeling.* Applied Surface Science, 2016. **376**: p. 79-90.
140. Zhu, Y.-A., et al., *DFT studies of dry reforming of methane on Ni catalyst.* Catalysis Today, 2009. **148**(3): p. 260-267.
141. Iyer, M.V., et al., *Kinetic Modeling for Methane Reforming with Carbon Dioxide over a Mixed-Metal Carbide Catalyst.* Industrial & Engineering Chemistry Research, 2003. **42**(12): p. 2712-2721.
142. Tsuji, M., T. Miyao, and S. Naito, *Remarkable support effect of ZrO2 upon the CO2 reforming of CH4 over supported molybdenum carbide catalysts.* Catalysis Letters, 2000. **69**(3): p. 195-198.
143. LaMont, D.C., et al., *The effect of Mo2C synthesis and pretreatment on catalytic stability in oxidative reforming environments.* Applied Catalysis A: General, 2003. **255**(2): p. 239-253.
144. Kurlov, A., et al., *Exploiting two-dimensional morphology of molybdenum oxycarbide to enable efficient catalytic dry reforming of methane.* Nat Commun, 2020. **11**(1): p. 4920.
145. Wan, W., B.M. Tackett, and J.G. Chen, *Reactions of water and C1 molecules on carbide and metal-modified carbide surfaces.* Chemical Society Reviews, 2017. **46**(7): p. 1807-1823.
146. Porosoff, M.D., et al., *Molybdenum Carbide as Alternative Catalysts to Precious Metals for Highly Selective Reduction of CO2 to CO.* Angewandte Chemie International Edition, 2014. **53**(26): p. 6705-6709.
147. Xiao, T.-c., et al., *Study on the mechanism of partial oxidation of methane to synthesis gas over molybdenum carbide catalyst.* Physical Chemistry Chemical Physics, 2002. **4**(18): p. 4549-4554.
148. Zheng, Y., et al., *Molybdenum Oxide, Oxycarbide, and Carbide: Controlling the Dynamic Composition, Size, and Catalytic Activity of Zeolite-Supported Nanostructures.* The Journal of Physical Chemistry C, 2019. **123**(36): p. 22281-22292.
149. Wang, H., et al., *H2 Production from Methane Reforming over Molybdenum Carbide Catalysts: From Surface Properties and Reaction Mechanism to Catalyst Development.* ACS Catalysis, 2022. **12**(24): p. 15501-15528.
150. Brush, A., et al., *Evidence of methane adsorption over Mo2C involving single C–H bond dissociation instead of facile carbon exchange.* Reaction Chemistry & Engineering, 2016. **1**(6): p. 667-674.

151. Hwu, H.H., M.B. Zellner, and J.G. Chen, *The chemical and electronic properties of oxygen-modified C/Mo(110): a model system for molybdenum oxycarbides.* Journal of Catalysis, 2005. **229**(1): p. 30-44.
152. Bkour, Q., et al., *A highly active and stable bimetallic Ni-Mo2C catalyst for a partial oxidation of jet fuel.* Applied Catalysis B: Environmental, 2019. **245**: p. 613-622.
153. LaMont, D.C. and W.J. Thomson, *Dry reforming kinetics over a bulk molybdenum carbide catalyst.* Chemical Engineering Science, 2005. **60**(13): p. 3553-3559.
154. Darujati, A.R.S., D.C. LaMont, and W.J. Thomson, *Oxidation stability of Mo2C catalysts under fuel reforming conditions.* Applied Catalysis A: General, 2003. **253**(2): p. 397-407.
155. Liang, P., et al., *Simple synthesis of ultrasmall β-Mo2C and α-MoC1−x nanoparticles and new insights into their catalytic mechanisms for dry reforming of methane.* Catalysis Science & Technology, 2017. **7**(15): p. 3312-3324.
156. Sehested, J., et al., *Activity and Stability of Molybdenum Carbide as a Catalyst for CO2 Reforming.* Journal of Catalysis, 2001. **201**(2): p. 206-212.
157. Du, X., et al., *Dry reforming of methane over ZrO2-supported Co–Mo carbide catalyst.* Applied Petrochemical Research, 2014. **4**(1): p. 137-144.
158. Brungs, A.J., A.P.E. York, and M.L.H. Green, *Comparison of the group V and VI transition metal carbides for methane dry reforming and thermodynamic prediction of their relative stabilities.* Catalysis Letters, 1999. **57**(1): p. 65-69.
159. Shamsi, A., *Methane Dry Reforming over Carbide, Nickel-Based, and Noble Metal Catalysts*, in *CO₂ Conversion and Utilization*. 2002, American Chemical Society. p. 182-196.
160. LaMont, D.C. and W.J. Thomson, *The influence of mass transfer conditions on the stability of molybdenum carbide for dry methane reforming.* Applied Catalysis A: General, 2004. **274**(1): p. 173-178.
161. Gavrilova, N., et al., *Synthesis of Mo2C by Thermal Decomposition of Molybdenum Blue Nanoparticles.* Nanomaterials, 2020. **10**(10): p. 2053.
162. Thakur, R., et al., *Insights into the Genesis of a Selective and Coke-Resistant MXene-Based Catalyst for the Dry Reforming of Methane.* ACS Catalysis, 2020. **10**(9): p. 5124-5134.
163. Katsuhiko, O., N. Masatoshi, and O. Shinzo, *Active Species of Molybdenum Carbide Catalysts in Methane Reforming: η-Mo3C2.* Chemistry Letters, 2000. **29**(9): p. 1086-1087.
164. Hirose, T., Y. Ozawa, and M. Nagai, *Preparation of a Nickel Molybdenum Carbide Catalyst and Its Activity in the Dry Reforming of Methane.* Chinese Journal of Catalysis, 2011. **32**(5): p. 771-776.
165. Kurlov, A., et al., *The structural evolution of Mo2C and Mo2C/SiO2 under dry reforming of methane conditions: morphology and support effects.* Catalysis Science & Technology, 2022. **12**(18): p. 5620-5628.
166. Duan, Y., et al., *In-situ synthesis of NiMo2C/Al2O3 catalysts for dry reforming of methane.* International Journal of Hydrogen Energy, 2016. **41**(47): p. 21955-21964.
167. Darujati, A.R.S. and W.J. Thomson, *Stability of supported and promoted-molybdenum carbide catalysts in dry-methane reforming.* Applied Catalysis A: General, 2005. **296**(2): p. 139-147.
168. Gao, H., et al., *Simple and large-scale synthesis of β-phase molybdenum carbides as highly stable catalysts for dry reforming of methane.* Inorganic Chemistry Frontiers, 2018. **5**(1): p. 90-99.

169. Roohi, P., R. Alizadeh, and E. Fatehifar, *Dry reforming of methane over nano-Mo2C/Al2O3 catalyst: Effect of carburization conditions on excess carbon deposition.* Energy Sources, Part A: Recovery, Utilization, and Environmental Effects, 2016. **38**(24): p. 3565-3571.
170. Zhang, S., et al., *Catalytic role of β-Mo2C in DRM catalysts that contain Ni and Mo.* Catalysis Today, 2015. **258**: p. 676-683.
171. Brungs, A.J., et al., *Dry reforming of methane to synthesis gas over supported molybdenum carbide catalysts.* Catalysis Letters, 2000. **70**(3): p. 117-122.
172. Cheng, J. and W. Huang, *Effect of cobalt (nickel) content on the catalytic performance of molybdenum carbides in dry-methane reforming.* Fuel Processing Technology, 2010. **91**(2): p. 185-193.
173. Shi, C., et al., *Synergism in NiMoOx precursors essential for CH4/CO2 dry reforming.* Catalysis Today, 2014. **233**: p. 46-52.
174. Brush, A., et al., *Tunable Syn-gas ratio via bireforming over coke-resistant Ni/Mo2C catalyst.* Fuel Processing Technology, 2016. **153**: p. 111-120.
175. Barbosa, R.D., et al., *Nickel–Promoted Molybdenum or Tungsten Carbides as Catalysts in Dry Reforming of Methane: Effects of Variation in CH4/CO2 Molar Ratio.* Catalysis Letters, 2021. **151**(6): p. 1578-1591.
176. Darujati, A.R.S. and W.J. Thomson, *Kinetic study of a ceria-promoted Mo2C/γ-Al2O3 catalyst in dry-methane reforming.* Chemical Engineering Science, 2006. **61**(13): p. 4309-4315.
177. Treacy, D. and J.R.H. Ross, *Carbon dioxide reforming of methane over supported molybdenum carbide catalysts*, in *Studies in Surface Science and Catalysis*, X. Bao and Y. Xu, Editors. 2004, Elsevier. p. 193-198.
178. Frontera, P., et al., *Effect of support surface on methane dry-reforming catalyst preparation.* Catalysis Today, 2013. **218-219**: p. 18-29.
179. Horiuchi, T., et al., *Suppression of carbon deposition in the CO2-reforming of CH4 by adding basic metal oxides to a Ni/Al2O3 catalyst.* Applied Catalysis A: General, 1996. **144**(1): p. 111-120.
180. Kambolis, A., et al., *Ni/CeO2-ZrO2 catalysts for the dry reforming of methane.* Applied Catalysis A: General, 2010. **377**(1): p. 16-26.
181. Özdemir, H., M.A. Faruk Öksüzömer, and M. Ali Gürkaynak, *Preparation and characterization of Ni based catalysts for the catalytic partial oxidation of methane: Effect of support basicity on H2/CO ratio and carbon deposition.* International Journal of Hydrogen Energy, 2010. **35**(22): p. 12147-12160.
182. Lucrédio, A.F., J.M. Assaf, and E.M. Assaf, *Methane conversion reactions on Ni catalysts promoted with Rh: Influence of support.* Applied Catalysis A: General, 2011. **400**(1): p. 156-165.
183. Trimm, D.L., *Catalysts for the control of coking during steam reforming.* Catalysis Today, 1999. **49**(1): p. 3-10.
184. Zhang, Y., et al., *Dry reforming of methane over Ni/SiO2 catalysts: Role of support structure properties.* Fuel, 2023. **340**: p. 127490.
185. Aw, M.S., et al., *Insights into durable NiCo catalysts on β-SiC/CeZrO2 and γ-Al2O3/CeZrO2 advanced supports prepared from facile methods for CH4–CO2 dry reforming.* Applied Catalysis B: Environmental, 2015. **164**: p. 100-112.

186. Haug, L., et al., *Zirconium Carbide Mediates Coke-Resistant Methane Dry Reforming on Nickel-Zirconium Catalysts.* Angewandte Chemie International Edition, 2022. **61**(50): p. e202213249.
187. Pritchard, M.L., et al., *The effects of sulfur and oxygen on the catalytic activity of molybdenum carbide during dry methane reforming.* Applied Catalysis A: General, 2004. **275**(1): p. 213-220.
188. Gao, H., et al., *Improvement of the catalytic stability of molybdenum carbide via encapsulation within carbon nanotubes in dry methane reforming.* Catalysis Science & Technology, 2018. **8**(3): p. 697-701.
189. Li, R., et al., *Nanostructured molybdenum carbide on biochar for CO2 reforming of CH4.* Fuel, 2018. **225**: p. 403-410.
190. Kurlov, A., et al., *Molybdenum carbide and oxycarbide from carbon-supported MoO3 nanosheets: phase evolution and DRM catalytic activity assessed by TEM and in situ XANES/XRD methods.* Nanoscale, 2020. **12**(24): p. 13086-13094.
191. Huang, J., et al., *Mo2C/SBA-15 Modified by Ni for the Dry Reforming of Methane.* Energy Sources, Part A: Recovery, Utilization, and Environmental Effects, 2011. **33**(24): p. 2249-2256.
192. France, L.J., et al., *The effect of lanthanum addition on the catalytic activity of γ-alumina supported bimetallic Co–Mo carbides for dry methane reforming.* Applied Petrochemical Research, 2014. **4**(1): p. 145-156.
193. Yao, L., et al., *Ni–Mo2C supported on alumina as a substitute for Ni–Mo reduced catalysts supported on alumina material for dry reforming of methane.* Comptes Rendus. Chimie, 2018. **21**(3-4): p. 247-252.
194. Tao, Q., et al., *Enhanced catalytic activity of Ni–Mo2C/La2O3–ZrO2 bifunctional catalyst for dry reforming of methane.* Journal of Materials Science, 2018. **53**(20): p. 14559-14572.
195. Silva, C.G., F.B. Passos, and V. Teixeira da Silva, *Effect of Carburization Conditions on the Activity of Molybdenum Carbide-Supported Catalysts Promoted by Nickel for the Dry Reforming of Methane.* Energy & Fuels, 2021. **35**(21): p. 17833-17847.
196. Osazuwa, O.U., et al., *An insight into the effects of synthesis methods on catalysts properties for methane reforming.* Journal of Environmental Chemical Engineering, 2021. **9**(2): p. 105052.
197. Jung, K.T., et al., *Effects of Transition Metal Addition on the Solid-State Transformation of Molybdenum Trioxide to Molybdenum Carbides.* Chemistry of Materials, 2004. **16**(2): p. 307-314.
198. Li, S., W.B. Kim, and J.S. Lee, *Effect of the Reactive Gas on the Solid-State Transformation of Molybdenum Trioxide to Carbides and Nitrides.* Chemistry of Materials, 1998. **10**(7): p. 1853-1862.
199. Lee, J.S., S.T. Oyama, and M. Boudart, *Molybdenum carbide catalysts: I. Synthesis of unsupported powders.* Journal of Catalysis, 1987. **106**(1): p. 125-133.
200. Lee, J.S., M.H. Yeom, and D.S. Lee, *Catalysis by Molybdenum Carbide in Activation of C-C, C-O and C-H bonds.* Journal of Molecular Catalysis, 1990. **62**(3): p. L45-L51.
201. Liu, F., et al., *A Comparison of NiMo/Al2O3 Catalysts Prepared by Impregnation and Coprecipitation Methods for Hydrodesulfurization of Dibenzothiophene.* The Journal of Physical Chemistry C, 2007. **111**(20): p. 7396-7402.
202. Gavrilova, N., et al., *Synthesis of Molybdenum Blue Dispersions Using Ascorbic Acid as Reducing Agent.* Colloids and Interfaces, 2020. **4**(2): p. 24.

203. Wan, C., N.A. Knight, and B.M. Leonard, *Crystal structure and morphology control of molybdenum carbide nanomaterials synthesized from an amine–metal oxide composite.* Chemical Communications, 2013. **49**(88): p. 10409-10411.
204. Gao, Q., et al., *Synthesis of Nanoporous Molybdenum Carbide Nanowires Based on Organic−Inorganic Hybrid Nanocomposites with Sub-Nanometer Periodic Structures.* Chemistry of Materials, 2009. **21**(23): p. 5560-5562.
205. Jia, L., et al., *Interfacial engineering of Mo2C–Mo3C2 heteronanowires for high performance hydrogen evolution reactions.* Nanoscale, 2019. **11**(48): p. 23318-23329.
206. Wan, C. and B.M. Leonard, *Iron-Doped Molybdenum Carbide Catalyst with High Activity and Stability for the Hydrogen Evolution Reaction.* Chemistry of Materials, 2015. **27**(12): p. 4281-4288.
207. Koizumi, R., et al., *Origami-Inspired 3D Interconnected Molybdenum Carbide Nanoflakes.* Advanced Materials Interfaces, 2018. **5**(6): p. 1701113.
208. Mondal, A., et al., *Large scale synthesis of Mo2C nanoparticle incorporated carbon nanosheet (Mo2C–C) for enhanced hydrogen evolution reaction.* International Journal of Hydrogen Energy, 2020. **45**(37): p. 18623-18634.
209. Ghayour, H., M. Abdellahi, and M. Bahmanpour, *Optimization of the high energy ball-milling: Modeling and parametric study.* Powder Technology, 2016. **291**: p. 7-13.
210. Abdellahi, M. and M. Bahmanpour, *Rapid synthesis of nanopowders in high energy ball milling; Optimization of milling parameters.* Ceramics International, 2015. **41**(1, Part B): p. 1631-1639.
211. Kim, J. and S. Kang, *WC platelet formation via high-energy ball mill.* International Journal of Refractory Metals and Hard Materials, 2014. **47**: p. 108-112.
212. Xia, Z.P., et al., *Mechanosynthesis of molybdenum carbides by ball milling at room temperature.* Journal of Alloys and Compounds, 2008. **453**(1): p. 185-190.
213. Ye, L.L. and M.X. Quan, *Synthesis of nanocrystalline TiC powders by mechanical alloying.* Nanostructured Materials, 1995. **5**(1): p. 25-31.
214. Razavi, M., M.R. Rahimipour, and A.H. Rajabi-Zamani, *Synthesis of nanocrystalline TiC powder from impure Ti chips via mechanical alloying.* Journal of Alloys and Compounds, 2007. **436**(1): p. 142-145.
215. Baklanova, O.N., et al., *Molybdenum carbide synthesized by mechanical activation an inert medium.* Journal of Alloys and Compounds, 2017. **698**: p. 1018-1027.
216. Vassilyeva, Y.Z., et al., *Synthesis of molybdenum carbide catalyst by DC arc plasma in ambient air for hydrogen evolution.* Materials Chemistry and Physics, 2020. **254**: p. 123509.
217. Yang, R., et al., *Molten salt synthesis of Mo2C powder using a mechanically milled powder.* Materials Letters, 2007. **61**(26): p. 4815-4817.
218. Hu, Z., et al., *Self-supported nickel-doped molybdenum carbide nanoflower clusters on carbon fiber paper for an efficient hydrogen evolution reaction.* Nanoscale, 2021. **13**(17): p. 8264-8274.
219. Ge, J., et al., *Electrochemical preparation of carbon films with a Mo2C interlayer in LiCl-NaCl-Na2CO3 melts.* Applied Surface Science, 2015. **347**: p. 401-405.
220. Chen, Y., et al., *Dual-phase MoC-Mo2C nanosheets prepared by molten salt electrochemical conversion of CO2 as excellent electrocatalysts for the hydrogen evolution reaction.* Nano Energy, 2021. **90**: p. 106533.

221. Tu, X. and J.C. Whitehead, *Plasma-catalytic dry reforming of methane in an atmospheric dielectric barrier discharge: Understanding the synergistic effect at low temperature.* Applied Catalysis B: Environmental, 2012. **125**: p. 439-448.
222. Khoja, A.H., M. Tahir, and N.A.S. Amin, *Dry reforming of methane using different dielectric materials and DBD plasma reactor configurations.* Energy Conversion and Management, 2017. **144**: p. 262-274.
223. Vakili, R., et al., *Plasma-assisted catalytic dry reforming of methane (DRM) over metal-organic frameworks (MOFs)-based catalysts.* Applied Catalysis B: Environmental, 2020. **260**: p. 118195.
224. Khoja, A.H., M. Tahir, and N.A.S. Amin, *Cold plasma dielectric barrier discharge reactor for dry reforming of methane over Ni/ɤ-Al2O3-MgO nanocomposite.* Fuel Processing Technology, 2018. **178**: p. 166-179.
225. Zeng, Y., et al., *Plasma-catalytic dry reforming of methane over γ-Al2O3 supported metal catalysts.* Catalysis Today, 2015. **256**: p. 80-87.
226. Chung, W.-C. and M.-B. Chang, *Review of catalysis and plasma performance on dry reforming of CH4 and possible synergistic effects.* Renewable and Sustainable Energy Reviews, 2016. **62**: p. 13-31.
227. Zeng, Y.X., et al., *Low temperature reforming of biogas over K-, Mg- and Ce-promoted Ni/Al2O3 catalysts for the production of hydrogen rich syngas: Understanding the plasma-catalytic synergy.* Applied Catalysis B: Environmental, 2018. **224**: p. 469-478.
228. Zhang, X., et al., *Elucidating the promoting role of Mo2C in methane activation using Ni-xMo2C/FAU to catalyze methane steam reforming.* Applied Catalysis B: Environmental, 2022. **310**: p. 121250.
229. Christofoletti, T., J.M. Assaf, and E.M. Assaf, *Methane steam reforming on supported and non-supported molybdenum carbides.* Chemical Engineering Journal, 2005. **106**(2): p. 97-103.
230. Zhu, Q., et al., *The effect of secondary metal on Mo2C/Al2O3 catalyst for the partial oxidation of methane to syngas.* Journal of Molecular Catalysis A: Chemical, 2004. **213**(2): p. 199-205.
231. Mounfield, W.P., III, A. Harale, and Y. Román-Leshkov, *Impact of Morphological Effects on the Activity and Stability of Tungsten Carbide Catalysts for Dry Methane Reforming.* Energy & Fuels, 2019. **33**(6): p. 5544-5550.
232. Xiao, T.-c., et al., *Methane partial oxidation to synthesis gas over bimetallic cobalt/tungsten carbide catalysts and integration with a Mn substituted hexaaluminate combustion catalyst.* Catalysis Today, 2009. **147**(3): p. 196-202.
233. Ren, P. and Z. Zhao, *Unexpected coke-resistant stability in steam-CO2 dual reforming of methane over the robust Mo2C-Ni/ZrO2 catalyst.* Catalysis Communications, 2019. **119**: p. 71-75.
234. Zou, H., et al., *Effect of additives on the properties of nickel molybdenum carbides for the tri-reforming of methane.* International Journal of Hydrogen Energy, 2016. **41**(38): p. 16842-16850.
235. Zou, H., et al., *Effect of impregnation sequence on the catalytic performance of NiMo carbides for the tri-reforming of methane.* International Journal of Hydrogen Energy, 2017. **42**(32): p. 20401-20409.
236. Wysocka, I., et al., *Novel sugar-based nickel-tungsten carbide catalysts for dry reforming of hydrocarbons.* Journal of Industrial and Engineering Chemistry, 2023. **124**: p. 431-446.

237. Lee, W.J., et al., *Microstructure formation on exposure of silicon carbide surfaces to the partial oxidation of methane.* Catalysis Today, 2011. **178**(1): p. 85-97.
238. García-Vargas, J.M., et al., *Methane tri-reforming over a Ni/β-SiC-based catalyst: Optimizing the feedstock composition.* International Journal of Hydrogen Energy, 2013. **38**(11): p. 4524-4532.
239. García-Vargas, J.M., et al., *Influence of alkaline and alkaline-earth cocations on the performance of Ni/β-SiC catalysts in the methane tri-reforming reaction.* Applied Catalysis B: Environmental, 2014. **148-149**: p. 322-329.
240. García-Vargas, J.M., et al., *Preparation of Ni–Mg/β-SiC catalysts for the methane tri-reforming: Effect of the order of metal impregnation.* Applied Catalysis B: Environmental, 2015. **164**: p. 316-323.
241. Yan, Q., et al., *Synthesis of tungsten carbide nanoparticles in biochar matrix as a catalyst for dry reforming of methane to syngas.* Catalysis Science & Technology, 2015. **5**(6): p. 3270-3280.
242. Grigoryan, R.R., et al., *Dry Reforming of Methane over Nanosized Tungsten Carbide Powders Obtained by Mechanochemical and Plasma-Mechanochemical Methods.* Petroleum Chemistry, 2019. **59**(11): p. 1256-1263.
243. Li, S., et al., *Enhanced activity of Co catalysts supported on tungsten carbide-activated carbon for CO2 reforming of CH4 to produce syngas.* International Journal of Hydrogen Energy, 2021. **46**(56): p. 28613-28625.
244. Gavrilova, N.N., V.N. Sapunov, and V.V. Skudin, *Intensification of dry reforming of methane on membrane catalyst.* Chemical Engineering Journal, 2019. **374**: p. 983-991.
245. Iyer, M.V., et al., *Catalysis for Synthesis Gas Formation from Reforming of Methane.* Topics in Catalysis, 2004. **29**(3): p. 197-200.
246. Shao, H., et al., *Effect of Temperature on Structure and Performance of In-House Cobalt−Tungsten Carbide Catalyst for Dry Reforming of Methane.* Industrial & Engineering Chemistry Research, 2005. **44**(14): p. 4914-4921.
247. Shao, H., *Bimetallic carbides as catalysts for dry reforming and steam reforming.* 2006.
248. Serrano-Lotina, A. and L. Daza, *Influence of the operating parameters over dry reforming of methane to syngas.* International Journal of Hydrogen Energy, 2014. **39**(8): p. 4089-4094.
249. Neylon, M.K., et al., *Catalytic properties of early transition metal nitrides and carbides: n-butane hydrogenolysis, dehydrogenation and isomerization.* Applied Catalysis A: General, 1999. **183**(2): p. 253-263.
250. Koc, R. and S.K. Kodambaka, *ChemInform Abstract: Tungsten Carbide (WC) Synthesis from Novel Precursors.* ChemInform, 2000. **31**(49).
251. Swift, G.A. and R. Koc, *Formation of WC powders using carbon coated precursors.* Journal of Materials Science, 2000. **35**(9): p. 2109-2113.
252. Lin, H., et al., *Tungsten carbide (WC) nanopowders synthesized via novel core–shell structured precursors.* Ceramics International, 2013. **39**(3): p. 2877-2881.
253. Wu, Y., et al., *Ultrafine/nano WC-Co cemented carbide: Overview of preparation and key technologies.* Journal of Materials Research and Technology, 2023. **27**: p. 5822-5839.
254. Yang, R., et al., *Molten salt synthesis of tungsten carbide powder using a mechanically activated powder.* International Journal of Refractory Metals and Hard Materials, 2011. **29**(1): p. 138-140.
255. Zhang, K., et al., *Molten salt synthesis of continuous tungsten carbide coatings on graphite flakes.* Ceramics International, 2017. **43**(11): p. 8089-8097.

256. Qiu, W., et al., *Molten salt synthesis and growth mechanism of WC platelet powders.* Powder Technology, 2017. **310**: p. 228-233.
257. Li, S., et al., *Highly stable activity of cobalt based catalysts with tungsten carbide-activated carbon support for dry reforming of methane: Role of tungsten carbide.* Fuel, 2022. **311**: p. 122512.
258. Zhang, Y., et al., *Highly active and stable cobalt catalysts with a tungsten carbide-activated carbon support for dry reforming of methane: effect of the different promoters.* Catalysis Science & Technology, 2022. **12**(15): p. 4871-4883.
259. Bolatova, Z., et al., *Ni, Co and Ni-Co-Modified Tungsten Carbides Obtained by an Electric Arc Method as Dry Reforming Catalysts.* Catalysts, 2022. **12**(12): p. 1631.
260. Zhang, X., et al., *Co–Ni/WC-AC catalysts for dry reforming of methane: The role of Ni species.* International Journal of Hydrogen Energy, 2023. **48**(40): p. 15065-15076.
261. Vertongen, R., et al., *Sorption-Enhanced Dry Reforming of Methane in a DBD Plasma Reactor for Single-Stage Carbon Capture and Utilization.* ACS Sustain Chem Eng, 2024. **12**(29): p. 10841-10853.
262. Gao, X., et al., *Recent Developments in Dielectric Barrier Discharge Plasma-Assisted Catalytic Dry Reforming of Methane over Ni-Based Catalysts.* Catalysts, 2021. **11**(4): p. 455.
263. Zeng, Y., et al., *Unraveling Temperature-Dependent Plasma-Catalyzed CO(2) Hydrogenation.* Ind Eng Chem Res, 2023. **62**(46): p. 19629-19637.
264. Heijkers, S., M. Aghaei, and A. Bogaerts, *Plasma-Based CH4 Conversion into Higher Hydrocarbons and H2: Modeling to Reveal the Reaction Mechanisms of Different Plasma Sources.* The Journal of Physical Chemistry C, 2020. **124**(13): p. 7016-7030.
265. Lin, S.-S., et al., *Plasma Promotes Dry Reforming Reaction of CH4 and CO2 at Room Temperature with Highly Dispersed NiO/γ-Al2O3 Catalyst.* Catalysts, 2021. **11**(12): p. 1433.